Cape Peninsula
University of Technology

OPTIMISATION AND VALIDATION OF AN X-RAY FLUORESCENCE METHOD FOR THE ANALYSIS OF MINERAL SANDS OXIDES

by

Cramwell Badla

Dissertation submitted in fulfilment of the requirements for the degree

Master of Applied Science in Chemistry

in the Faculty of Applied Sciences

at the Cape Peninsula University of Technology

Supervisor: Dr Francois Wewers

Bellville

Declaration

I, Cramwell Badla, declare that the contents of this dissertation/thesis represent my own unaided work, and that the dissertation/thesis has not previously been submitted for academic examination towards any qualification. Furthermore, it represents my own opinions and not necessarily those of the Cape Peninsula University of Technology.

---------- ----------

Signed Date

Abstract

Namakwa Sands is a heavy mineral mining and beneficiation business within Tronox, and produces two major products, zircon ($ZrSiO_4$ 99.9 %) and rutile (TiO_2 99.9 %). Heavy mineral sand deposits occur naturally and are mined for minerals such as Zircon ($ZrSiO_4$), Rutile (TiO_2) and Ilmenite ($FeTiO_3$). The heavy mineral concentrates are exported to international markets to make specialist coatings for the paints and ceramics industries and both industries are very strict on the purity of the minerals used. Namakwa Sands prides itself in being able to produce zircon and rutile at the customer requirements however, strict requirements, especially in terms of Fe impurities (Fe_2O_3 content in zircon concentrate must be < 600ppm), limit the productivity and come at a cost to recovery.

Production comes from an open pit where dry mining is employed. The ore is transported by loaders and conveyors to a primary and secondary mineral separation plant where wet spirals (seawater) and magnetic and electrostatic separators are used to produce the marketable concentrates. The ability to control the mineral characterisation of feedstock materials or to monitor intermediate, products and waste streams allows better process control and increased efficiency. Heavy mineral sands concentrate samples are analysed by an X-ray fluorescence spectrometer (XRF) in the form of a fused bead. A worldwide shortage of certified reference materials for the calibration of an XRF instrument for the analysis of heavy mineral sands has resulted in the need to synthesise calibration standards. This was done using synthetic standards made from high purity compounds and mineral sands reference materials.

This study addresses the optimisation of X-ray fluorescence calibration through the introduction of synthetic standards for the determination of mineral sands oxides. It examines the application of synthetic standards made from high purity compounds and mineral sands reference materials for the calibration of an XRF spectrometer and enabling it to analyse for major, minor and trace elements (Mg, Al, Si, P, Hf, Ca, Ti, Zr, Fe, Th and U) in heavy mineral sands processing. The analytical conditions suitable for the samples were optimized considering sensitivity, precision, and the lower limit of detection. The fusion method was investigated as a universal method that can yield quality fusion beads and retain all the elements of interest on both the calibration standards and samples.

Calibration standards were synthesised by mixing pure compounds and mineral sands reference materials, to mimic matrices similar to that of the routine samples and cover the required analytical range. The aliquots were mixed in % fractions and fused with a 1:9 sample/ borate dilution to make glass beads. The matrix-matched standards and dilution have shown that the matrix effect can be

reduced. During XRF analysis interference effects such as spectral overlaps and background correction were compensated to ensure accurate analysis. The main parameters studied were the influence of different flux compositions and sample/flux ratio.

The optimum sample preparation conditions were evaluated and confirmed by visual inspection of beads to check dissolution, clearness, shattering and infinite thickness. The optimised calibration was validated as per SANAS TR 26-02 criteria for linearity, the limit of detection and quantification, precision, specificity, and accuracy. It passed all the validated parameters. The calibration lines were developed from synthetic standards and the results were accurate, substantiating that the fusion method can eliminate the mineralogical, matrix and particle size effects. The working range for all the lines was satisfactory. The limit of quantification (LOQ) of analytes was reliably low which shows that the predefined goals for bias and imprecision are met. The correlation coefficients (r^2) of the resulting calibration curves were > 0.999 showing excellent linearity. The precision of the calibration was sufficiently high, and the accuracy was of adequate quality with z(MAD) < 2. These observations support the successful synthesis and use of a well-selected set of synthetic standards. The low dilution fused glass technique effectively eliminates particle size effect, and allows accurate determination of both major, minor and trace elements from single glass beads.

The study confirmed that the newly developed fusion method can be successfully used to analyse a variety of heavy mineral sand samples to assist in the daily routine analysis of ilmenite, rutile, zircon production. The proposed XRF method can replace the *Original method* since its calibration can enable quick and effective analysis of elements across a wide range of concentrations in different types of heavy mineral sands streams, giving accurate and trustworthy results.

Acknowledgements

I want to thank Tronox Namakwa Sands, for their financial support and providing the necessary facilities for all the research work. Special thanks to unknown reviewers who generously gave their time and provided valuable suggestions to improve the quality of the document. I further wish to acknowledge the assistance of Tronox laboratory analysts who prepared most of the samples.

Table of Contents

List of Figures

List of Tables

Abbreviations and Symbols

ANOVA	Analysis of variance (Minitab function)
BG	Analyte background intensity
COLA	Comprehensive Lachance
CRM	Certified Reference Material
DF	Degrees of freedom
FP	Fundamental parameters method. XRF quantitative method
FPC	Flow Proportional Counter
H_0	Null hypothesis
H_1	Alternative hypothesis
I	Spectral line intensity
ICP-MS	Inductively Coupled Plasma – Mass Spectrometer
ICP-OES	Inductively Coupled Plasma - Optical Emission Spectroscopy
IFAC	Interference factor
kcps	Kilo counts per second
kV	Kilo volt
Kα	K-alpha photons or spectral lines
Kβ	K-beta photons or spectral lines
LiF	Lithium Fluoride
LiM	Lithium Metaborate
LiI	Lithium Iodide
LiT	Lithium Tetraborate
LOD	Limit of detection
LOQ	Limit of quantification
mA	milli ampere

nm	nano meter (10^{-9} m)
PET	penta-erythritol
PHA	Pulse height analyser. XRF energy distribution analyser
PHD	Pulse height distribution
ppm	Parts per million. Relative unit
r^2	Linear regression value
sec	second(s)
SEE	Standard estimate error
t_{calc}	Calculated t-value (*t*-test)
t_{crit}	Critical t-value (*t*-test)
UV-VIS	Ultraviolet–visible spectroscopy
WDXRF	Wavelength dispersive X-ray fluorescence
XRF	X-ray fluorescence
λ	Wavelength
μ	True concentration value
%RSD	Percentage relative standard deviation
2θ	Bragg angle (expressed as sin θ)

CHAPTER 1

INTRODUCTION

This study was conducted at Tronox Namakwa Sands on the West Coast of South Africa, 350 km north of Cape Town. The Namakwa Sands operation is a world-class producer of valuable heavy minerals (VHM) such as ilmenite ($FeTiO_3$), followed in abundance by leucoxene (an alteration product of ilmenite), zircon ($ZrSiO_4$) and rutile (TiO_2) from mainly semi-consolidated marine and dune sands. The processes encompass mining, mineral concentration and separation, and smelting operations. Heavy mineral sands are minerals with specific gravities higher than 3 kg/m^3.

Ilmenite is smelted using direct current (dc) open arc furnaces to produce titanium slag (TiO_2) and several grades of pig-iron (FeO). Titanium slag is used in the manufacture of paint pigment, while pig-iron is used in the foundry industry for the casting of automotive and engineering components and various other applications. Zircon is a hard mineral with a high refractive index and is ideally suited for the ceramics industry as an opacifier in the production of tiles and sanitary ware, other applications include refractories, TV screens, foundries and zirconium chemicals and zirconium metal. Rutile is high strength and low-weight mineral used in the manufacture of welding rods and paint pigment and is processed into titanium metal for use in aircraft parts amongst others.

1.1 Background

The production of VHM from a heavy mineral deposit requires the physical separation of individual mineral grains. Grains refer to individual sand grains on mm scale. Separation is accomplished by exploiting differences in four mineral characteristics: density, grain size, magnetic susceptibility, and electrical conductivity. Therefore, there is a continually increasing need for quick and accurate chemical analysis across a wide concentration range in mineral sands processing operations. Such a need is necessary to further improve heavy mineral yields and recoveries. X-ray fluorescence (XRF) spectroscopy has been proven successful in the analysis of elements (as oxides) from Ilmenite, Rutile and Zircon minerals. It delivers a very rapid, precise, and accurate analysis of minerals and ores across a broad range of elements (Be-U) and concentrations ranging from parts per million (ppm) trace amounts to one hundred percent (wt. %) (Potts, 2013).

The most common elements found in mineral sands are Al, Ca, Ce, Cr, Fe, Hf, Mg, Mn, Nb, P, Si, Sn, Th, Ti, U, V and Zr. The aim of mineral sand processing is therefore to separate the valuable minerals from the gangue to produce enriched Zircon ($ZrSiO_4$), Rutile (TiO_2) and Ilmenite ($FeTiO_3$) concentrates. With large-scale mineral concentrating operations, "trustworthy" analysis will play a major part in the future development of automatic control systems for optimisation of the electrostatic, magnetic, and wet gravity separations. Mineral sands processing plants undergo many separation stages and recycling paths to separate the feed into its constituent mineral species, thus leading to wide analysis ranges and requiring analysis of trace elements.

The accuracy of XRF analysis depends mainly on factors such as the stability of the spectrometer, the quality of the certified reference materials (CRMs) or other 'standard samples' used for calibration, the homogeneity of the samples analysed, the effectiveness of the calibration of the matrix effect and particle size effect (Willis, 2010). Matrix effects are created by the varying XRF intensities when reading the same element bonded to different components. The higher the complexity of a component, the higher the apparent intensity is, even if the element is present at the same concentration. Particle size: a more accurate term would be heterogeneity. It represents any small volume of material that has a composition different from that of the surroundings.

There are several sample preparation procedures for quantitative analysis, including between powder pellets and fused glass beads. In XRF, most solid samples are prepared as pressed pellets, whereby the achievable precision suffers from so-called particle size effects. It is described that the intensity of X-ray fluorescence is depending on particle size and shape. If the achieved precision with pressed pellets is not sufficient, the sample must be prepared using a fusion process. Since XRF analysis is a comparative method, the accuracy of calibration lines relies on the homogeneity of the standards and the reliability of their certified values. Thus, for accurate analysis, samples are generally fused with flux into glass beads to reduce matrix effects and particle size effects, while retaining low detection limits. Many authors have examined the fusion techniques involving various samples to flux ratios, e.g. (Claisse & Samson, 1962; Norrish & Hutton, 1969). They reported that dilution of the samples has the effect of reducing the inter-element influence and matrix effects.

Sieber (2002) stated that an XRF spectrometer traditionally requires its methods to be calibrated using certified reference materials (CRMs). As stated in the abstract, this means choosing from a limited selection of CRMs, which are costly and not widely available. Due to the scarcity of commercial mineral sands calibration standards, various international mineral sands industries have opted to synthesize calibration standards. The introduction of synthetic standards made from pure compounds for XRF method calibrations has been studied and yielded accurate results (Sieber,

2002). These studies were done using stoichiometric mixtures of high purity and stable compounds via the standard addition method. XRF traditionally suffers from significant matrix effects which can make calibration challenging. Calibration methods for XRF include the use of matrix-matched standards (standards that closely match the routine samples), adding an internal standard to the sample matrix, dilution to reduce matrix effects, and fusion of standards and samples with a suitable flux (Sieber, 2002).

The current work describes techniques of XRF calibrations through the introduction of matrix-matched synthetic standards for the precise and accurate analysis of oxides. These standards were made from commercially available high purity compounds to calibrate a method for 11 oxides, namely, ZrO_2, SiO_2, HfO_2, Fe_2O_3, TiO_2, Al_2O_3, CaO, MgO, P_2O_5, U_3O_5 and ThO_2. The aim is for the calibration to enable quick and effective analysis of elements across a wide range of concentrations in different types of heavy mineral sands streams, giving accurate and trustworthy results.

1.2 Research problem

The existing analytical method for most of the intermediate stream samples is used outside its intended scope. The calibration standards do not cover the whole range of concentrations required in the subsequent analyses. Therefore, concentrations of routine samples are determined by extrapolation which compromises the precision and accuracy of the results. Additionally, the calibration standards are depleted in the laboratory and are not available on the market, thus the method cannot be reproduced. Furthermore, the method is not fit to partake in interlaboratory comparison and quality assurance activities. The laboratory has received numerous complaints from external and internal customers about the precision and accuracy of the method.

1.3 Research questions

- Will the XRF calibration protocols developed in the present work yield a successful synthesis of standards to obtain a well-selected set of synthetic calibration standards?
- Will the XRF method enables a quick and effective analysis of elements across a wide concentration range in different types of heavy mineral sands streams giving accurate and trustworthy results?

- What effect will the method have in ore characterisation methodologies and perhaps the development of elemental composition-based markers to predict extraction performance?

  What validation parameters are more important to verify that the method is fit for purpose?

1.4 Objectives

- Investigate and optimise the sample preparation process.
- Synthesize calibration standards that have a similar matrix to the routine samples to be analysed and cover the required analytical range using high purity compounds.
- Re-develop a suitable analytical method that will enable quick and effective analysis of elements across a wide range of concentrations in different types of heavy mineral sands streams, giving accurate and trustworthy results for the analysis of ZrO_2, SiO_2, HfO_2, Fe_2O_3, TiO_2, Al_2O_3, CaO, MgO, P_2O_5, U_3O_5 and ThO_2.
- Validate the analytical method according to international quality standards (ISO17025).
- Testing the method by laboratory comparison technique.

1.5 Delimitations

All mineral processing samples are analysed by XRF; thus, other analytical techniques will not be discussed.

1.6 Thesis outline

The current study encapsulates six chapters presented as follows:

Chapter 1: Introduction

Discusses the general topic and give some background. Outlines the current situation. Evaluate the current situation and identify the gap.

Chapter 2: Literature review

Gives an overview of previous studies as well as all areas investigated including experimental techniques that are used regarding the synthesis of standards, XRF method development and method validation. The aim is to gain insight into how researchers apply the concepts to real-world problems.

Chapter 3: Experimental

Describe each step of the experimental procedures used in this study. It also provides a clear and complete description of the specific procedure including sample preparation, synthesis of calibration standards techniques.

Chapter 4: Results and Discussion

The validation and optimisation parameters are being presented and discussed. It also presents the results obtained from the study to estimate inaccuracies or systematic errors between the *Original and the Optimised method*. This was evaluated using the confidence limits method to estimate the systematic errors on the basis of the differences observed between the methods.

Chapter 5: Conclusion and Recommendations

Provides a summary of the purpose, methodology, results of this study. Then, conclusions are based on research insights gained regarding study findings and limitations. In addition, recommendations are presented.

References

Lists references cited within the text.

CHAPTER 2

LITERATURE REVIEW

2.1 Sample preparation

The variety of materials that can be analysed routinely for major (> 10 %), minor (0.5 - 10 %) and trace (< 0.5 %) elements using XRF is substantial. Most materials have broad 'industrial standard' analysis requirements in terms of analytes, concentration ranges and required precision and accuracy. X-ray fluorescence analysis is a widely accepted technique for obtaining rapid chemical analyses of geologic samples. Depending upon the application and the required precision and accuracy, laboratories use either pressed powder and/or borate fusion methods (Amosova et al., 2019).

The use of pressed powders gives accurate results. However, large errors are possible due to differences in the granulometric (particle size) and phase compositions of the substance under analysis and the reference materials (mineralogy). These effects increase when samples contain abundant silicate minerals, quartz, and accessory minerals. These errors can be minimized to a certain extent by pressing powders to a constant volume (Li et al., 2018). Particle size effects could be significantly reduced when the sample particle size is small enough, which can be achieved by employing milling methods. The best way to avoid the mineralogical effect is to fuse both the unknown samples and the calibration standards under the same conditions.

Willis (2010) reported that to improve accuracy, homogeneous beads had to be prepared, and this motivated the development of the borate flux fusion method. For obtaining optimum analysis results in the XRF method, the samples and standards must be excited under entirely identical conditions. Fusion provides an ideally homogeneous sample with a defined density and without particle size effects. In addition, homogeneity, and a perfect surface lead to a much smaller calibration error. To ensure representativity, Marguí et al. (2016) stated that the material should be finely ground, the finer the particles the faster the fusion since borate fusion is a dissolution. Thus, the grinding of samples to < 75 µm or finer is recommended as large particles take long to dissolve and if dissolved are the cause of cracking and crystallisation. Willis et al. (2011) discovered that refractory minerals such as zircon, chrome and quartz are hard and difficult to grind finely as well as being difficult to dissolve.

Fusion techniques for sample preparation in X-ray fluorescence analyses are being more widely adopted for the analysis of powdered materials when dealing with routine production control. Low dilution fused glass XRF methods have thus been developed to eliminate particle size effects, sample heterogeneity, and sampling errors for the analysis of silicate rock materials (Eastell & Willis, 1993). Factors to be considered for the fusion technique were identified and discussed by Smoliński et al. (2016) and include the sample type, particle size, fusing agent (flux), sample to flux ratio, fusion temperature as well as fusion time. The quality of the analysis is dependent on the sample specimen homogeneity, which in turn is dependent on the fusion process. The two essential constituents of a fusion are a sample and borate flux. Smoliński et al. (2016) defined borate fusion as a chemical reaction that occurs at high temperatures using a platinum crucible to melt borates to become solvents for oxides. The melt is cooled in a platinum mould without crystallizing to yield an amorphous homogeneous solid glass bead. The Pt-Au alloy is the most universally used due to it possessing the best non-wetting properties (Willis, 2010). Boron oxide is obtained from dehydrated boric acid and cools down to a stable glass after melting.

The borate fusion method was found to be advantageous for the preparation of synthetic standards (Claisse, 1994). It gained popularity for its high transparency for X-rays at long wavelengths making the sensitivity of light elements higher (Potts, 2013). The lithium borates from which current fluxes are made are the tetraborate and the metaborate. Lithium tetraborate (Li_2BO_7) is the most used flux in XRF analysis. Since it is relatively more acidic compared to lithium metaborate ($LiBO_2$), it is suitable for fusing samples such as limestone and cement which contain basic oxides (CaO, MgO, etc.) (Willis et al., 2011). However, its 930 °C melting point is the highest among the flux types and consequently, the fusion temperature must be relatively high. Therefore, this flux requires special attention to sample and flux volatilisation as well as damage to the fusion crucible. $LiBO_2$ being more basic compared to Li_2BO_7 is therefore more suitable for fusing samples such as silicates, rocks and refractories which contain acidic oxides (SiO_2, ZrO_2, TiO_2, etc.). It has a lower melting point of 845 °C and tends to cause crystallization instead of vitrification when cooled (Marguí et al., 2016).

Samples can be classified as either acidic or basic, and the fluxes are classified based on their ability to react with these two sample types (Willis et al., 2011). The flux must be chosen to make sure the sample components will dissolve readily. Claisse (1994) stated that the acidity or alkalinity of oxides determines their solubility in a specific flux and the stability and mechanical properties of the resulting fused glass bead. He prescribed that an acidic oxide should be dissolved using the more alkaline flux, thus lithium metaborate, and vice versa. Fluxes are classified by their acidic index, which is the proportion of the oxygen to metal atoms. An acidic index is expressed as the number

of oxygen atoms in the oxide divided by the number of metal atoms. All the oxides with an acidity index greater than one are specified as acidic. He also prescribed a lithium tetraborate-metaborate mixture for any oxide with an acidity index between 1.25 and 2.

Claisse & Samson (1962) suggested the use of a lithium borate combination as it is more efficient than pure tetraborate or metaborate for most oxides. It has a lower melting point, therefore, leads to lower viscosity, producing a more stable fusion bead, and decreasing the possibility of residual sample in the crucibles and moulds. Norrish & Hutton (1969) advocated Claisse & Samson (1962) suggestions and proposed the so-called 12:22 flux that contains 12 parts lithium tetraborate and 22 parts lithium metaborate. Bennett & Oliver (1992) expanded the studies and established a mixture of 1-part lithium tetraborate and 4 parts lithium metaborate as the composition is close to the eutectic thus, making the preparation of glass beads easier. A more recent study by Marguí et al. (2016) reported that a 50 % lithium tetraborate: 50 % lithium metaborate composition is the most universal flux. It is widely used due to its optimised performance for all acidic oxides.

There is a limit to the quantity of a given sample that can be dissolved in a given flux. At a higher sample-to-flux ratio, the matrix effects are normally high thus requiring matrix correction (Willis et al., 2011). The advantage of increasing the sample to flux ratio will be lower weighing errors and a good representation of production. The intensities will be constant from sample to sample with improved repeatability and reproducibility (Marguí et al., 2016). A lower sample-to-flux ratio would mean an easy dissolution of the sample due to the high amount of flux present however, the sensitivity of the XRF when analysing low concentration elements will decrease, which in turn means a decreased repeatability due to decreased instrument precision. This will also lead to a low analyte peak to background ratio and high detection limit due to low intensities (Beckhoff et al., 2006). To analyse for major, minor and trace elements on a single fusion specimen the dilution ratio must be low enough to produce high count rates for the trace elements but high enough to produce homogeneous specimen (Eastell & Willis, 1990).

Lee & McConchie (1982) successfully determined selected trace elements using lithium tetraborate and lithium carbonate with a flux-to-sample ratio of 2:1. Bower & Valentine (1986) critically compared sample preparation methods for major and trace element determinations using XRF spectroscopy. They concluded that any dilution ratio could be adopted, depending on the type of analysis and the degree of accuracy required. They also concluded that pressed powder pellets for trace element analysis have no real advantage over glass fusion discs as the latter are homogeneous and particle size, mineralogical and chemical effects are eliminated. A low dilution fusion technique,

based on those of Eastell & Willis (1993) has been developed for the determination of major, minor and trace element contents in geological samples.

Borate fusions were found to be advantageous for the preparation of synthetic standards (Claisse & Blanchette, 2004). Pure oxides can be mixed in any desired combinations and proportions to make standards that contain only desired elements (Claisse, 1998). A calibration with pure oxides has the further advantage of calibration curves with a regression coefficient closer to 1. Claisse & Blanchette (2004) reported that flux is available as fine powders or in granular and globular forms. It should be completely dry and must be dried before use as is hygroscopic. The appropriate purity grade must be chosen and since impurity levels can vary from batch to batch, it is desirable to have a substantial amount of one batch to minimise analysis error.

The features of an ideal fusion procedure as defined by Bennett & Oliver (1992) is the retention of all elements in the sample and the flux. Volatile elements such as Al, Mg and P may be lost during the fusion process. According to Willis (2010) the evaporation behaviour of these elements is dependent on the chemical composition of the sample, added reagents and the mineralogy of the samples. An element mechanically mixed into a matrix as an oxide is less stable than an element located in a lattice position in a mineral.

2.2 Preparation of calibration standards

There are various preparation techniques that are well suited for making synthetic standards from pure compounds. One involves standard addition where certified material or a pure chemical compound is added to a sample to form a mixture. This technique was used by Yamasaki (2014), where large batches of reference materials and pure compounds were homogenised using blending operations (i.e. ball-mill, mortar, and pestle, etc.). This aids the preparation of standards closely matched to the matrix of the test samples. Chiweshe et al. (2016) successfully trialled the method in preparation of precious metal calibration standards. The use of the standard addition method has been reported as one of the preferred methods to reduce matrix effects. The application of the standard addition method for mineral sands determination is not very common due to the complexity of mineral sand composition. The Australian Standard, however, reported the use of the standard addition method using only pure compounds (no matrix matching). The standard proved that this method is very sensitive to unmatched matrices, especially in the presence of titanium as the major element since it suffers matrix effect challenges (AS, 1996). The matrix is the same for each reference sample and matches that of the unknown samples. This method requires an extensive

reference sample set along with the knowledge of all elements present in both the reference and unknown samples (Bouchard et al., 2014). Any error in the preparation of the stock will propagate through the other standards leading to a bias in the calibration. Bouchard et al. (2014) reported that precise and accurate results can be achieved when synthetic standards are prepared by blending reference materials with pure compounds using a lithium borate fusion method. Staats (1989) discovered that the planning stage is crucial to ensure all required analyte elements are included as it is a challenging task to add additional analyte elements later.

(Mashima & Mori, 2005; Mashima, 2016) studied the standard dilution method, where the standard stocks are combined in known and varying amounts of the analyte to build the calibration curve. They found that the method is very accurate because it allows for the direct quantification of original analytes and simultaneously corrects for matrix effects. The disadvantages of this method are that it requires a large number of samples and is very time-consuming and labour intensive. Making standards from high-purity compounds eliminates homogeneity concerns and allows customization of concentration ranges to fit specific needs but having to weigh multiple reagents increases the chance for errors (Nettles, 2000).

The customisation allows calibration standards to cover the complete concentration range for each element to be determined and to prevent extrapolation during quantitative analysis which may cause erroneous results. The standard concentrations should cover, at least, the range of concentrations encountered during the analysis of test samples and be evenly spaced across the range. Ideally, the calibration range should be established so that most of the test sample concentrations fall towards the centre of the range. This is the area of the calibration range where the uncertainty associated with predicted concentrations is at its minimum (Nettles, 2000). The studies of Giles et al. (1995) and Sieber (2002) in this field exemplified that the methods require an inventory of high purity compounds. Furthermore, all the compounds must be dried or roasted prior to use. This is done at the temperature specified on the product certificate to ensure the compound has the correct stoichiometry. Mashima & Mori (2005) cautioned that failure to pre-treat compounds can result in weighing errors during the standard addition as some compounds are hygroscopic.

2.3 Selection of XRF analytical parameters

A wavelength-dispersive XRF spectrometer consists of the X-ray tube (generates primary X-rays to excite secondary characteristic X-rays from atoms in the sample), collimators (to direct a parallel beam of X-rays from the sample to the analysing crystal), the analysing crystal (to disperse the X-

rays from the sample into individual wavelengths) and the detector which measures photon energy from the sample and converts it into electrical signals.

After the elements in the sample have been excited by the primary X-rays from the tube, each element emits secondary X-ray photons with a characteristic wavelength (fluorescence). These secondary X-ray photons from the sample are focused onto an analysing crystal using a collimator that intercepts the photons from the sample to ensure that a parallel photon beam is projected onto the crystal. The collimator, which is situated between the sample and crystal also ensures that only X-rays that arise from the sample are allowed to reach the crystal. The function of the analysing crystal is to separate all the characteristic secondary X-ray wavelengths emitted by the elements in the sample into distinct wavelengths by means of diffraction. The instrument parameters over which an analyst commonly has control are illustrated in Figure 2.1.

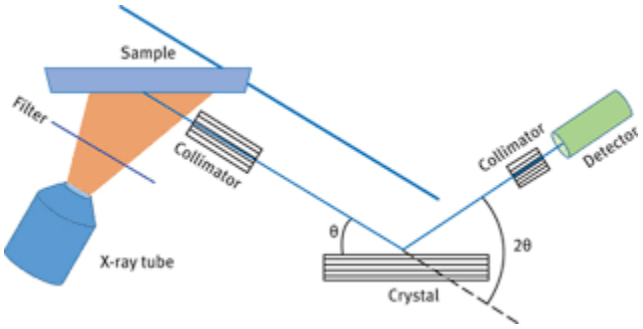

Figure 2.1. A schematic of a wavelength dispersive XRF-spectrometer.

In setting up a good XRF program the first requirement must be knowledge of the concentration of the analytes and the samples to be analysed. This will enable the better choice of selecting analyte lines that are free from possible spectral interferences. There are two factors that control whether the interference is significant or not; i.e. the angular separation of the analyte line from the interfering line and the relative concentration of the analyte. According to Willis et al. (2014) when setting up a good XRF for quantitative analysis, there are crucial aspects that one must consider obtaining accuracy and good precision. Selection of analyte lines/channels is amongst one of the aspects.

For X-ray measurements, the optimum conditions must be chosen. Optimum measurement conditions depend on what the analyst requires, for example, the highest intensity, the lowest background, or the minimum line overlap. The maximum intensity is achieved when the energy of the tube radiation is three to four times the absorption edge of the element. In terms of line overlaps, the choice of crystals and collimators in a Wavelength dispersive XRF spectrometer will have a

large effect. Willis et al. (2014) suggested that the best combination of analytical parameters that will yield the lowest limits of detection and smallest counting error must be properly selected. Instrumental parameters are usually selected for maximum intensity to compensate for the addition of flux to the sample which leads to a decrease in fluorescence intensity.

In fusions, the diluent is made of light elements that are highly transparent to X-rays. Consequently, the dilution has little effect on short wavelengths/high energy elements. In the case of long wavelengths/low energy elements such as Mg and Al, the dilution ratio is more important, as these may yield significant low intensities (Haukka & Thomas, 1977; Eastell & Willis, 1990). The X-ray interaction depends on the thickness of the sample as well as the density of the sample. More focus will be given to the X-ray interaction, which is the principle of X-ray fluorescence spectrometers. The only parameters under the control of the analyst with regards to the tube are the kV and mA settings.

2.3.1. Tube kV and mA Selection

Potts (2013) indicated that the tube anode is chosen based on whether it will provide the most efficient excitation of the elements to be analysed. The Rhodium (Rh) tube has been found to be the best multipurpose tube for exciting elements from Fluorine to Uranium (Schlotz & Uhlig, 2006). It has a maximum voltage setting of 60 to 70 kV and operating power of up to 4000 W (kV x mA). The tube is fitted with a 30 to 150 µm thick beryllium window. The Beryllium is selected as window material since it is the lowest-atomic-number material that is available as a foil with appropriate mechanical properties to form a vacuum-tight seal and it allows good transmission of both the K- and, especially, L- lines to be used for exciting the sample (Beckhoff et al., 2006). The wavelength and intensity distribution of the tube is determined by the voltage (kV) and current (mA) applied to the X-ray tube. It is recommended by the XRF suppliers to keep the power of the tube constant and therefore change the voltage (kV) and current (mA) so that the power setting remains at maximum.

2.3.2. Collimator Selection

After the elements in the sample have been excited by the primary X-rays from the tube, each element emits secondary X-ray photons with a characteristic wavelength (fluorescence). These secondary X-ray photons from the sample are focused onto an analysing crystal using a collimator that intercepts the photons from the sample to ensure that a parallel photon beam is projected onto

the crystal. The collimator, which is situated between the sample and crystal also ensures that only X-rays that arise from the sample are allowed to reach the crystal.

The primary collimator is usually made of a series of parallel blades. The length and spacing of the blades determine the angular divergence admitted by the collimator. This angular divergence determines the final resolution of the spectrum. One can improve the resolution by closing the collimators to minimise the divergence, however, the photon flux will decrease thus leading to a decrease in intensity. Thus, a compromise between the final resolution (necessary to avoid important spectral overlaps) and the sensitivity (related to the intensity) is made (Beckhoff et al., 2006). Generally, the collimators are adopted in accordance with the crystal's intrinsic divergence, which varies from one type of crystal to another. Some of the crystals offer excellent resolution while others have a very wide diffraction profile (Grieken & Markowicz, 2001). For this purpose, spectrometers offer three types of collimators: fine, medium, and coarse. The fine collimator is used for most of the heavy elements, medium for the mid-range elements and coarse for the light elements.

2.3.3. Analysing Crystal Selection

The crystal separates the wavelengths by diffraction and directs them to the detector. The crystal consists of crystal lattice which consists of sets of parallel atom planes. In Bragg´s Law, the distance between the atom planes is referred to as "d" and it determines the angular separation between peaks, the resolution being inversely proportional to the distance (Schlotz & Uhlig, 2006). Two main qualities of the crystal are its reflection ability which affects the peak intensities and the crystal d-spacing which affects the resolution. The reflectivity is usually proportional to the *d*-spacing. Optimal crystal choice is determined by the wavelength of the element and generally, crystals with longer d-spacing are used with light elements and crystals with shorter *d*-spacing are used with heavier elements.

An XRF spectrometer is equipped with three crystalline materials i.e. Lithium fluoride (LiF), Penta-erythritol (PET) and Germanium (Ge). The intensity, angular dispersion and resolution of the secondary X-ray photons are controlled by the analysing crystal. LiF crystal is used for short and long wavelengths, and where lines are very close to each other. Ge is used for chlorine, sulphur and phosphorus because it has no second-order (n=2) reflections and Ca-Kβ_2 which interferes particularly with P-Kα. PET is used mainly for silica and aluminium. According to Willis et al., (2014) a good analysing crystal must have some important properties which are,

- Wavelength range appropriate for the lines to be measured
- High diffraction intensity
- High resolution
- High peak to background ratio
- Absence of interfering elements
- Low thermal coefficient of expansion
- High stability in air and on exposure to X-rays
- Good mechanical strength

The maximum angle that can be measured by the spectrometer is 10 - 147 ˚2θ. Below 10 ˚2θ, the radiation from the specimen will pass over the top of the analysing crystal resulting in un-diffracted radiation entering the detector and giving false results. Above 147 ˚2θ, the mechanical arm on which the detector is mounted will strike the primary collimator housing or the specimen chamber (Willis et al., 2014).

2.3.4. X-Ray Detector Selection

The intensity of characteristic secondary X-ray photons (seen as spectra lines) produced during XRF analysis is measured with relevant detectors. The detectors convert the X-ray photons from the sample into electrical pulses and the height of the pulse will be proportional to the energy of the incoming radiation. The most important characteristics of a detector are efficiency, dead time, and energy resolution. All the detectors are proportional detectors; the magnitude of the output electronic pulse for an incoming individual X-ray photon is proportional to the energy of the photon (Beckhoff et al., 2006). Detectors suffer from two problems namely dead time and the production of escape peaks. Spectrometer electronics need a certain amount of time to process a pulse, during which no other pulse can be registered. This period is called counter channel dead time for an individual pulse. As the pulse formation is different for the flow counter and the scintillation counter, the dead times (typically 300 to 400 ns) are also different for each detector.

For sequential XRF spectrometers, it is possible to use the detector per element. For this reason, a wide range of gas detectors is used such as He, Ne, Kr and Xe gas-filled proportional detectors (FPC), in addition to scintillation detectors (Potts, 2013). The gas proportional counter comprises a cylindrical metallic tube in the middle of which a thin wire (counting wire) is mounted. This tube is filled with a suitable gas (e.g., 10 % Ar + 10 % CH4). A positive high voltage is applied to the wire. The tube has a lateral aperture or window that is sealed with a material permeable to X-ray. The

scintillation counter (SC) used in XRF comprises a sodium iodide crystal in which thallium atoms are homogeneously distributed "NaI(Tl).

Scintillation counters are used for wavelengths less than 0.2 nm. In scintillation, the incoming photons diffracted by the analysing crystal are absorbed with a NaI(TI) scintillator and produce a flash of light. A photomultiplier tube converts the flash of light into an electronic pulse. The voltage of the output pulse is proportional to the brightness of the light flash and to the energy of the measured X-ray photon. The pulses are then passed on to a pulse height selector (PHS) (Giles et al., 1995). The technical problems with scintillators are mainly ineffective and uniform light detection.

The gas flow proportional counters are used for wavelengths longer than 0.2 nm. It is filled with Ar-gas mixed with methane as quenching gas. An X-ray photon from an analyte element enters the detector and ionises the gas to form an electron pair. The number of electrons produced is proportional to the energy of an incoming X-ray photon. The electric field inside the detector forces the electrons towards the central anode wire where they produce a drop in the detector high voltage and generate an output pulse which is proportional to the number of electrons. The voltage of the pulse is therefore proportional to the energy of the detected X-ray photon. This process will give rise to the pulse height peak (Schlotz & Uhlig, 2006).

If the incoming X-rays have energies greater than the binding energy of Ar, then such X-rays can cause excitation of the secondary Ar X-rays. When Ar X-rays are reabsorbed in the detector gas the result is the generation of an output pulse of the same size (pulse height) as that produced by the incoming X-ray photon. The Ar X-rays 'escape' from the detector, either through the detector window then a smaller output pulse known as the escape peak is produced on the low energy side of the main peak (Grieken & Markowicz, 2001). Escape peaks are only produced when the X-rays from the element can excite the gas of the detectors. Gas-filled detectors have good detection efficiency. Their main disadvantages are the gas supply and thin entrance windows. These foils can easily be damaged resulting in gas leakage.

2.4. Qualitative analysis

Qualitative analysis assesses possible peak overlaps. The procedures used for correcting the line overlaps from elements present in the sample are the same for interference from other analyte or matrix elements. No spectral overlaps are really expected for the elements with low atomic numbers like Si, Mg and P because the line wavelengths for these elements are not as close together as those or elements with higher atomic numbers (Willis et al., 2011). To determine the effects of spectral

interference from analyte or matrix elements it is necessary that interference standards be prepared for all the interfering elements. These interference standards are blank samples with no detectable concentration of any of the analyte but with only the interfering elements to correct the interference.

The concentration of the interfering element in these standards should be more than the maximum expected in the suite of unknown samples to be analysed (Willis et al., 2011). However, it should not be less than 1000-2000 ppm, or the counting statistics will be inadequate for precise determination of the correction factors. When preparing such standards, it is strongly recommended that very high purity chemicals should be used as additives to ensure that only the element of interest is being added to the blank material (Beckhoff et al., 2006)

2.5. Quantitative analysis

The intensity of the fluorescent X-rays is dependent on the concentration of an element in the sample. The higher the concentration of an element, the higher the count intensity will be in its corresponding energy channel. Thus, if the fluorescent X-ray intensity and concentration of an element contained in a standard sample are both known, then calibration can be established to determine the concentration of an element from its fluorescent X-ray count intensity. Obtaining this calibration function is the main objective of all quantitative XRF analysis methods. In the quantitative method also measuring conditions can be fine-tuned if needed and background positions and PHA windows are set.

2.5.1. Analyte background correction

Wavelength scans for the elements are determined to verify the 2θ angle at which each element line is diffracted by crystal and to evaluate possible spectral overlaps and selection of background positions. Any additional L- lines appearing in the wavelength scans will be identified by comparing the 2θ angle value obtained in the scan to 2θ angle values commonly available in literature tables (Grieken & Markowicz, 2001).

Overlaid wavelength scans from the typical sample are used to facilitate the evaluation of potential overlaps of the analyte peak and background positions. In quantitative analysis the net peak intensity is proportional to concentration and the analyte peaks are superimposed on a background; the intensity changes with wavelength and with sample composition. Therefore, to obtain the net peak intensity, it is necessary to subtract the background intensity at the peak position from the measured gross peak intensity.

Willis et al. (2014) discussed several different methods available for determining the background beneath the peak position; most of them involve measuring the background at one or more interference-free positions close to the peak. They found that background intensities ideally should be measured on both sides of the peak, if possible. This is due to the fact the background is generally sloping and has some curvature, especially at the shorter wavelengths. Therefore, methods of background correction must take into account both the slope and the curvature of the background. If only a single background-position is measured the analytical results are usually less accurate.

2.5.2. Pulse height analyser setup

By careful selection of detector window, it is possible to efficiently absorb the radiation of interest, while filtering crystal fluorescent radiation in the detector window and allowing higher-order radiation to partially pass through the detector. The pulse height analyser (PHA) is the pulse height selection, and it is an electronic way of removing unwanted pulses which are present in the measured signal, but which do not originate from the element of interest. The unwanted pulses can be created by low voltage electronic noise, reflections from the crystals and crystal fluorescence. The fluorescence can only be removed provided that the energy is sufficiently different from the element that is being measured. The pulse height distribution is an energy spectrum in which the pulse height of the measured signal is proportional to the energy of the incoming X-ray photons (Schlotz & Uhlig, 2006).

The pulse height analyser window is made up of lower and upper levels. Setting up the PHA window is critical for accurate and precise analyses; it must be set properly as is strongly affected by the detector pulse height resolution. The scintillation counter must be set symmetrical and sufficiently wide to accept at least 95 % of the total peak. When the gas flow counter is used and escape peaks are generated, the escape peaks must be included in the PHA window.

2.5.3. XRF method calibration

In setting up calibration lines for the elements, standards with known concentrations of each element are measured on the XRF spectrometer to determine the spectral-line intensity (kcps) related to the known concentration (%) for each element. The spectral-line intensity is a function of concentration, when a sample with an unknown concentration is analysed, the concentration can be determined by relating the intensity of the element spectral line obtained from the sample back to the calibration line (François et al., 2008). It is also useful to make at least duplicate measurements at each

concentration level, particularly at the method validation stage, as it allows the precision of the calibration process to be evaluated at each concentration level. The replicates should ideally be independent – making replicate measurements on the same calibration standard gives only partial information about the calibration variability, as it only covers the precision of the instrument used to make the measurements and does not include the preparation of the standards.

The calibration lines must be validated for specific quality control parameters using relevant statistical methods, the focus point must be to set up linear response curves for each element (Sieber, 2002). The ideal for setting up good calibration lines is to use Certified Reference Materials (CRMs). The uncertainty related to the concentration is known for CRMs. Additionally, the accuracy of any calibration depends on the accuracy of the standards used. It is not always possible to use CRMs due to the limited availability of these standards. In these cases, secondary standards (also known as synthetic standards or reference standards) must be prepared, and the concentrations of the relevant elements are determined using an alternative validated analytical procedure. These secondary standards are prepared from high purity compounds. Standards used to set up calibration lines must also contain the elements necessary to determine and correct for possible matrix effects in the sample. This ensures good matrix matching between standards and the samples.

A matrix correction step is used after raw count data are smoothed and peak areas are calculated. This step is essentially a final calibration to obtain the best estimate of elemental concentrations from processed energy spectrum versus count data. Matrix corrections can be categorized into two types: empirical methods and fundamental parameter (FP) methods. The empirical method may be constructed without any XRF principles which would require knowledge of the instrument and material parameters. The empirical method produces a calibration curve to determine the chemical concentration for elements in the sample from processed XRF energy count data. Two empirical methods widely used in commercially available XRF instruments are the Lucas-Tooth & Price (1961) and Lucas-Tooth & Pyne (1964) calibration algorithms. The Lucas-Tooth & Pyne algorithm uses a non-linear interpolation step to correct for inter-element interactions, whereas the Lucas-Tooth and Price use linear interpolation. Interelement interactions are caused when the XRF intensity from one element is absorbed by, or enhanced by, another element. The Lucas-Tooth & Price matrix correction algorithm is used for most commercial XRF applications.

Although the empirical methods are mathematically simple, they require a large number of reference standards with chemical and physical properties similar to those of the unknown samples. The preparation of the calibration standards is the critical step in the calibration process. This step must be carried out with great care, and all standard samples must be prepared in exactly the same manner

as the unknown sample. Thus, the same sample preparation steps and experimental conditions must be used for both standards and unknown samples. This requirement for sample preparation limits many potentials uses for XRF in practical applications.

The fundamental parameter (FP) method which was first introduced by Sherman (1955) describes very well the relationship between the measured intensities emitted by specimen and its composition. Basically, through a calibration step, the fundamental parameter method converts the element's peak intensities to an elemental concentration where the related parameter is independent of the sample matrix. Other popular FP-based calibration methods include those studied by Rousseau (2006). These methods utilize knowledge of the instrument and material parameters such as theoretical X-ray beam intensity, beam, and detector angles, inter-element effects, and spectral background to estimate elemental concentrations. The FP models are computationally demanding and impractical for near real-time applications; however, FP methods require as little as one reference sample to produce acceptable calibration results. Further, the reference sample does not have to exactly match the properties of the unknown sample. Due to the mathematical simplicity of empirical methods and the small number of calibration standards required for the FP methods, researchers have focused their efforts on the development of semi-empirical matrix correction algorithms to combine the strengths of empirical and FP methods. Specifically, these combine the mathematical models from the empirical methods with theoretical coefficients obtained from instrument parameters. These types of matrix correction methods have been an ongoing research area for XRF spectral analysis since mid the 1960s. Researchers such as Lachance & Traill, (1966) and Rasberry & Heinrich (1974) have developed various semi-empirical algorithms for the matrix correction step. Although the complication of mathematical models is somewhat reduced from the full FP method, this semi-empirical method often requires reference samples consisting of pure elements, which are generally very difficult to obtain.

2.6. Analytical method validation

Optimizing the measurement conditions of calibrant, analytical lines, dispersive crystal, operating conditions such as pulse height, peak angle, the X-ray tube, and background have proven to introduce additional errors in quantitative analysis (Potts, 2013). When a new analytical method is developed, it is done to minimise the possibility of errors that may lead to inaccurate results. Errors form part of almost every aspect of analysis from sampling and sample preparation, right up to results. They are an inevitable part of the method development but can be minimised. They are

classified into gross, random or systematic errors. Gross errors are of such a nature that the entire analysis must be abandoned. When multiple analyses are conducted on a sample and a systematic error occurs, all individual results will be biased, yielding values that are either higher or lower than the true analytical value which has a direct influence on the accuracy of the results (Miller & Miller, 2018). Errors effectively influence the precision of results due to the wide range over which the results appear. Therefore, it is important to identify and quantify as they contribute to high uncertainties in analytical results. Measurement uncertainty, as well as accuracy, is thus a combination of random and systematic effects. A good validation procedure will ensure a good predictive ability of the method in terms of results obtained.

Prichard & Barwick (2007) reported that the validation of the method for the analysis of oxides is to determine if the method is fit for its intended purpose of analysis. Based on international best practices, method validation is a requirement in analytical laboratories to demonstrate its qualification and competence. ISO/IEC (2005) emphasises that: Laboratories shall validate standard methods and in-house methods, in a manner that amplification and modification confirm that the method is fit for its intended use.

The primary aim of validating an analytical method is therefore to ensure and provide the evidence to prove that the chosen analytical method can yield correct and trustworthy results in conformity with standards and specifications established by the test laboratory (Prichard & Barwick, 2007). In the process of validating the method, various statistical methods are used to validate relevant parameters to prove the reliability and efficiency of the test method. The parameters validated include the following:

- Linearity
- Determination of Limit of Detection (LOD) and Limit of Quantification (LOQ)
- Precision (robustness/ruggedness)
- Specificity
- Accuracy

2.6.1. Linearity

Almost all analyses involve the use of calibration graphs. These plots are the response of the analytical system against the concentration of a series of standards of known analytical composition. These graphs with the aid of the regression analysis function are used to determine and assess calibration parameters. The regression analysis function is mainly used to validate parameters such

as the analytical range, the limit of detection (LOD) and limit of quantification (LOQ) values, and linear regression.

Regression analysis is a deterministic model, which allows predicting the values for a dependent variable (*Y*) when an independent variable (*X*) is known. The model determines the kind of relationship between *X* and *Y*. The experimental values rarely fit the mathematical model, and there are differences between the observed and the predicted values provided by the model, which are called residual. The simplest regression model is the linear one in which the relationship between *X* (known with error) and *Y* (known without error) is a straight line, $Y = bX + a$, where a is the *y*-intercept and *b* is the slope of the line (Eurachem, 2014). The relationship between instrument response and the known concentrations of an analyte (standards), which is used as the calibration curve can be explained by a similar regression model.

Linearity is the ability of a method to obtain test results proportional to the concentration of the analyte within a given working range. Linearity of the calibration curve is usually expressed through the coefficient of correlation, r^2. A correlation coefficient close to unity ($r^2 = 1$) is considered by some authors sufficient evidence to conclude that the calibration curve is linear (Eurachem, 2014). A clear curved relationship between concentration and response may also have an r^2 value close to one. A linear regression model between calculated standard points and the nominal ones used to evaluate the quality of the fit should have a unit slope and a zero intercept. In the case of the linear calibration method, the slope should be statistically different from 0, the intercept should not be statistically different from 0 and the regression coefficient should not be statistically different from 1. In case of having a significant non-zero intercept, the accuracy of the method must be demonstrated (Eurachem, 2014).

The r^2 -values obtained in the instrumental analysis are normally very high, so a calculated value, together with the calibration plot itself, is often sufficient to assure that a useful linear relationship has been obtained. In some circumstances, however, much lower r^2 -values are obtained. In these cases, it will be necessary to use a proper statistical test to see whether the correlation coefficient is significant, bearing in mind the number of points used in the calculation. The simplest method of doing this is to calculate a *t*-value and compare it with the tabulated value at the desired significance level, using a two-sided *t*-test and (n - 2) degrees of freedom. The null hypothesis, in this case, is that there is no correlation between *x* and *y*. If the calculated value of *t* is greater than the tabulated value, the null hypothesis is rejected, and we conclude that a significant correlation does exist (Eurachem, 2014).

2.6.2. LOD and LOQ

In validation, it's vital to indicate the level at which detection is not reliable. The instrumental limit of detection is the concentration at which the instrument can detect with certain reliability while the limit of quantification is the concentration that can be quantitatively expressed with certain reliability. Limit of Detection (LOD) represents the lowest amount of an analyte in a sample that can be detected by an analytical method. It is the signal that is greater than the statistical fluctuation of the background noise (Eurachem, 2014; Potts, 2013). It can also be defined as the smallest measure that can be confidently analysed (based on a 99.9 % confidence level).

LOD only becomes important for very low concentrations, mostly ppm's. The LOD was not considered satisfactory for quantitative analysis and for this reason limit of quantification (LOQ) was invented. This is to ensure additional confidence is designed to estimate the limit of quantitative analysis. Limit of quantification (LOQ) refers to the lowest concentration of analyte that can be determined with acceptable precision and accuracy. The analyte signal at the LOQ level should be at least 10 times the signal of the blank sample and the accuracy and precision within 20 % of the nominal concentrations (Eurachem, 2014; Potts, 2013).

The slope of the calibration curve can be used to estimate the detection limit of the analyte. If the calibration curve is linear, "*a*" is constant, and the estimation of LOD is easy to calculate. It is assumed that a validated analytical method should have a constant slope throughout sample analysis. Variation in the slope might be due to laboratory errors during sample preparations and instrument variations such as changes in calibrations. Although there is no criterion in the international guidelines to report the slope, monitoring the slope can provide valuable information regarding the quality of the sample analysis.

The analytical working range of an analytical method is the interval over which acceptable accuracy and precision can be expected and stretches from LOQ to the highest calibration standard of the analyte. The analytical working range is normally expressed in the same units as the test results obtained by the analytical method (Eurachem, 2014).

2.6.3. Precision

Precision is defined as the spread or variation between results for the multiple analysis of one homogeneous sample. It is usually expressed as the standard deviation or relative standard deviation (coefficient of variance) and maybe a measure of either the degree of reproducibility and /or repeatability (Eurachem, 2014; Potts, 2013). The two common precision measures are

reproducibility and repeatability, which describe the two-extreme measures of precision. Repeatability is an interpretation of variation to anticipate when a method is performed in replicate by an analyst on given equipment over a brief timescale. This type of precision can be used in a single laboratory and referred to as intermediate precision (sometimes also called ruggedness). Good validation practice involves the use of typical 'real' test materials preferably not reference materials, which may be typically homogeneous. A ruggedness study evaluates a method's capacity to remain unaffected by small variations in method parameters. It involves deliberately introducing small changes to the method and examining the consequences.

2.6.4. Specificity

Specificity is the parameter concerning the extent to which other substances interfere with the identification or quantification of the analyte(s) of interest in mixtures or matrices. Specificity tells us about the degree of interference by other substances also present in the sample while analysing the analyte. For analytical methods, specificity defines the identity of an analyte among a mixture of similar components in a sample where the identity of the components is not important. It can be achieved by analysing either a known analyte among a mixture of structurally similar compounds or a mixture of structurally similar molecules without the analyte. The second approach is popularly used in XRF analysis and may also be termed "matrix-interference" and is applied to check whether the matrix may have an influence on the results by enhancing or quenching effects (Eurachem, 2014).

2.6.5. Accuracy (trueness)

Studies of the accuracy of an analytical method are key validation criteria, it is a critical part of measurement uncertainty. Accuracy of an analytical method is the extent to which test results generated by the method and the true value agree. Method validation evaluates the accuracy of results by estimating both systematic and random error effects on results. Trueness asserts the closeness between the mean set of results to the true value. Bias estimate is used to express trueness, using mean and standard deviation results from a method, and comparing with known values of certified reference material. The accuracy is evaluated using the paired *t*-test (Eurachem, 2014; Potts, 2013). The *t*-test aims to determine statistically whether there is a significant difference between the average analytical result (x) and the true value (μ) of the analyte in the sample. A high level of trueness is equivalent to a lack of bias in the method.

CHAPTER 3

EXPERIMENTAL

3.1 Introduction

3.1.1 Health and Safety

Risk assessment was conducted to evaluate hazardous conditions or behaviours to prevent any potential impacts on quality, health safety, environment, and radiation. The risk assessment summary is shown in Table 3.1. The heavy mineral sands sample were handled carefully to prevent contamination from the natural concentrations of U and Th which are slightly highly radioactive.

XRF spectrometer uses X-ray tubes as the X-ray source, x-rays are relatively low energy (40 to 100 kV). X-rays are in a form of ionising radiation, and exposure to ionising radiation can cause cancer and genetic effects. However, the XRF spectrometer is constructed so that no harmful levels of X-ray radiation escape from the spectrometer and are fully interlocked. For example, if a panel that allows access to an area of possible radiation exposure is removed, the X-ray generator will immediately switch off.

Nieka fusion machines have integrated locking safety doors, real-time ¬flame monitoring and automatic shut off features, regulatory shutdown button.

The RS200 RETSCH Vibratory Disc Mill is designed with a grinding set clamping system for a convenient and safe tightening clamp for the vessel and the disc.

Table 3.1: Risk assessment summary.

	Hazard	Risk	Control
Quality	Weighing errors; Incorrect flux; inadequate flame conditions; sample residue remaining in crucible	Incorrect results	Training of personnel; yearly preventative maintenance of equipment
OHS	Sharp and rough edges; noise; fumes; trip and fall	Injuries; hearing loss; diseases; Fire; explosion	Supply PPE; yearly personnel medical surveillance; supply first kits and fire extinguishers, signages
Environmental	Incorrect disposal of chemicals; chemical containers; sample and sample containers and spillage	Pollution	Use of MSDS; waste disposal designated area
Radiation	Exposure	Contamination; pollution	Contamination, pollution

3.1.2 Sample handling

During the mineral processing, 2 kg samples are taken to the laboratory every 2 hours for chemical analysis from an automatic sampler by the Production Controller. The laboratory records the sample and applies proper labelling to ensure that sample identity is maintained throughout the processing steps. Samples are split with vibratory rotary splitters to reduce the size into a workable portion and to ensure that this workable portion is still representative of the initial sample in both matrix and composition. Homogeneity is necessary for chemical analysis to ensure all elemental components of the sample are present in all sub-fractions of the material measured out for analysis.

Samples need to be pulverised to obtain a fine homogeneous composition. The milled sample is mixed with flux and is placed in a fluxer where the material is fused at 900 ^{o}C for 15 minutes and cooled for 5 minutes. The fused sample bead is sent to the X-ray spectrometer for analysis. The laboratory analyses the sample every two hours and transmits the results into Plant Management Information System, and it will be available for the Section Grade Controllers, Shift Supervisor and Process Controller. Results undergo laboratory quality control to identify deviations on sample preparation and instrument, to ensure the accuracy and precision of results to customers.

3.2 Optimisation of sample preparation

The largest proportion of analytical error in results is from the sample preparation step. The objective of sample preparation is to obtain a homogenous glass bead with a mirror surface, no crystallisation,

and no undissolved solids. It is known that the particle size in fusion has an influence on dissolution. The sample type, particle size, flux, sample to flux ratio, fusion temperature as well as fusion time have an influence on the fusion procedure (Willis, 2010). These can cause incomplete dissolution which leads to crystallisation and cracking thus, were investigated in this study. The laboratory receives dry samples thus, sample pre-treatment is not needed, the only parameters that could affect the results are the amount of sample taken for pulverization and the time that samples are grinded to obtain a fine powder. Therefore, it was decided to investigate the technique that would prove successful for the process samples and analytes of interest.

The sample powder used for fusion must be < 75 µm particle size so that the flux is more active in its dissolution effects and the finer the sample powder the more efficient the dissolution. The continuous grinding and mixing of raw material for a specific period result in a fine homogeneous composition. During the investigation, five 100 g mass aliquots of the sample were taken and each one was milled on an automatic Retsch 200 milling machine. Parameters such as adequate milling time and motor revolutions per second (rpms) were investigated. For the grinding, a carbon steel grinding vessel was used. Potential contaminants from carbon steel vessels are mostly iron, however, contamination will be insignificant since iron is one of the major elements in the sample. Every vessel material has its contaminant risks and therefore carbon steel vessel was suitable for this work, as the contamination was insignificant due to a high composition of iron in heavy mineral sand samples.

This was followed by a sieving process to determine the effect of sample size, milling time and motor rpms on particle size. The aim was to obtain the maximum amount of sample with particle sizes of < 75 µm. For this, a sieve with an aperture of 75 µm was used. The 100 g sample aliquots were weighed before milling. After milling the samples were sieved and the mass retained on the sieve (> 75 µm) was subtracted from the mass that passed through the sieve (< 75 µm). This calculation was used to determine the percentage sample with particle sizes < 75 µm. The other way of solving the particle size effect is to fuse with a high flux-to-sample ratio. Possible solutions for this effect are discussed by Marguí et al. (2016). The other solutions investigated include the reduction of the sample particle size.

Fusion was carried out with an automated propane gas fluxer (Nieka GS4). It has predefined fusion programs, but customised programs can also be created by the user. Each program contains seven steps, including an oxidation step, four fusion steps, a pouring step and cooling steps. Each step contains parameters that can be changed such as % gas power, duration and % cooling power. The propane gas power was adjusted to 50 % in the main fusion steps to reach 950 ^{o}C which is slightly

above the borate melting point of 870 ^{o}C. The aim was to fuse below 1050 ^{o}C to avoid flux volatilisation (Loubser et al., 2004). The duration of the initial heating steps is 240 seconds and that of the main fusion steps including agitation to make the melt homogeneous without any bubbles is 660 seconds. After the casting step, an initial cooling cycle of approximately 300 seconds is started. The cooling was gradually to keep the moulds hot enough to avoid the thermal shock that would lead to crystallization associated with rapid cooling. Thus, the total cycle time, excluding the pouring step, is approximately 20 minutes.

3.3 Preparation of synthetic stock standards

For the quantitative analysis of mineral sands by XRF the following types of fusion specimens were required: blanks, interference standards and calibration standards. The preparation of blank specimens is very important but can be problematic as they usually contain either a pure oxide or a mixture of two oxides which can be difficult to dissolve (Beckhoff et al., 2006). Blank specimens were used to calculate background factors for elemental analysis.

Sample preparation optimisation was followed by the preparation of multi-element synthetic calibration standards for method calibration and determining spectral overlap and background correction factors. In the preparation of calibration standards, it is important to take into consideration that the analytes might interfere with each other. Overlapping elements and matrix effects might affect the calibration and possible interfering needs to be detected. Therefore, for a successful XRF calibration, it was essential to alternate element concentrations in the calibration samples.

In this work, there were 11 analytes, from a wide elemental spectrum namely, Al_2O_3, CaO, Fe_2O_3 HfO_2, MgO, P_2O_5, SiO_2, TiO_2, ZrO_2, U_3O_5 and ThO_2. The concentration range of each oxide was calculated to have standards lower and higher than the routine samples. The oxides were blended with reference materials to be able to correct for inter-elemental interferences as well as possible line overlaps. This fabrication approach has been discussed in considerable detail by Staats (1989). Prior to mixing, directions on the pure oxides and CRM certificates for pre-treatment were carefully followed, as certified values on the certificate are based on the specified pre-treatment i.e. drying or heating before use (Mashima & Mori, 2005). Thus, compounds were dried in an oven at 105 °C and some heated in a muffle furnace at 1000 °C. Pre-treatment conditions of reagents are summarised in Table 3.2.

Table 3.2: Pre-treatment conditions of reagents.

Material	Pre-treatment / °C
Al_2O_3	Heated at 1000 for 2 hours
CaO	Heated at 1000 for 2 hours
Fe_2O_3	Heated at 1000 for 1 hours
HfO_2	Heated at 1000 for 1 hours
MgO	Heated at 1000 for 1 hours
P_2O_5	No treatment
SiO_2	Heated at 1000 for 2 hours
TiO_2	Heated at 1000 for 1 hours
ZrO_2	Heated at 1000 for 1 hours
U_3O_5	Heated at 500 for 1 hours
ThO_2	Heated at 1000 for 1 hours
Zircon SARM13	Dried at 105 for 2 hours
Rutile SARM61	Dried at 105 for 2 hours
Quartz SARM49	Dried at 105 for 2 hours

They were all stored in a desiccator after cooling as some are hygroscopic. The composition of the calibration standard must approximate that of the matrix of the routine samples. Therefore, three mineral sands reference materials (quartz SARM49, Rutile SARM61 and Zircon SARM13) provided by the South African Reference Materials (SARM) were used to make standard stocks. A 5-figure Mettler Toledo analytical balance (M104TS) was used to weigh the compounds. Accurate weighing is one of the most important factors of the XRF calibration. Synthetic standard samples were prepared following the procedures used by Yamasaki (2014) and Lezzerini et al. (2014) as they involve standard addition where certified material and pure chemical compounds are added to form a mixture.

For the standard with low concentrations of P_2O_5, ZrO_2, HfO_2 and TiO_2, 0.010 g of P_2O_5, TiO_2, HfO_2 and 0.020 g of ZrO_2 (> 99.9 %, Alfa Aesar Puratronic) were added to 19.950 g of quartz SARM49 to make a Quartz stock. For the standard with low concentrations of HfO_2, U_3O_8, ThO_2 and MgO, 0.001 g of U_3O_8 and ThO_2, 0.010 g of HfO_2 and 0.02 g of MgO (> 99.9 %, Alfa Aesar Puratronic) were added to 19.968 g of Rutile SARM61 to make a Rutile stock. For the standard with high concentrations of U_3O_8 and ThO_2, 0.01 g of U_3O_8 and ThO_2 were added to 19.980 g of Zircon SARM13 to make a Zircon stock.

SiO_2, TiO_2 and ZrO_2 are three major oxides typically found in mineral sands. The concentration ranges of the calibration standards needed to be extended widely for the accurate quantification of these elements. Therefore, a heavy mineral sand matrix standard (HMC stock) with high concentrations of Al_2O_3, CaO, Fe_2O_3, SiO_2, TiO_2 and ZrO_2 was prepared using the addition of 2.000

g of Al_2O_3 and CaO, 4.000 g of TiO_2 and ZrO_2, 3.000 g of Fe_2O_3 and 5.000 g of SiO_2 (> 99.9 %, Alfa Aesar Puratronic).

The compounds were weighed to a total weight of exactly 20 g and well homogenised for 1 hour using a hand-held mortar and pestle. The duration for homogenization is longer than 15 s used by Mashima & Mori (2005) but shorter than the 2 h used by Mashima (2016). The bulk compositions of the synthetic standards were recalculated using actual weight measurements. The concentration of each oxide was calculated by dividing the weighed mass of oxide with the standard stock total mass and multiplied by a hundred to get the percentage of the oxide present. Compositions of synthetic standard stocks are shown in Table 3.3. To precisely evaluate and determine the background of trace elements and possible line overlaps, a major ZrO_2 oxide high concentration interference standard was prepared for the line overlap of Zr-Lα on P-Kα line and to calculate background factors for trace oxides (P_2O_5, U_3O_5 and ThO_2).

Table 3.3: Recalculated concentrations of elements in synthetic standard stocks.

Calibration standards	Al_2O_3 %	CaO %	Fe_2O_3 %	HfO_2 %	MgO %	P_2O_5 %	SiO_2 %	TiO_2 %	ZrO_2 %	U_3O_5 %	ThO_2 %
Quartz Stock	0.050	0.010	0.050	0.050	0.050	0.050	99.35	0.050	0.100	-	-
Rutile Stock	0.928	0.090	0.679	0.050	0.050	0.030	2.026	93.10	1.337	0.010	0.010
Zircon Stock	0.609	0.140	0.187	1.289	0.044	0.230	32.53	0.295	63.95	0.090	0.084
HMC Stock	10.00	10.00	15.00	-	-	-	25.00	20.00	20.00	-	-

* HMC – Heavy Mineral Concentrate

3.4 Preparation of calibration standards

Stock standard samples were weighed in a petri dish and dried in an oven for 2 hours at 105 °C and cooled in a desiccator, as some of the constituent compounds are hygroscopic. A total of 15 calibration standard specimens were prepared following the standard dilution approach by (Mashima, 2016; Mashima & Mori, 2005). They were prepared by mixing percentage fractions of standard stocks to mimic the heavy mineral sand matrix and to ensure that the required analytical ranges were covered. To precisely evaluate and determine the background of trace elements and possible line overlaps, a 66%ZrO_2:33%SiO_2:1%HfO_2 high concentration interference standard was

prepared for the line overlap of Zr-Lα on P-Kα line and to calculate background factors for trace oxides (P_2O_5, U_3O_5 and ThO_2) (Bouchard et al., 2014). Compositions of calibration standards are shown in Table 3.4. The lithium borate fusion method was chosen because of its excellent repeatability and accuracy to prepare homogeneous calibration standards glass specimens for XRF analysis (Claisse & Samson, 1962).

Table 3.4: Composition of calibration standards mixed in percentage fractions.

Mixing	Calibration standards	Al_2O_3 %	CaO %	Fe_2O_3 %	HfO_2 %	MgO %	P_2O_5 %	SiO_2 %	TiO_2 %	ZrO_2 %	U_3O_5 %	ThO_2 %
25%Q:75% H	STD-1	7.512	7.502	11.26	0.013	0,013	0.013	43.59	15.01	15.03	-	-
50%Q:50% H	STD-2	5.025	5.005	7.525	0.025	0,025	0.025	62.18	10.03	10.05	-	-
10%Q:90% H	STD-3	9.005	9.001	13.50	0.005	0.005	0.005	32.44	18.01	18.01	-	-
40%RT:60% H	STD-4	6.371	6.036	9.271	0.020	0.020	0.012	15.81	49.24	12.53	0.004	0.004
70%ZR:30% H	STD-5	3.427	3.098	4.631	0.902	0.031	0.161	30.27	6.206	50.76	0.062	0.059
75%ZR:25% H	STD-6	2.957	2.605	3.890	0.967	0.033	0.172	30.65	5.221	52.96	0.066	0.063
20%RT:80% H	STD-7	8.186	8.018	12.14	0.010	0.010	0.006	20.41	34.62	16.27	0.002	0.002
60%RT:40% H	STD-8	4.557	4.054	6.407	0.030	0.030	0.018	11.22	63.86	8.802	0.006	0.006
90%ZR:10% H	STD-9	1.548	1.126	1.668	1.160	0.040	0.207	31.77	2.265	59.55	0.080	0.076
50%RT:50%ZR	STD-10	0.769	0.115	0.433	0.669	0.047	0.130	17.28	46.70	32.64	0.049	0.047
20%RT:80%ZR	STD-11	0.673	0.130	0.285	1.041	0.045	0.190	26.43	18.86	51.42	0.073	0.069
90%RT:10%ZR	STD-12	0.896	0.095	0.629	0.174	0.049	0.050	5.076	83.82	7.598	0.017	0.018
10%ZR:90% H	STD-13	9.061	9.014	13.519	0.129	0.004	0.023	25.75	18.03	24.39	0.009	0.008
40%ZR:60% H	STD-14	6.244	6.056	9.075	0.515	0.018	0.092	28.01	12.12	37.58	0.035	0.034
60%ZR:40%H	STD-15	4.366	4.084	6.112	0.773	0.026	0.138	29.52	8.177	46.37	0.053	0.050

ZR – Zircon stock, Q - Quartz stock, RT – Rutile stock, H – Heavy mineral sands Stock

The calibration specimens were made using a convenient sample/flux weight ratio of 1 g sample and 9 g of 50/50 lithium tetraborate/lithium metaborate flux to ensure proper dissolution. A Mettler M104TS four-decimal-digit electric balance was used to weigh the sample and the flux. As the Thermo XRF generally accommodates glass beads of 32 mm in diameter as a standard, the weights of the sample and flux used are suitable for the preparation of glass beads of this diameter. It is

important to have the sample-to-flux ratio be precisely 1:9. The mixtures were thoroughly mixed with a vortex mixer to ensure homogeneity between the sample and the flux. The mixture was put into a platinum crucible (95 % Pt &5 % Au alloy). Fusion was carried out with an automated propane gas fluxer (Nieka GS4) producing good quality 3 mm glass beads. To improve the precision of the calibration and to aid in the identification of 'bad' fused specimen, the calibration specimens were prepared in duplicates. The synthetic specimens do not last indefinitely, as the intensities for long wavelength analytical lines (e.g. Mg-Kα) change. Therefore, samples were prepared periodically. After work, the platinum ware was cleaned with the citric acid solution in an ultrasonic bath. The citric acid is sufficient to digest any residual melt stuck to the platinum ware and is safer than a hydrochloric acid solution. The glass beads were kept in plastic sample trays and stored in a desiccator until measurement.

3.5 Selection of XRF analytical parameters

The success and accuracy of the analysis depend on the correct selection of spectral lines (K- or L-series lines), XRF tube voltage and current (kV and mA), analysing crystal and detectors. Required experimentations were conducted to select the best combination of instrumental parameters that will yield the lowest limits of detection and the best counting statistics (smallest counting error). The Kα lines were used for the elements with $\lambda > 0.2$ nm and Lα- lines were used for the elements with $\lambda <$ 0.2. Zr-Lα was preferred rather than Zr-Kα due to the fused beads that are typically 2-3 mm thick, so it, therefore, does not have sufficient thickness for the required critical depth (~ 5 mm) for Zr-Kα (Willis et al., 2011).

3.5.1 Tube (kV and mA) selection

The study was conducted on a Thermo ARL 9900 XRF instrument equipped with a Rh anode, end window X-ray tube with a maximum operating power of up to 3.6 kW. The spectrometer is fitted with instrumental parameters which the analyst can adjust to achieve the best analytical conditions. Various analytical parameters have to be optimized to perform efficient and accurate analysis. Instrumental parameters were selected to obtain the highest count rates from each element to compensate for the dilution of the sample with flux which leads to a decrease in fluorescence intensity. This was done by setting up X-ray tube at 30 kV and 120 mA for long-wavelength analytical lines such as Ca-Kα, P-Kα, Si-Kα, Al-Kα, Zr-Lα, Fe-Kα, Ti-Kα and Mg-Kα, at 60 kV and 50 mA for short-wavelength lines, Hf-Lβ1, Th-Lα and U-Lα. Having too many X-ray tube power

settings may affect the lifespan of the X-ray tube. Thus, to have only two power settings, for Ca-Kα, Fe-Kα and Ti-Kα the 30 kV setting was used, even though it is not optimum, it is sufficient to excite these elements as minors. The kilovolts (kV) and milliamps (mA) used in the method for efficient excitation are shown in Table 3.5.

The X-ray generator of Thermo XRF is maintained at eco-mode of 10 kV and 10 mA when not in use, the increase from 10 kV and 10 mA to 60 kV and 120 mA for measurement does not require a long wait time. Changing the kV changes both the intensity and the wavelength distribution of the tube spectrum. Changing the mA on the tube changes only the intensity of the tube spectrum but has no effect on its wavelength (Potts, 2013). Generally, a high voltage is recommended to be used with heavy elements and high current with light elements (Beckhoff et al., 2006). This is due to the fact that as the wavelength of the analyte increases the absorption of the intense Rh K-lines and high energy continuum decrease (Potts, 2013). The Kα lines were used for the elements with $\lambda > 0.2$ nm and Lα- lines were used for the elements with $\lambda < 0.2$. Zr-Lα was preferred rather than Zr-Kα due to the fused beads that are typically 2-3 mm thick, so it therefore does not have sufficient thickness for the required critical depth (~ 5 mm) for Zr-Kα (Willis et al., 2011).

Table 3.5: kV and mA used in the method for efficient excitation.

Channel	Voltage (kV)	Current (mA)
Al-Kα	30	120
Ca-Kα	30	120
Fe-Kα	30	120
Hf-Lβ1	60	50
Mg-Kα	30	120
P-Kα	30	120
Si-Kα	30	120
Th-Lα	60	50
Ti-Kα	30	120
U-Lα	60	50
Zr-Lα	30	120

3.5.2 Collimator selection

The Thermo 9900 has three types of collimators that can be selected to direct a parallel beam of X-rays from the sample to the analysing crystal namely, fine (150 µm), medium (250 µm), and coarse (600 µm). To achieve high sensitivity a 600 µm collimator is used for Mg, and the collimator used for other elements is a 250 µm collimator due to its good sensitivity and peak resolution. A medium collimator will remove some background noise which will make the identification of the analyte lines easier. The fine collimator was not considered due to its low sensitivity.

3.5.3 Analysing crystal selection

Bragg's law states that for a given crystal plane and for a given order of diffraction of X-ray radiation, each wavelength in the incident XRF spectrum is diffracted at a unique angle. To cover the necessary wavelength range for the mineral sand samples, the four X-ray dispersive crystals listed were used, a multilayer AX06, PET, Ge111 and LiF200. The AX06 crystal is a synthetic crystal. The analysing crystals were selected according to their sensitivities, angular dispersion and resolution of the secondary spectrum. Resolution is more important for elements where the peaks

are closer to one another. The LiF200 crystal has high intensities and good dispersion and is useful for both the short and medium wavelength analytical lines. The PET crystal was used for Al-Kα and Si-Kα due to its good diffraction efficiency. As we go from short wavelengths to long wavelengths, the interplanar spacing of the crystal also increases, as a result for Mg-Kα the multilayer AX06 crystal was chosen since it has a d-spacing of > 1 nm. The Ge111 crystal was used for P-Kα and Zr-Lα because it has no second-order lines (n=2) from Ca-Kβ_2 that interferes with P-Kα. The crystals used are summarised in Table 3.6.

Table 3.6: Analysing crystal and 2θ diffraction angles of the analytical lines.

Channel	Analysing crystal	Angle (2θ)
Al-Kα	PET	144.71
Ca-Kα	LIF200	113.09
Fe-Kα	LIF200	57.52
Hf-Lβ	LIF200	39.93
Mg-Kα	AX06	19.93
P-Kα	Ge111	141.0
Si-Kα	PET	109.01
Th-Lα	LIF200	27.47
Ti-Kα	LIF200	86.14
U-Lα	LIF200	24.15
Zr-Lα	Ge111	136.65

3.6 Analytical method validation

3.6.1 Linearity and detection limit and quantification limit

Linear regression was used to confirm a relationship between an analytical signal and the concentration of the analyte. A total of nineteen synthetic standards of which only four are CRMs (stocks) were used, emphasising the limited availability of CRMs. The empirical calibration was done per element; the concentration of the element was calibrated against its net intensity, without making any matrix effect correction. It was possible to use this type of calibration since the calibration standards and sample matrix compositions were the same, and fused glass discs were

made at high dilution ratio. Accurate results are possible when calibration standards are prepared properly and measured under the same conditions. The calibration standards were selected to cover the whole range of concentrations required in the quantitative analysis to prevent extrapolation which may cause erroneous results.

Before carrying out any linear regression calculations the calibration plots were examined for possible outliers and points of influence; points of influence are points that have one or two effects on a regression line i.e. high leverage and bias and are known as systematic errors. Systematic errors arise from Instrumental errors which are caused by the spectral interferences and instabilities in instrument components. X-ray fluorescence measurements are based on the 'line only' principle, there might be interference with other peaks or be affected by secondary enhancement effects from other low-atomic elements that are routinely present in mineral sands and flux.

The calibration data for each element was used to do statistical analysis of the variances that are influential on the analyte range, LOD, LOQ and linear regression parameters. The characteristics of the regression were calculated using the Regression Analysis function in Minitab stats pack.

3.6.2 Precision

It is known that precision is not an indication of accuracy; results may have good repeatability and precision but may nevertheless be completely inaccurate. The precision was evaluated in two parts, by the within-laboratory reproducibility and instrument precision. Within-laboratory reproducibility was determined with the top-down method where a homogeneous typical sample was independently prepared and analysed. The measurement data were collected within a minimum period of six months. The aim was to cover varying conditions in the laboratory. This ensures that variations due to different operators, re-calibrations, routine instrument maintenance are captured. The % RSD (Rw, n=40) is chosen as an indication of the precision because this value represents all the results obtained during a multiple analysis of the same sample for the same element(s). For the precision to be good, the % RSD should be ≤ Acceptable % RSD indicating little deviation between results falling within the results population. Although the % RSD gives a measure of the % spread of a set of results about the mean value, it does not indicate the shape of the distribution.

3.6.3 Specificity

The specificity of the method was scrutinized by assessing each element spectrum in the sample and stripping overlapping lines (Kα was used for most elements). This ensures each element

characteristic line was not interfered with by another element signifying that the fluorescence peak was specific to the element analysed. Theoretically, it is known (Table 3.8) that the Zr-Lα background tails onto that of P-Kα. The effect of a possible overlap is based on its concentration in the sample. If an element line next to a measured element has major intensity, it most likely will affect the calibration, for example, Zr-$L\alpha_1$ background tails onto that of P-Kα line. Therefore, spectral line overlap correction is necessary. It was corrected by calculating interference correction factors from intensity measurements made on specially prepared "interference standards" containing 66%ZrO_2:33%SiO_2:1%HfO_2.

The correction was done by subtracting a fraction of the Zr-Lα overlapping peak from the P-Kα peak after background correction as shown in Equation 3.1. From the corrections above it was found that 35 % of the P-Kα peak is attributed by both background and spectral overlap. The formula was inserted as the pseudo equation in the software for the quantification of Phosphorus.

$$\text{P-K}\alpha\text{net} = \text{P-K}\alpha - ((BG_1\_\ \text{P-K}\alpha - BG_2\_\ \text{P-K}\alpha) * 0.1656 + BG_2\_\ \text{P-K}\alpha)) - (\text{Zr-L}\alpha * 0.004) \quad 3.1$$

where,

0.004 = Interfering factor

3.6.4 Accuracy

The accuracy using CRMs could not be tested due to the unavailability of CRMs. However, it was rather tested through a proficiency testing (PT) scheme. Proficiency testing is an important component of any system of laboratory quality assurance (ISO/IEC, 2005). ISO/IEC (2005) lists participation in proficiency testing programs as an important component of the quality assurance of test results. The principal aim of a PT exercise is to evaluate the competence of the calibration and thus provide the laboratory with a tool to improve the accuracy and traceability of the measurements. It also enables the laboratory to assess its performance relative to domestic and international peer laboratories, hence improving the comparability of results between laboratories and between countries (Rousseeuw & Hubert, 2018). For this procedure, a bulk of milled typical heavy mineral sand sample was homogenised in a tubular mixer for 18 hours. The sample was named RR005/18 and weighed into 50 g portions and sealed in plastic bags and circulated to multiple laboratories. The particle size was tested to determine the pulp of the samples and the sample pass the pulp criteria of 90 % of the sample passing 75 µm sieve on the wet screen. Due to the scarcity of CRM's, it was not possible to send out a sample with "known" contents. The sample was in essence "unknown"

and therefore “a best” estimate of the real content, called the consensus value, was used for evaluation purposes. The participating laboratory used the test method that they believe was technically appropriate. Various analytical techniques were used for the analyses such as:

- XRF – fusion and powder pellet
- Wet Chemistry, Volumetric, Gravimetric, Auto-titration, UV Vis
- ICP-MS
- ICP-OES

All laboratories stated the method used on the reporting templates. Participant results were captured and evaluated using the Robust statistics *z*-score method discussed by Rousseeuw & Hubert (2018). The criterion described by Thompson et al. (1999) was used for the classification of the results, where *z*-scores in the range $-2 < z < 2$ are considered to be satisfactory (Thompson et al., 1999). The statistics of a normal distribution means that 95 % of data points will lie between a *z*-score of –2 and +2. The *z*-scores represent a measure of how far a result is from the consensus value. For *z*-score values of any element that fell outside this range, the calibration will be examined to ensure that determinations were not subject to unsuspected analytical bias. Thompson et al. (1999) stated that the magnitude of the *z*-score allows the laboratory to assess the accuracy of results in comparison with other participating laboratories.

For calculation of z-score the following formula is used:

$$z(\mathrm{MAD}) = \frac{\mathrm{xi} - \mathrm{Me}}{\mathrm{MAD}} \qquad 3.6$$

where;

MAD (Median of all deviations converted to an equivalent scale)

Me = Reference material Median of x_i

x_i = Value of participant

1.483 = correction factor which makes the MAD consistent for Gaussian distributions.

The MAD x_i of observations is median (abs (x – median (x))) multiplied by the default constant 1.4826 (correction factor for MAD for non-normal distribution), which is used to put MAD on the same scale as the data and assumes normally distributed data. The normal distribution here is not an "assumption" but rather a calibration tool; the MAD is multiplied with a factor that under normality

will give (asymptotically at least) the same as the standard estimator. This means that the size of the robust z-scores is also comparable with the size of the standard z-scores from the normal distribution can be used, for example, for outlier detection. This does not mean that the data have to be normal, as the MAD is not affected by outliers regardless of whether multiplied by 1.4826 or not. It rather means that if the majority of the data look like coming from a normal distribution, robust z-scores can be used to detect outliers that are not in line with normality, because they are unaffected by these outliers, as opposed to the standard z-scores, and multiplication by 1.4826 makes sure that expected robust z-scores for non-outliers are in the same ballpark as non-robust z-scores in case no outliers exist.

CHAPTER 4

RESULTS AND DISCUSSION

This chapter comprises the analysis, presentation and interpretation of the findings resulting from this study. The analysis and interpretation of data are carried out in two phases. The first part, which is based on the results of the XRF method development, deals with the sample preparation improvement, XRF parameters setup and quantitative analysis. The second is based on statistical validation, to assess whether the method is fit for purpose.

4.1 Optimisation of sample preparation

4.1.1 Particle Size

It was established that 2 minutes milling time and 80 – 100 g at 1000 rpm is sufficient to give the largest amount of sample with particle sizes < 75 µm. The results obtained are shown in Table 4.1. The efficiency of the mill and milling vessel will be tested on a regular basis to ensure the mill is consistently producing samples with < 75 µm particle size as deterioration of the milling vessels causes the efficiency to decrease.

Table 4.1: Milling efficiency determination.

Sample ID	Sample(g)	Sieve(g)	Sample + Sieve(g)-before screen	Sample + Sieve(g)-after screen	Retained Sample(g)	%Efficiency	%Target
Rutile	50	257.4	307.4	260.1	47	94.6	90
Zircon	50	262.0	312.0	264.0	48	96.0	90
Ilmenite	50	256.1	306.1	259.0	47	94.2	90

4.1.2 Fusion technique

Eastell & Willis (1990) and Lee & McConchie (1982) have successfully developed low dilution fusion techniques for the determination of major, minor and trace element contents in geological samples to the flux-to-sample ratio of 2:1. However, the low flux-to-sample ratio requires higher fusion temperatures than usual, in the region of 1050 - 1100 °C. The first flux-to-sample ratio considered was 5:1, however, the samples did not dissolve completely, the mould was not filled with glass during casting, came out milky and cracked. To test the flux-to-sample ratio a mixture of 66%ZrO_2:33%SiO_2:1% HfO_2 oxides from Alfa Aesar Puratronic oxides was used. Willis et al., (2011) observed that a very low ratio, for example 1/100, results in line intensities proportional to concentrations; calibration curves are nearly free of matrix effects. However, the contrast, line/background ratio, is low and the detection limit is relatively high. At high sample/flux ratios, for example 1/5, the matrix effects are relatively high; it is necessary to make matrix corrections. There is no lower limit on the sample/flux ratio except that some lithium fluxes tend to crystallize when the ratio is too low. There is, however, an upper limit that should not be approached too close on account of the slow dissolution rate and the increasing risk of disk cracking. Sample/flux ratios that are reasonably high yet sufficiently not too close to the solubility limits.

Therefore, it was decided to rather consider a 9:1 ratio to achieve homogeneous glass disks and reduce inter-element matrix effects to an acceptable level. The sample easily dissolved due to the high amount of flux present however, the sensitivity of the XRF when analysing low concentration elements decreased, which in turn means a decreased repeatability due to decreased instrument precision. This also led to low analyte peak- to-background ratios and high detection limits for trace elements. The specimen came out completely dissolved, clear, and intact. The flame reached 950 ^oC, a high enough temperature to completely dissolve the sample and flux. After the fusion, the concentration of the elements present in the sample was quantified. The X-ray spectrometer did indicate all the known constituents present in the samples. To enable the use of fundamental parameters as a correction model for inter-element effects the sample to flux ratio must be constant for both the calibration standards as well as the samples.

The type of fluxer and flames used to fuse the samples are of utmost importance as discussed by Willis (2010. If the gas is oxygen-enriched, it can reach very high temperatures that exceed the borate melting point leading to flux volatilisation which is a serious risk for damaging platinum ware, subsequently leading to poor reproducibility and repeatability of the results. Propane gas heating burners were used for the fusion of the samples as they are user-friendly, provide easy control of gas flow, good reproducibility and stable heating conditions that are independent of the number of burners used.

The fluxer parameters were selected to maximize the efficiency of sample preparation and the complete dissolution of hard zircon mineral as being difficult to dissolve (Beckhoff et al., 2006). It was observed that the melting point differs from oxide to oxide but is always lower than the original flux melting point. The dilution of the sample in the flux results in a decrease in fluorescence intensities. Lithium metaborate and lithium tetraborate are important fluxing reagents. Lithium metaborate (LiM) is a more reactive flux than lithium tetraborate (LiT). It rapidly attacks most silicates and many non-silicates, yielding a glass that is mechanically strong and reasonably non-hygroscopic. A suitable flux was required for this study that would dissolve the sample completely during the fusion process in a dilution ratio that would allow the analysis of trace elements in addition to major and minor elements. Therefore, 49.75%LiT:49.75%LiM:0.5%LiI flux composition discovered by Claisse (1998) was chosen as an optimum in this work due to its best performance in both basic and acidic oxides. Lithium Iodide (LiI) was used as the releasing agent which is one of the improvements by Blank & Eksperiandova (1998) to ensure no residue is left in the crucible during casting since the borates tend to adhere to the platinum ware. The flux recommended is readily available in South Africa from Afrifusion and Analytical industrial. Fusion program parameters are shown in Table 4.2.

Table 4.2: Fusion program parameters for the preparation of standards and samples.

Parameters	**Step 0 Oxidation**	**Step1 Pre-fusion**	**Step 2 fusion 1**	**Step 3 fusion 2**	**Step 4 fusion 3**	**Step 5 Pouring**	**Step 6 Cooling 1**	**Step 7 Cooling 2**	**Step 8 Cooling 3**
Duration (min)	02:00	02:00	02:00	05:00	04:00	00:30	01:00	01:00	03:00
Gas Power (%)	10	20	35	45	50	0	0	0	0
Rotation speed (%)	0	10	40	60	40	0	0	0	0
Cooling Power (%)	0	0	0	0	0	0	10	70	100
Fusion Temp. (℃)	300	500	700	900	950	950	0	0	0

4.2 Qualitative analysis

The Zircon and Rutile concentrate samples were scanned for qualitative analysis of each analyte at their respective analytical parameters. Doing qualitative wavelength scans on a typical sample indicates the 2θ angles at which each element line of interest is diffracted by the crystal used for analysis. The resulting spectra were overlaid to evaluate for analyte peak selection and spectral overlap on both peak and background positions by graphical interpolation (Ogasawara et al., 2018). The theoretical overlaps are listed below in Table 4.3. The theoretical overlaps were compared with the practical wavelength scans. Any additional lines appearing in the wavelength scans were identified by comparing the 2θ degree value obtained in the scan to 2θ degree values commonly available in literature tables (Grieken & Markowicz, 2001). This was done to try and identify unknown lines in the wavelength scans, keeping in mind the known composition of the sample. The obtained wavelenght spectra are attached in Appendices A.1 - A.11.

Table 4.3: Theoretical and empirical overlaps.

Analyte	Overlap	Overlap Order	Correction
Al-Kα	-	-	-
Ca-Kα	-	-	-
Fe-Kα	MnKβ	1	adjusting pulse high
Hf-Lβ	Zr-Kβ1	2	choosing Hf-$L\beta_1$
Mg-Kα	Ca-Kα	3	adjusting pulse high
P-Kα	Ca-Kβ1, Zr-Lα	2	Using the Ge111
Si-Kα	Sr-Lα1	1	Adjusting pulse high
Th-Lα	-	-	-
Ti-Kα	I-Lβ1	1	Adjusting pulse high
U-Lα	-	-	-
Zr-Lα	P-Kα	1	Calculated correction factor

No spectral overlaps were really expected for the elements with low atomic numbers like Si, P, Mg and Al because the line wavelengths for these elements are not as close together as those for elements with higher atomic numbers (Willis et al., 2014). The overlap of Ca-Kα on Mg-Kα was corrected by adjusting pulse high to minimise the intensity of Ca-Kα. There was another overlap identified of Hf-$L\alpha_1$ by the second-order Zr-Kα lines. However, it was solved by choosing Hf-$L\beta_1$ as the Hf analyte

line. The Hf-Lβ_1 line could be overlapped by second-order Zr-Kβ_1. However, Hf-Lβ_1 is slightly more intense than Hf-Lα_1, and Zr-Kβ_1 is much less intense than Zr-Kα and its intensity is minimised by the correct pulse high adjustment. The overlap of Ca-Kβ_2 on P-Kα was corrected by using the Ge111 crystal because it has no second-order lines (n=2) from Ca-Kβ_2 that interferes with P-Kα. On the wavelength scan, it can be seen that the Si-Kα line overlaps with the Sr-Lα_1-line. Another overlap is found between the FeKα and MnK$\beta_{1,3}$ lines. These overlaps are of no significance since none of these lines form part of the quantitative analysis of this study. A Nb-Kα line with a low intensity appears on the wavelength scan which indicates the possible presence of very low amounts of Nb in heavy mineral sand. After investigation of all the wavelength scans the conclusion was drawn that no significant spectral overlaps occur at the element lines of interest for the quantitative analysis.

4.3 Quantitative analysis

4.3.1 Analyte background correction

The background corrections for all trace elements such as Th and U were made by measuring the intensity at peak and interference-free spectral positions. Background factors were calculated by measuring a matrix “blank" sample 66%ZrO_2:33%SiO_2:1%HfO_2 ("matrix blank" sample). The selected sample does not contain any elements which cause spectral interference at the analyte peak positions. Trace element analysis requires attention when determining background intensities beneath analyte peaks. Ideally, the background intensities should be measured on both sides of the peak at interference-free positions close to the peak, if possible. This is due to fact that the background is generally sloping and has some curvature, especially at the shorter wavelengths.

It was noticed that the background in the region of Nb-Kα to U-Lα is sloping and highly curved. Thus, background intensities were measured on both sides of the peak at interference-free positions close to the peak (Beckhoff et al., 2006). The aim is to obtain the most accurate possible net intensities for the analyte peaks which are subject to large proportionate corrections for background. Therefore, to calculate the estimated background at the peak positions, Method A as reported by Willis and Duncan (2011) was employed. This method only measures the intensities of the peak and background positions. It was preferred in this study as it accommodates both the sloping and curvature of the background. It is recommended for trace element analysis as it requires the use of a blank sample in calculating a background factor.

In quantitative analysis the net peak intensity is proportional to the analyte concentration. To obtain the net peak intensity, it was necessary to subtract the background intensity at the peak position from

the measured gross peak intensity. For the P-Kα background-position determination, the lower angle background was positioned at 130 ° just below the Zr-Lα (137 °). This is because the lower angle background has the potential to be overlapped by the intense Zr-Lα tailing onto P-Kα. The wavelength scan of Zr-Lα and P-Ka is shown in Figure 4.1. Since U-Lα and Th-La share background positions, it was difficult to select interference-free background positions for the LiF200 crystal because of its fair resolution. Thus, their peaks are tailing to each other's background positions, and it is therefore, not possible to locate background positions. The wavelength scan of U-Lα and Th-La is shown in Figure 4.2. It is illustrating the degree of spectral overlap and shared background positions constituted as BG_1 and BG_2. The high-angle "tail" of the U-Lα peak interferes at the Th-Lα peak position and the low-angle "tail" of the Th-Lα peak interferes at the U-Lα peak position. A repetition multiplier was used with a multiplier of three, meaning that the element peak and the background points were analysed thrice. The average intensities were used to calculate net peak intensities using Equations 4.1 - 4.3 below:

The background correction was then calculated as follows:

$$\text{P-K}\alpha\text{net} = \text{P-K}\alpha - ((BG_1\_\ \text{P-K}\alpha - BG_2\_\ \text{P-K}\alpha) * 0.167 + BG_2\_\ \text{P-K}\alpha)) \quad 4.1$$

$$\text{Th-L}\alpha\text{net} = \text{Th-L}\alpha - ((BG_1\_\ \text{Th-L}\alpha - BG_2\_\ \text{Th-L}\alpha) * 0.392 + BG_2\_\ \text{Th-L}\alpha)) \quad 4.2$$

$$\text{U-L}\alpha\text{net} = \text{U-L}\alpha - ((BG_1\_\ \text{U-L}\alpha - BG_2\_\ \text{U-L}\alpha) * 0.597 + BG_2\_\ \text{U-L}\alpha)) \quad 4.3$$

where;

BG_1 = Intensity of background 1 (kilo counts per second - kcps)

BG_2 = Intensity of background 2 (kilo counts per second - kcps)

0.167, 0.392, 0.597 = Determined background factors

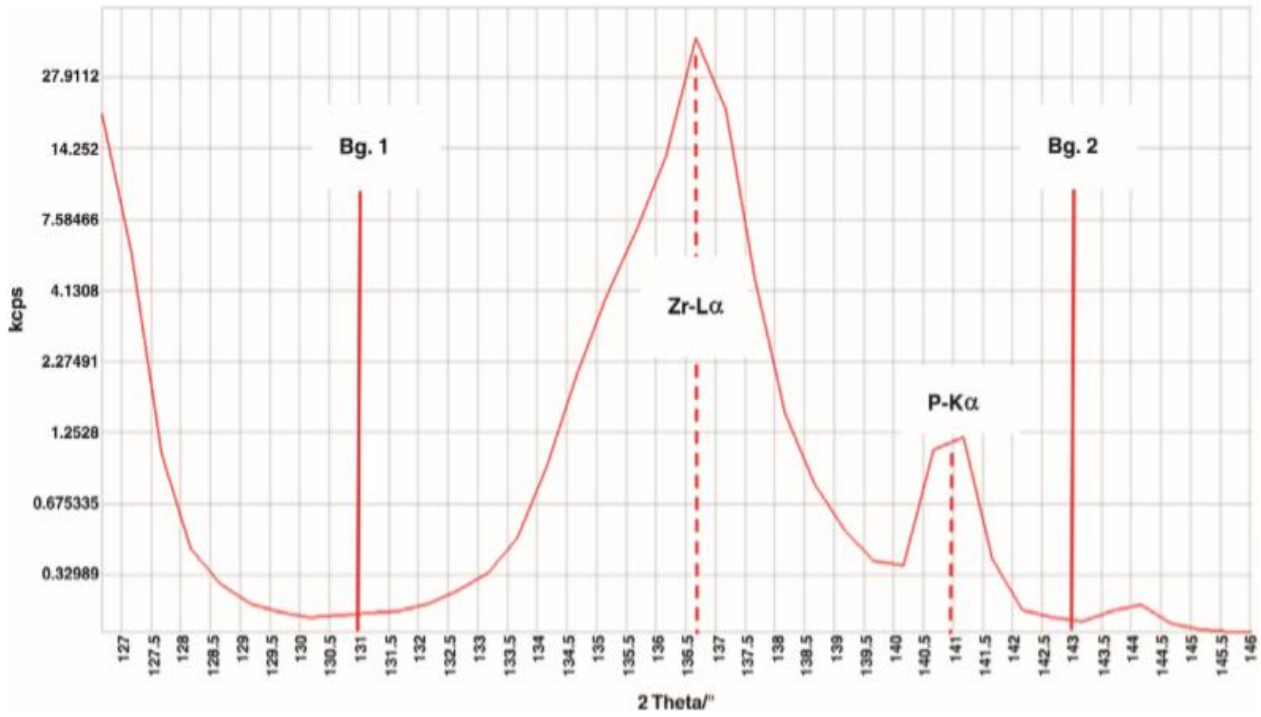

Figure 4.1: Wavelength scans of Zr-Lα and P-Ka lines illustrating spectral overlap.

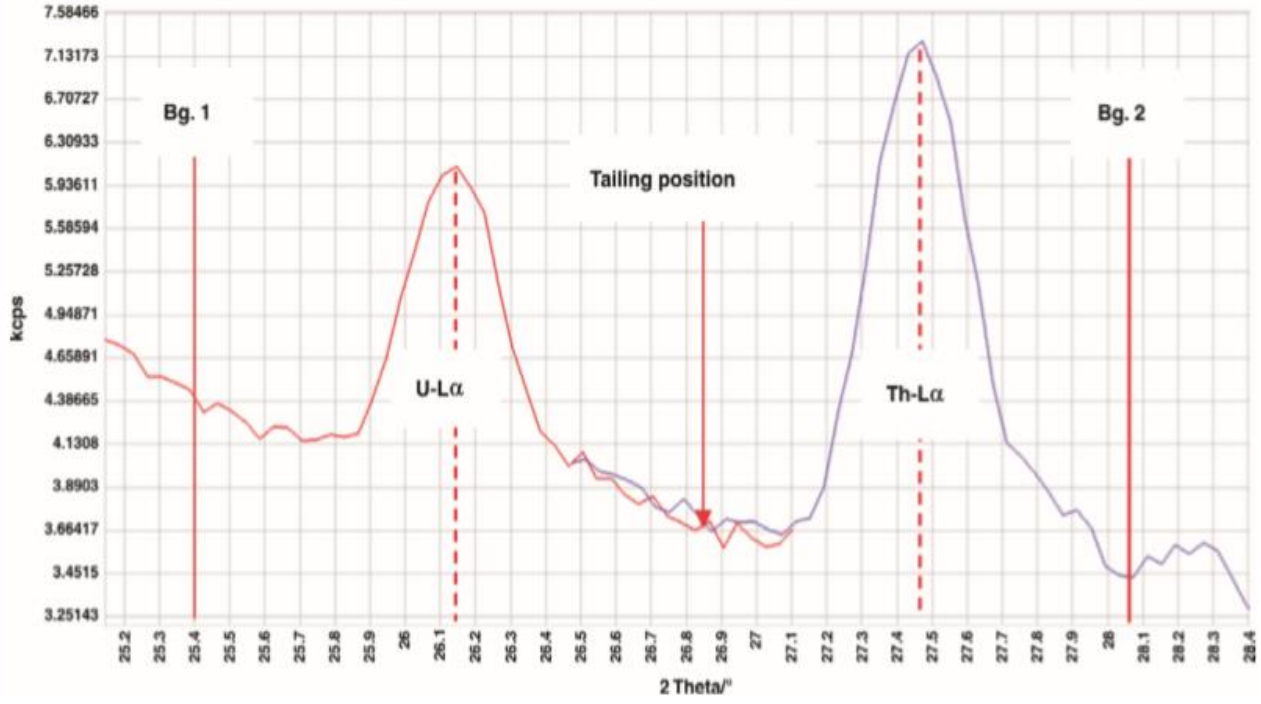

Figure 4.2: Wavelength scans of U and Th in a mineral sand sample.

4.1.2. Pulse height analyser setup

Both Ar-CH_4 Gas and Scintillation counters used in XRF are proportional detectors in the sense that the energy of the incident X-ray photons determines the magnitude of the voltage pulse produced by the circuitry (pulse height measured in mV). A pulse height analyser (PHA) makes use of this effect to select only a narrow range of voltage pulses, thus rejecting all those unwanted pulses. A pulse height analyser was used to reduce interference from higher-order spectral lines and reduce backgrounds giving improved limits of detection for trace elements. A pulse height analyser includes adjustable upper and lower electronic thresholds forming a window. In Thermo ARL instruments the energy distribution is from 35 to 160 %, however, the ideal energy profile of an element line should have a lower threshold of 40 % and an upper threshold of 140 % (100 % window). The energy of the measured element line is assumed to be around 85 %. All pulses with energies within the window are passed on to a detector and all pulses outside the window are excluded. The upper and lower thresholds for Ar-CH_4 Gas must be checked for potential drift every six months due to changes in gas pressure and temperature (Potts, 2013). According to the factory-calibrated parameters of the XRF spectrometer used during this study, the ideal PHA of an element line must generate a count rate - of > 10 kcps. The values obtained during the PHA runs are summarised in Table 4.4 and the PHA spectra are attached in Appendices B.1 - B.11. Relatively low count rates for Mg-Kα are caused by lower excitation of the Rh tube at longer wavelengths. For Th-Lα and U-Lα, the low count rates were due to background corrections since in quantitative analysis the net peak intensity is proportional to concentration. Before the subtraction of the background, the count rates were 74.10 and 67.14 kcps respectively, in essence, ±90 % of the peak was background.

Table 4.4: Summary of the PHA runs.

Analyte	Count rate (kcps)	% PHA window
Al-Kα	33.22	60
Ca-Kα	50.03	45
Fe-Kα	738.98	70
Hf-Lβ1	79.28	70
Mg-Kα	9.37	40
P-Kα	14.61	50
Si-Kα	93.49	45
Th-Lα	2.73	70
Ti-Kα	811.68	60
U-Lα	6.77	70
Zr-Lα	478.44	45

4.1.3. Removal of Tube interfering lines

If any component of the tube provides interference on an analyte line, the first step is to eliminate or minimise the interference. Setting the pulse height selector (PHS) is useful to check that the highest intensity to be measured does not saturate the detector electronics. If it does, a different filter, collimator or analysing crystal, or analyte line must be used (Willis et al., 2014). As evidenced in Figure 4.3, the PHA of Fe-Kα was too broad with poor resolution, and as a result, an Aluminium 0.5 mm primary beam filter (PBF) was used to reduce disturbances of the Bremsspectrum (rhodium X-ray tube photons). This resulted in a loss in primary beam intensity and at least some reduction in the excitation efficiency of Fe-Kα. The pulse distribution data from detectors were evaluated and modified in the pulse height. Figures 4.3 and 4.4 illustrate the PHS with and without PBF application for Fe-Kα.

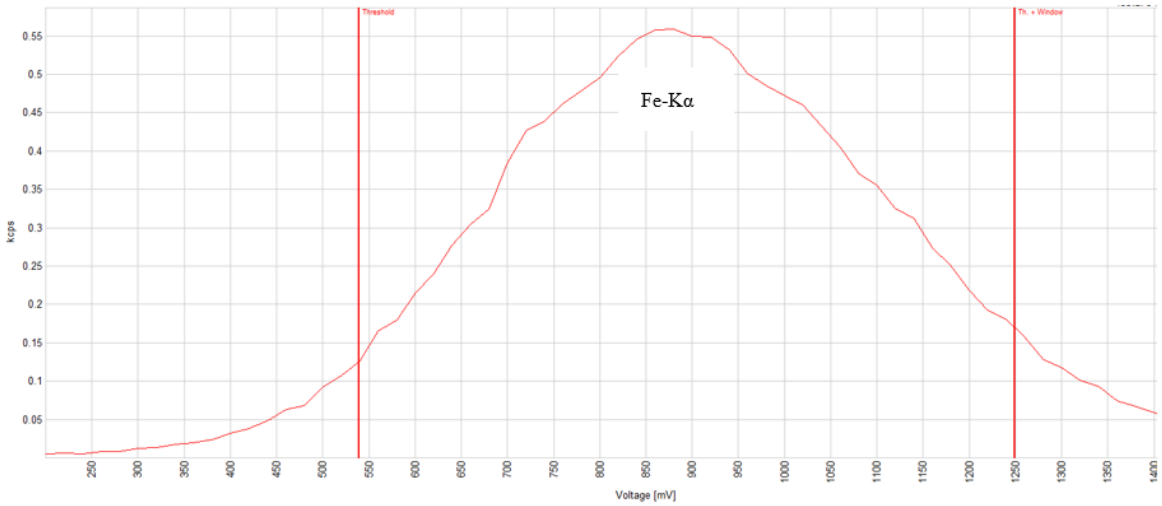

Figure 4.3: The Bremsspectrum of a rhodium X-ray tube in Fe without primary beam filter (PBF).

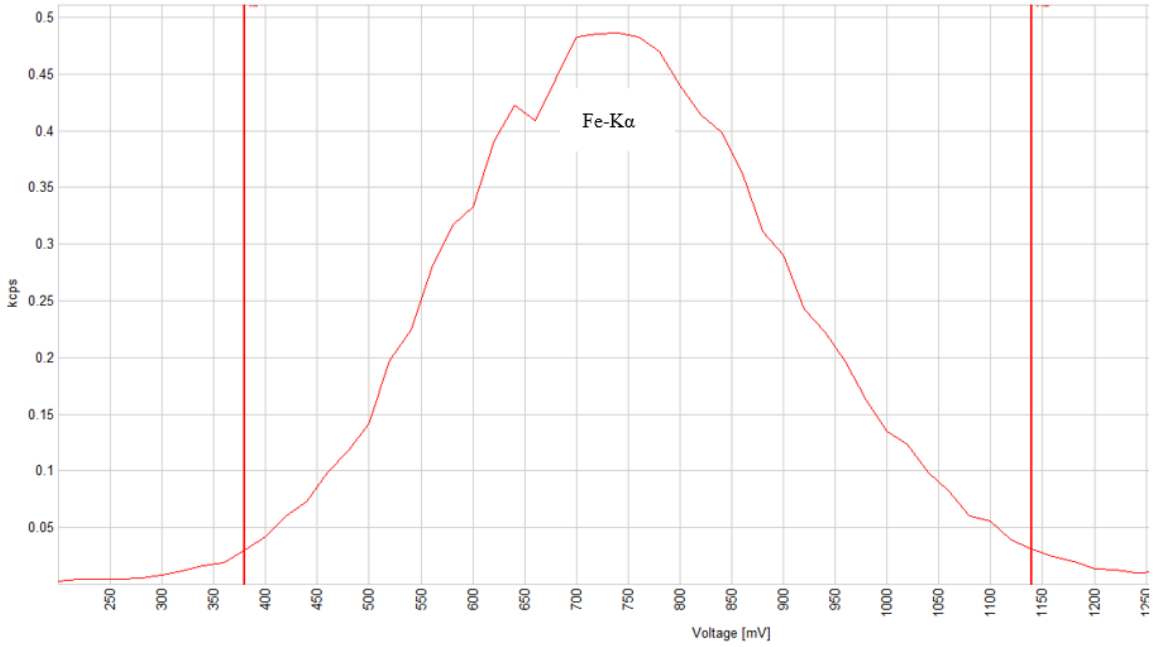

Figure 4.4: The Bremsspectrum of a rhodium X-ray tube in Fe with primary beam filter (PBF).

4.1.4. Removal of crystal fluorescence interfering lines

For phosphorus there were Germanium crystal fluorescence lines that appeared on the lower side of the main pulse height. Crystal fluorescence occurs when an element in the analysing crystal is excited by radiation from the elements in the sample and thus emits characteristic X-rays. The PHS

window was set to exclude the Germanium crystal fluorescence peak as recommended by (Willis et al., 2011). The PHS spectrum of P-Kα is shown in Figure 4.5. The plot shows the removal of interfering Ge111-L crystal fluorescence lines in the pulse height selector window set for P-Kα peak. The lower and upper voltage levels which define the "window" are shown as LL and UL. With these settings, only the P-Kα peak falls in the pulse height selection window and the pulses comprising the peak of Ge-Lines will be discarded by the pulse height selector.

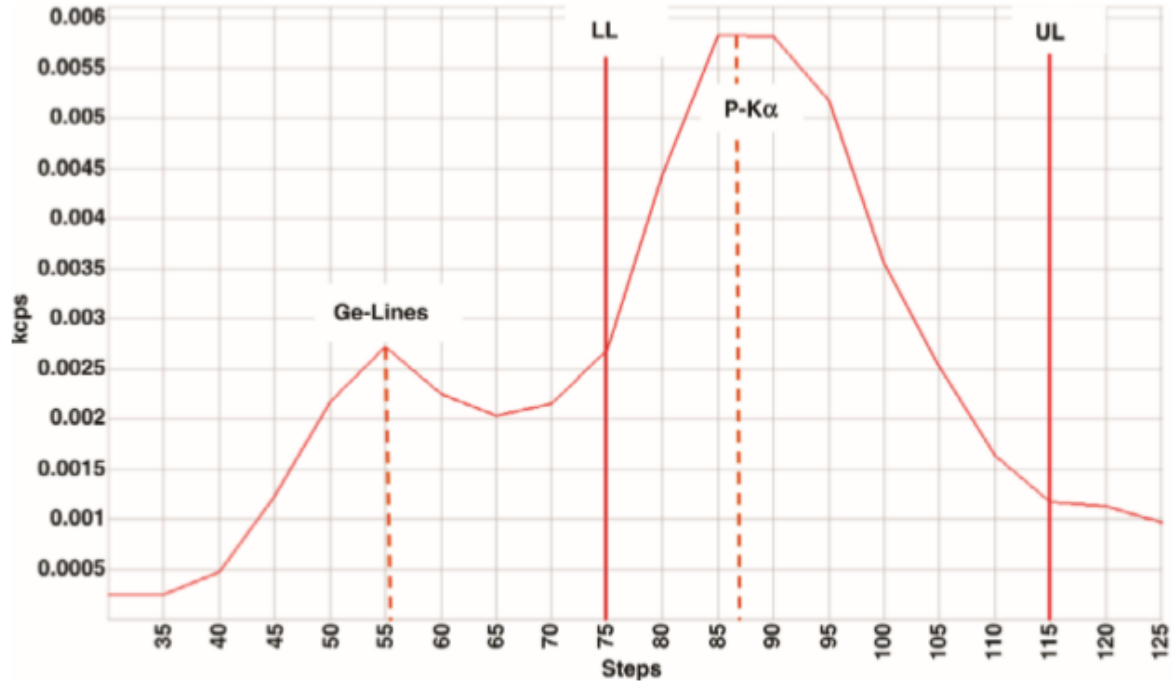

Figure 4.5: An Ar-CH_4 gas flow pulse height distribution plot for P-Kα using Ge111 analysing crystal.

4.1.5. Removal of electronic noise interfering lines

Escape peaks for Ti and Ca-Kα- lines are close to lower-level electronic noise (< 40 %) therefore, the lower limit was selected to exclude the noise pulse. The PHS spectrum of Ti-Kα is shown in Figure 4.6. The plot shows the removal of interfering electronic noise in the pulse height selector window set for the Ti-Kα peak. The lower and upper voltage levels which define the "window" are shown as LL and UL. With these settings, only the Ti-Kα peak falls in the pulse height selection window and the pulses comprising the peak of Noise will be discarded by the pulse height selector.

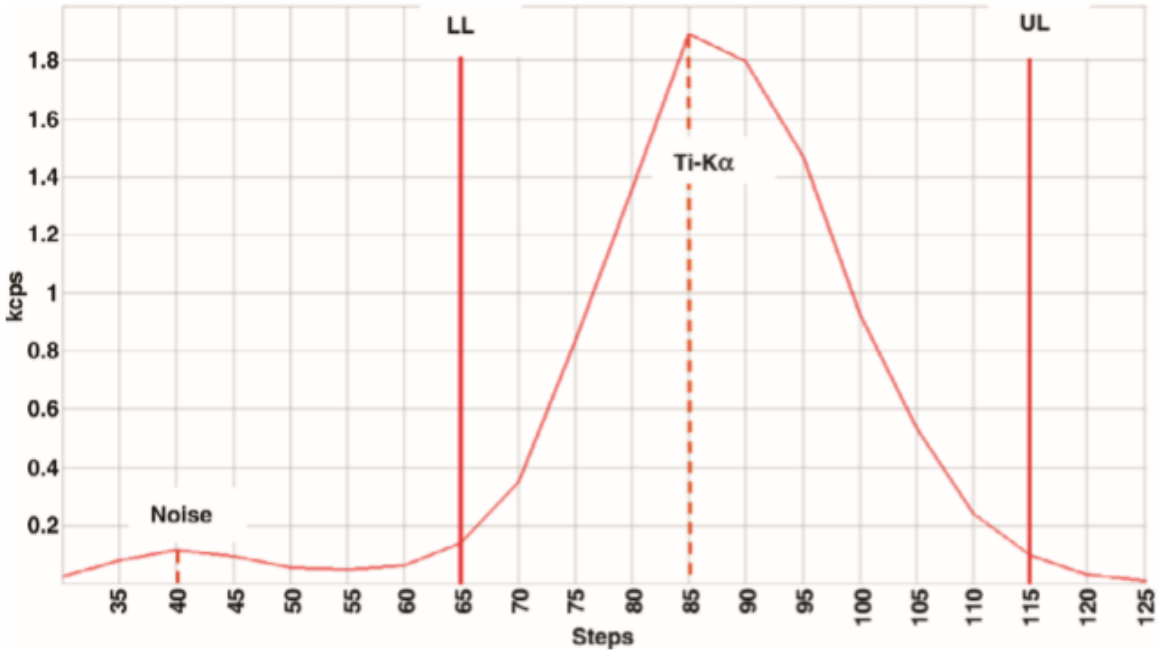

Figure 4.6: An Ar-CH_4 gas flow pulse height distribution plot for Ti-Kα using LIF200 analysing crystal.

4.2. Analytical method validation

The calibration lines have only been evaluated using a mathematical fit calculation according to the SEE value (standard estimated error). This is not good enough to assume that each line will be able to give accurate results during analysis. Other validation parameters were determined using specific statistical calculations to prove that all the lines are able to give accurate and trustworthy results and are fit for the intended analysis of mineral sands samples. The optimised calibration was validated as per ISO/IEC (2005) TR 26-02 criteria for its linearity, limit of detection (LOD), the limit of quantification (LOQ), analytical working range, precision and accuracy.

4.2.2. Linearity

The concentrations of the standards were plotted on the *x*-axis (lower uncertainty) and the instrument signals (high uncertainty) on the *y*-axis. The linear regression of the calibration line is acceptable if $r^2 > 0.997$. All the calibration lines had $r^2 > 0.999$, indicating that excellent calibration lines have been established (Table 4.6). Data points of the calibration standards were narrowly fitted to the calibration lines, except for Th and U. The plots of calibration lines are attached in Appendices C.1 - C11. Several points deviate noticeably from the 'best' straight line and are possibly attributed to matrix error, the r^2 is very close indeed to 1. It is observed that even quite poor-looking calibration

plots give very high r^2-values. The lesson learned is that the calibration curve must also be inspected visually, otherwise, a straight-line relationship might wrongly be deduced from the calculation of r^2. The r^2-values obtained in the instrumental software are normally very high, so a calculated value, together with the calibration plot itself, was sufficient to assure that a useful linear relationship has been obtained. Nevertheless, several studies focused on the fact that r^2 might not be a useful indicator of linearity and other statistical tests including the two-sided *t*-test have been suggested to ascertain the goodness of fit of the calibration curve.

Thus, in addition to r^2, the Minitab Analysis of Variance (ANOVA) results of the calibration were used to confirm significant linearity by using a two-sided *t*-test. The Minitab Regression outputs are summarised in Table 4.5 and Appendices D.1 – D.11. The output shows the standard error (*S*) of regression which is a measure of the amount of error accrued in predicting a y value for each given *x* (or *Sy/x*). The r^2-value (called '*R-sq*' by this program because it indicates the percentage of how well the experimental points fit a straight line) is 99.87 % or 0.9987. The intercept coefficient (constant) is 0.1493. The slope of the regression, called '% Al_2O_3' because *b* is the coefficient of the *x*-term in the regression equation, is 0.7234. The regression equation will be used to predict the intensity (kcps) y_i for a value of Al_2O_3 in test samples by interpolation and to determine the limit of detection of the analytes.

Table 4.5: Regression Analysis function in Minitab stats pack.

Regression Analysis: INT (kcps) yi versus %Al2O3

Analysis of Variance

Source	DF	Adj SS	Adj MS	F-Value	P-Value
Regression	1	9,31600	9,31600	5331,77	0,000
%Al2O3	1	9,31600	9,31600	5331,77	0,000
Error	6	0,01048	0,00175		
Total	7	9,32648			

Model Summary

S	R-sq	R-sq(adj)	R-sq(pred)
0,0418003	99,89%	99,87%	98,49%

Coefficients

Term	Coef	SE Coef	T-Value	P-Value	VIF
Constant	0,1493	0,0190	7,86	0,000	
%Al2O3	0,72337	0,00991	73,02	0,000	1,00

Regression Equation

INT (kcps) yi = 0,1493 + 0,72337 %Al2O3

The calculated value of *t* was compared with the tabulated value, t_{crit}, at the 95 % significance level and (*n*-2) degrees of freedom. If the calculated value of $t_{calc} > t_{crit}$, the null hypothesis (H_0) is rejected, and we conclude that a significant correlation does exist between *x* and *y*. From the results summarised in Table 4.6 it is evident that the calculated values of *t* are greater than the tabulated values; confirming that a significant correlation does exist for all. As expected, the closer r^2 is to 1 the larger the values of *t*, indicating a strong linear relationship. The t_{calc} of TiO_2 is at a maximum of 233, this shows significant linearity. The respective intercepts are therefore significantly different to 0 and bias is present.

Table 4.6: Regression Summary.

Analyte	(r^2)	*SE*	t_{calc}	t_{crit}	Regression equation
Al_2O_3	0.9989	0.048	120	2.6	$y = 0.149 + 0.723x$
CaO	0.9992	0.900	115	2.6	$y = - 0.068 + 2.696x$
Fe_2O_3	0.9984	0.325	145	2.4	$y = 1.170 + 4.446x$
HfO_2	0.9991	0.098	68	2.8	$y = 0.146 + 7.816x$
MgO	0.9997	0.019	88	3.2	$y = 0.422 + 0.511x$
P_2O_5	0.9998	0.002	74	2.8	$y = -0.042 + 1.109x$
SiO_2	0.9997	0.933	89	2.8	$y = 1.933 + 2.810x$
TiO_2	0.9999	0.121	233	2.8	$y = -1.971 + 0.528x$
ZrO_2	0.9991	0.456	131	2.2	$y = 0.740 + 0.753x$
U_3O_5	0.9995	0.016	76	3.2	$y = 0.292 + 16.272x$
ThO_2	0.9996	0.002	94	2.8	$y = 0.210 + 17.441x$

Matrix corrections play a major role in the accuracy of XRF measurements since the main focus of this research is to generate reference spectra to use in the calibration process. The calibration lines were validated for accuracy by evaluating the standard error (SE) / (*Sy/x*) to see if any corrections for matrix effect were needed to be made. This value gives an indication of the accuracy of the correlation fit of all the standards (*n*) used on the calibration line and takes into account the absolute difference (Δ) between the true concentration value (μ) and the calculated value (*x*), as well as the number of calibration standards used. The value obtained for Δ must be close to zero showing that

the difference between the true value of the standard and the value calculated according to the linear response equation of the calibration line is insignificant (Lezzerini et al., 2014). The equation for calculating the SE is:

$$SEE = (\Sigma\Delta^2 / n-2)^{½} \quad 4.4$$

The matrix effect correction was applied to all the elements to maximize the accuracy using the COLA algorithm proposed by Lachance (1981). COLA uses theoretical influence coefficients studied by Rousseau (2006) and is applicable over very wide ranges of compositions and is calculating specific coefficients for every specimen. This program is built into the Thermo ARL software. The results show that matrix effects had no influence on all the calibration lines.

For Th and U, calibration standards remained scattered with the SE values > 2 %. The calibration data points that were not fitting in the calibration lines were removed and considerable improvement was observed on both Th and U without matrix correction. The SE values decreased to < 0.1 % respectively indicating the accuracy of the correlation of all the standards used on the calibration line. Referring to Table 4.6, it is evident that the concentration differences between the true analytical value and the calculated value are significantly small, especially considering the low concentration level of the standards. The two improved calibration lines of Th-Lα and U-Lα are shown in Figures 4.7 and 4.8. This proves that the matrix effect can be removed at ten times dilution but not at six times dilution (Kusano et al., 2015).

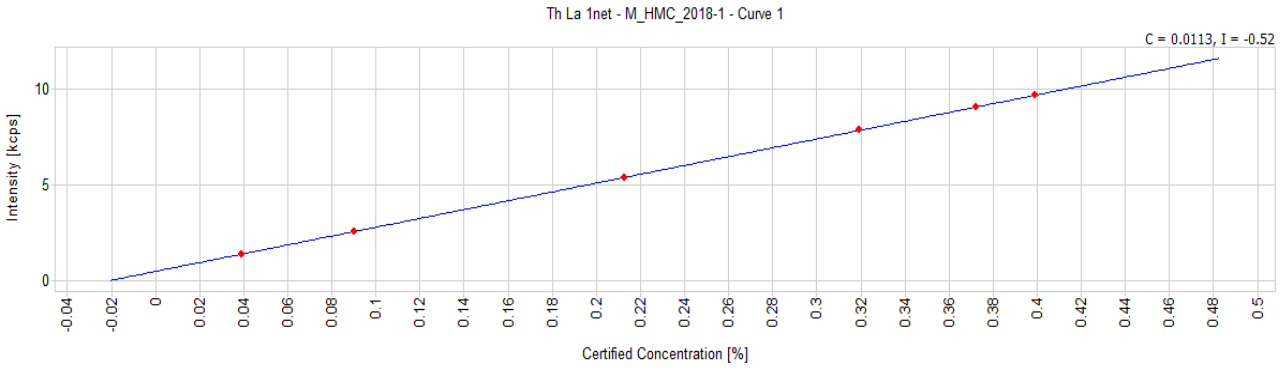

Figure 4.7: Calibration curve of Th-Lα, r^2 = 0.9999, % error = 0.016.

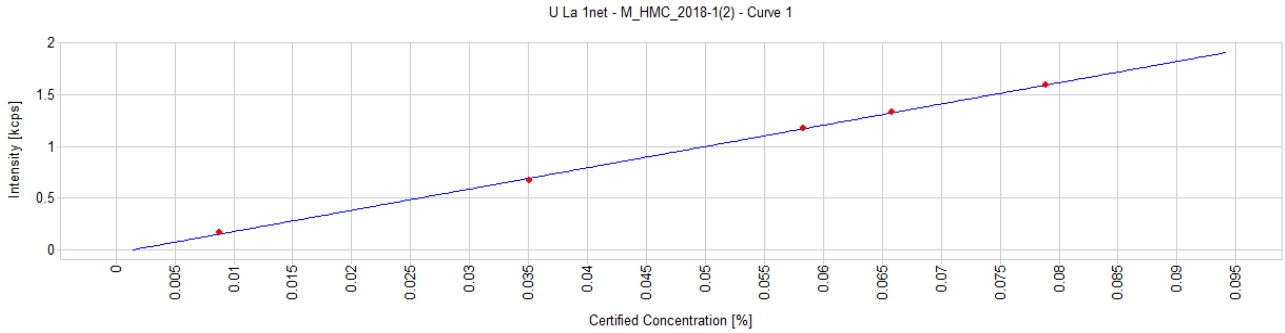

Figure 4.8: Calibration curve of U-Lα, r^2 = 0.9995, % error = 0.002.

4.2.3. LOQ and Working range

Every analyte in an analytical method has a detection limit (LOD), depending on the calibration line range and instrument hardware and software settings selected for that element. The limit of detection of an analyte may be described as that concentration that gives an instrument signal (y) significantly different from the 'blank' or 'background' signal. This description gives the analyst a good deal of freedom to decide the exact definition of the limit of detection, based on a suitable interpretation of the phrase. Therefore, in this work there was no blank measured as part of the calibration standard, the calibration data and regression statistics were used to theoretically determine the LOD.

The approach used for calculating detection limits includes the error (s_B) associated with measurements of the analytical sensitivity/slope (m) (Kadachi & Al-Eshaikh, 2012). The intercept error was neglected and was assumed to be 0 because the analytical measurements for trace elements are background corrected. The limit of detection was found by relating $3s_B$ (k = 3) to a concentration value by dividing by the slope of the calibration curve line obtained from the linear regression analysis. The use of k = 3 allows a confidence level of 99.9 %. The generally accepted rule in XRF is that if the concentration is lying at a $3s_B/m$ above the mean background, based on the normal distribution statistics there is a 99.9 % probability that the concentration does not belong to the background (Potts, 2013). LOQ was determined using $10s_B/m$ to ensure it is 10 times away from the background signal.

The counting times of elements were set at levels designed to produce LOQs of about 1000 ppm. The analytical working range in this study was defined as the interval between the limit of quantification (LOQ) and the upper calibration standard of an analyte. The obtained LOQs are adequately low extending the working range of all analytes. One of the fundamental problems when performing trace analysis with XRF is estimating characteristic peak amplitude in the presence of background noise.

For this work, LOQ is defined as $10s_B/m$ to ensure it is 10 times away from the background signal. Based on the definition of LOQ and the results of Table 4.7, four out of eleven oxides studied have LOQ values relatively higher than 1000 ppm and are caused by lower excitation of the Rh tube at longer wavelengths. It is apparent that X-ray fluorescence is a sensitive technique for detection of elements in heavy mineral sand samples at g/g concentration levels. Limits of quantification for Mg, P and Si (light elements) were higher than the other elements, but they are low enough if we consider that all three are present at minor concentrations in heavy mineral sand samples. SiO_2, TiO_2 and ZrO_2 are three major oxides typically found in mineral sands. SiO_2 is a major in Quartz, TiO_2 a major in Rutile and ZrO_2 a major in Zircon matrix samples, their respective working ranges are wide enough for accurate quantification.

Table 4.7: LOD and LOQ validation summary.

Analyte	% LOD $_{k=3}$	% LOQ	Working Range
Al_2O_3	0.03	0.08	0.08-5.0
CaO	0.03	0.09	0.09-9.0
Fe_2O_3	0.02	0.07	0.07-12.1
HfO_2	0.04	0.15	0.15-1.29
MgO	0.03	0.11	0.11-3.5
P_2O_5	0.04	0.13	0.13-0.23
SiO_2	0.03	0.11	0.11-55.2
TiO_2	0.01	0.04	0.04-83.8
ZrO_2	0.02	0.08	0.08-64.0
U_3O_5	0.003	0.01	0.01-0.1
ThO_2	0.004	0.01	0.01-0.1

4.2.4. Precision

The standard deviations of both methods were determined in Minitab descriptive statistics function. The Minitab descriptive statistics output is illustrated in Table 4.8 and Appendices E.1 - E.11. The output shows the mean, standard deviation, and Coefficient of variation (CV), also known as the relative standard deviation (% RSD).

Table 4.8: Descriptive Statistics function in Minitab stats pack.

Descriptive Statistics: 1 fused bead 10 measurements

Statistics

Variable	Mean	StDev	CoefVar
1 fused bead 10 measurements	2,3414	0,0132	0,56

Descriptive Statistics: 40 days

Statistics

Variable	Mean	StDev	CoefVar
40 days	2,3205	0,0471	2,03

The instrument precision was determined using the methodology studied by Richard (2001) whereby one specimen bead was analysed for ten days and the %RSD (n=10) technique was applied. The aim was to evaluate variation from the Rh-tube, detector, and goniometer of the instrument. The criteria in Table 4.9 were applied in the decision-making for both the instrument precision and within-laboratory repeatability. The relative standard deviation (RSD) is calculated and compared with recommended acceptable RSD's (APVMA, 2004).

Table 4.9: RSD evaluation criteria.

Concentration level	Acceptable precision (RSD)
≥ 10.0 %	≤ 2 %
1.0 % up to 10.0 %	≤ 5 %
0.1 % up to 1.0 %	≤ 10 %
<0.1 % (1000 ppm)	≤ 20 %

The ruggedness in this study is summarised in Table 4.10. In general, the higher the standard deviation, the higher the variation in the laboratory. On examining % RSD of both instrument precision and within-laboratory repeatability, the coefficients of variation for the major elements are mostly below ±2 % except 3 % of Mg. This is because of low energy elements such as Mg and Al yielding significant low intensities due to dilution. At low sample/flux ratio, the sensitivity of the XRF when analysing low concentration elements decreases, which in turn means a decreased

repeatability due to decreased instrument precision (Eastell & Willis, 1993). The U and Th coefficients of variation are high in the reproducibility exercise.

The repeatability of a method is normally expected to be poorer for the trace elements, due to larger random errors. Random errors affect the precision of an experiment. However, all the obtained coefficients of variation are below 10 % which is lower than the acceptable % RSD criteria (Table 4.9). This supports the assumption that the XRF instrument is stable and the sample preparation precise, due to the results being reproducible. This certifies that the variations are due to different operators, re-calibrations, routine instrument maintenance are insignificant. It also proves that the low dilution fusion approach developed was appropriate to eliminate particle size effects and sample heterogeneity. All the fusion parameters i.e. the particle size, fusing agent (flux), sample to flux ratio, fusion temperature as well as fusion time were adjusted optimally to achieve a quality fusion specimen. It is known that the quality of the analysis is dependent on the sample specimen homogeneity, which in turn is dependent on the fusion process.

Table 4.10: Precision validation summary.

Analyte	% RSD Instrument (n = 10)	% RSD Laboratory (n = 10)
Al_2O_3	0.6	2
CaO	0.3	2
Fe_2O_3	0.1	1
HfO_2	0.3	2
MgO	3.2	2
P_2O_5	0.6	1
SiO_2	0.1	0.3
TiO_2	0.3	0.7
ZrO_2	0.1	1
U_3O_5	2	5
ThO_2	2	3

4.2.5. Accuracy

As mentioned in Section 3.6.4 that the accuracy was tested through a proficiency testing (PT) scheme. Appendix F contains the raw data of key compounds as well as of additional compounds reported by some of the participants. It indicates Grubb's outliers in red and outliers based on visual inspection in blue. It also indicates the consensus values after outliers have been removed. The names of the participated laboratories are hidden to ensure confidentiality however, the newly developed XRF method is named Laboratory 3. Various analytical techniques were used for analysis by the participants. Most of the participants prefer not to disclose this information. Due to round robins being courtesy exercises, no pressure was put on participants to disclose information they are not comfortable sharing. Table 4.11 displays the *z*-score performance.

Limited statistical evaluation is applied to the data. The Grubbs test was used for detecting outliers and the *z*-score method was used to categorize data from satisfactory to unsatisfactory. The one-sided Grubbs test was used to confirm the minimum and/or maximum value of the data set as outliers. A value is regarded as a Grubbs outlier if the G_{calc} is greater than the G_{crit} obtained from the Table with Critical Values for the Grubbs Test, for a specific value of *n* (number of report results). This method does not cater for clustering of data close to the extremes, but due to the bulky manual calculations involved with G_2 and G_3, visual inspection was additionally used to assist with outlier elimination. Results reported as outliers are not considered in statistical calculations. There were no Grubbs outliers for the method developed in this study, only had P_2O_5 as an outlier based on visual inspection.

Robust statistics using *z*(MAD) was applied to calculate the *z*-scores. It was observed that *z*-scores do not work well with a limited number of results or where the results are very close to one another. As such, *z*-scores were evaluated in conjunction with the actual raw data. The *z*-score method is also dependent on the performance of the participating laboratories, especially where outlier results may impact the distribution of the data. Most of the oxides *z*(MAD) scores in Table 4.11 are ≤ 2 which was satisfactory in the PT scheme. The satisfactory criterion means the results are within the two-standard deviation (2σ) limit from the population average. This proves that the optimised calibration results are trustworthy, although some of the calibration curves were built without matrix-effects correction.

A questionable *z*-score (2.97) was obtained for P_2O_5. The P_2O_5 was the only oxide where the analytical working range was not wide enough to allow the determination of real samples by interpolation and not extrapolation. P_2O_5 in overall mineral sands chemistry is not usually present in significant quantities. After careful observation of the spectra, no interferences were observed

which could explain the bias observed. Relatively poor participation is noted in the laboratories, unfortunately, no CRM is available for quality control to evaluate the performance of laboratories.

Table 4.11: Accuracy validation summary.

CRITERIA	Al_2O_3	CaO	Fe_2O_3	HfO_2	MgO	P_2O_5	SiO_2	TiO_2	ZrO_2	U_3O_5	ThO_2
Study z(MAD)	1.98	1.97	1.47	0.95	0.10	2.97	0.88	0.31	0.78	0.05	1.59

4.2.6. Comparative study

Since the aim of this research is the optimisation of the XRF method, the *Original and Optimised methods* were compared. The key point for the successful implementation of the described approach is to firstly constitute a suitable collection of samples containing a broad range of analyte concentrations to ensure robust calibrations. Several factors that influence the results from XRF analysis and need to be evaluated before finalizing the protocol include the detection limits, matrix effects, sample preparation and instrument configuration.

The comparative study was done using Confidence Intervals derived from Matrix Reference materials (RMs). The two reference materials, RR014/16 (RR014 for Round-Robin number and 16 the year of certification), which has high TiO_2 content and RR002c/17 (RR014 for Round-Robin number and 17 the year of certification) which has high ZrO_2 content with relatively high SiO_2 content, were selected. These RMs were certified through interlaboratory studies, where the participants were reputable national and international laboratories, specialising in geochemical analysis. The 95% confidence limits of the standard deviation of the mean of means of the reported values were used since they provide the range within which the true value of the measured parameter is expected to lie. This makes it possible to use the measurement result, although the true value is not known. The 2*s* limits (95 % CI) are usually wide.

On examining the results shown in Table 4.12 the *Original method* is performing poorly, the majority of oxides measurements lie outside the confidence limits and are asterisked. An outside limit result (44.3 %) was obtained by the *Original method* for the TiO_2 in RR014/16, it was expected as the *Original method* was extrapolating above the calibration in Rutile matrix samples but the 20.7 % in RR002/17 is within working range. The results obtained for Al_2O_3 in RR002/17 are below the LOQ on the Original method. A 3.04 % in RR002/17 and 2.82 % RR014/16 for Fe_2O_3 were outside

the limits, it seems that the Fe_2O_3 analysis was erratic. Similarly, P_2O_5 and HfO_2 are outside the limits on both reference materials; it seems they were extrapolated above and below the calibration point, respectively. This is a confirmation that it is responding differently to the matrix reference materials; hence, it was earmarked for improvements.

P_2O_5 performed well on both RMs in the Optimised method despite the questionable *z*-score (2.97) in the PT exercise. The value 0.19 % for CaO on the Optimised method is located at the lower end of the confidence interval for RR002c/17 but, the 1.24 % in R014/16 is better on the higher sample. The Optimised method additionally includes U and Th for shipping purposes as some of the various concentrate streams are shipped to overseas markets; both performed well on both RMs. Heavy mineral sand fractions (e.g. Monazite, Rutile and Zircon) are often slightly radioactive and some countries have regulatory controls over the U and Th levels. The concentrations in certain heavy mineral fractions are often enhanced above those found in mineral sands as a result of beneficiation processes. The U and Th remained trapped inside the crystal structures of the minerals and therefore mineral sands. (Philander & Rozendaal, 2009).

Table 4.12: Comparison of the methods.

	RR014/16					RR002c/17				
Oxide	**Orig**	**Opt**	**Consensus**	**95 % LCL**	**95 % UCL**	**Orig**	**Opt**	**Consensus**	**95 % LCL**	**95 % UCL**
Al_2O_3	1.69	1.90	1.92	1.68	2.14	0.18*	0.54	0.54	0.49	0.61
CaO	1.44	1.30	1.34	1.24	1.45	0.20	0.19	0.23	0.19	0.27
Fe_2O_3	3.04*	1.29	1.47	1.24	1.67	2.82*	1.20	1.26	1.15	1.39
HfO_2	0.52*	0.65	0.72	0.58	0.92	0.91*	0.95	1.06	0.94	1.21
MgO	0.59	0.43	0.49	0.36	0.63	nr	0.12	0.10	0.08	0.14
P_2O_5	0.11*	0.29	0.27	0.23	0.33	0.15*	0.35	0.35	0.31	0.38
SiO_2	22.2	22.6	22.1	21.6	22.8	26.6	26.5	26.2	24.9	28.2
TiO_2	44.3*	39.0	39.6	37.6	41.5	20.7	20.5	20.3	19.8	21.8
ZrO_2	30.7	31.9	31.1	29.9	32.5	49.1	49.4	50.0	48.3	51.7
U	nr	274	337	255	411	nr	301	316	279	366
Th	nr	272	324	168	471	nr	614	635	512	766

* - values outside the 95 % confidence level, nr – not reported, RR – Round Robin, Orig – Original, Opt – Optimised.

CHAPTER 5

CONCLUSION AND RECOMMENDATIONS

In this study, each synthetic standard was made by homogenizing pure compounds with reference materials using blending operations. The calibration standards were prepared by carefully weighing, mixing and then homogenizing with borate flux. The calibration glass disks were made by mixing various quantities of stock standard samples with lithium tetraborate/ lithium metaborate mixtures and fused. Particle size effect (grain size) is one of the drawbacks of the fusion technique this was eliminated by pulverizing the samples to < 75 µm. All the calibration standards yielded good glass specimens. The 50/50 lithium tetraborate/ lithium metaborate flux performed well for all acidic oxides. The specimens of each standard were prepared in duplicates and analysed to check the repeatability of the results. Borate fusions were found advantageous for the preparation of synthetic standards.

Low intensities for trace elements such as Mg, Th and U were noticed. This loss of intensity was less than expected from direct proportionality with the dilution, and is not too inconvenient, because the spectrometer tube voltage and current settings were adjusted to achieve maximum excitation. The proper selection of tube voltage and current settings is very important in determining the excitation efficiency of different groups of elements.

For Mg, the voltage applied to the X-ray tube was reduced to 30 kV. For Hf, Th and U the voltage and current were adjusted to 60 kV/50 mA to change both the intensity and the wavelength distribution of the tube spectrum so that, their respective lines will be excited by the Rh K- lines. The use of theoretical Kα lines eliminates the error arising from the spectral distribution of the X-Ray tube using optimized analytical conditions.

A general principle of empirical calibration in XRF is that the calibration and test samples be as similar as possible and cover a similar range of concentrations, and this range is reflective of the actual range of analyte concentrations expected in the samples on which the method would be applied in the future. The calibrations developed in this research are robust enough to be applied to mineral sand samples. During the method validation phase, the main parameters that were validated to prove that the method is fit for purpose were:

- Linearity

- Determination Limit of Detection (LOD) and Limit of Quantitation (LOQ)
- Precision of results
- Specificity
- Accuracy

For all the calibration lines the linearity was found to be satisfactory $r > 0.997$ and showed almost perfect linearity. The obtained standard error values were between 0.002 - 0.933 proving the accuracy of the correlation fit. Differences in the standard error of calibration reported in this study appear to be the function of matrix differences in samples. Furthermore, the empirical coefficients (COLA) calculated by multiple regression analysis contain many potential pitfalls. Not only do empirical coefficients correct for matrix effects, but they can also prevent other error types that may be present, such as errors on measured intensities and poor sample preparation. Unfortunately, all these effects tend to change from sample to sample, so that unknown samples analysed using such calibration curves often may yield inferior quality analytical results. These errors might contribute to the significant bias obtained for P_2O_5 in this study.

Due to the higher standard deviation of the calibration slope for Mg, P and Si, the limits of quantification were higher as compared to the other elements reported. The calibration line of P is the only line that can be improved regarding the analytical ranges. The ranges for the rest of the calibration lines are satisfactory. The LOD and LOQ values for all the lines are low enough to prevent extrapolation below the lowest calibration point.

The precision RSD values were less than 10 %, this is an indication of the stability of the instrument's goniometer and good sample preparation. The hypothesis was that the XRF synthetic calibration technique can quantify the concentration of elements in mineral sands samples. One of the first characteristics that one would like to know about any method is whether the results reflect the true value of the analyte or not. The accuracy of the method is sensitive to varying conditions including the level of an analyte in the sample and matrix. Thus, accuracy was validated using Proficiency Testing. According to the results obtained from the *z*-scores used to validate accuracy, all the calibration lines used for the analysis of the elements and the oxides gave results that could be interpreted as accurate according to the *z*-scores criteria.

The data presented here support the successful synthesis and use of a well-selected set of synthetic standards. It also shows that precise and accurate analysis of samples can be achieved from robust sample preparation. The fact that synthetic standards are chemically pure and traceable offers

important support for compliance with company operating procedures and relevant legislation. It is to be hoped that the synthetic calibration protocols developed and tested in the present work will be adopted by other mineral sands researchers and industry operators to improve ore characterisation methodologies and perhaps develop elemental compositions-based markers to predict extraction performance.

The main concerns with fabricating synthetic standards are errors associated with the weighing of trace elements. The low cost and ready availability of the matrix-matched samples retained from the proficiency-testing exercise make it possible to use them routinely as control samples, allowing fast response times to problems once they have been identified. The general conclusion made after the validation procedures was that the method developed for the analysis of ZrO_2, SiO_2, HfO_2, Fe_2O_3, TiO_2, Al_2O_3, CaO, MgO, P_2O_5, U_3O_5 and ThO_2 is fit for purpose for the analysis of the mentioned analytes.

REFERENCES

Amosova A.A, Chubarov V.M., Pashkova G.V., Finkelshtein A.L., Bezrukova E.V., 2019. Wavelength dispersive X-ray fluorescence determination of major oxides in bottom and peat sediments for paleoclimatic studies Appl. Radiat. Isotopes,144, pp. 118-123.

APVMA., 2004. Guidelines for the validation of analytical methods for active constituent, agricultural and veterinary chemical products.

AS, 4392, 1996. Heavy mineral sands - Analysis by wavelength dispersive X-ray fluorescence spectrometry Titaniferous mineral sands.

Beckhoff, B., Kanngießer, B., Langhoff, N., Wedell, R., Wolff, H., 2006. Handbook of Practical X-Ray Fluorescence Analysis (Berlin: Springer).

Bennett, B. & Oliver, G., 1992. XRF Analysis, Minerals and Allied Materials. J Wiley & Sons.

Blank, A. B. & Eksperiandova, L. P., 1998. Specimen Preparation in X-ray Fluorescence Analysis of Materials and Natural Objects. X-ray Spectrometry, Volume 27, pp. 147-160.

Bouchard, M., Milliard, A., Rivard, S. & Ness, S., 2014. ISO 9516-1 Simplified borate fusion/WDXRF analytical method for Iron including total Iro analysis: Part 2. Cambridge university press.

Bower, N. W. & Valentine, G., 1986. Critical comparison of sample preparation methods for major and trace element determinations using X-ray fluorescence. X-Ray Spectrometry, 15(1) pp. 73 -78.

Chiweshe, T. T., Purcell, W. & Venter, J. A., 2016. Evaluation of different internal standards for precious metals quantification. Bull. Chem. Soc. Ethiop., 30(1), pp. 55-70.

Claisse, F. & Blanchette, J. S., 2004. Physics and chemistry of borate fusion-for x-ray fluorescence spectroscopists. Fernard Claisee Inc.

Claisse, F. & Samson, C., 1962. Heterogeneity Effects in X-ray Analysis. Advances in X-ray Analysis, 5(12), pp. 335-354.

Claisse, F., 1994. Fusion of Sulfide Ores and Minerals. Denver Conference.

Claisse, F., 1998. Choix de la composition optimale d'un borate de lithium dans la preparation des perles pour analyse par Fluo-X. France, J. Physique IV, Volume 8, pp. 379-384.

Eastell, J. & Willis, J. P., 1990. A low dilution fusion technique for the analysis of geological samples, 1 – Method and trace element analysis. X-Ray Spectrom., Volume 19, pp. 3-14.

Eastell, J. & Willis, J. P., 1993. A low dilution fusion technique for the analysis of geological samples, 2 – Major and minor element analysis and use of influence/alpha coefficients. X-ray Spectrom., Volume 22, pp. 71-79.

Eurachem, G., 2014. The Fitness for Purpose of Analytical Methods. A laboratory guide to method validation and related topics. 2 ed. Copyright LGC (Teddington) Ltd.

François, N., Govaerts, B. & Boulanger, B., 2008. Optimal designs for inverse prediction in univariate nonlinear calibration models. Chemometrics and Intelligent Laboratory Systems, 74(2).

Giles, H. I., Hurley, P. W. & Webster, H. W., 1995. Simple approach to the analysis of oxides, silicates and carbonates using X-ray fluorescence spectrometry. X-ray Spectrom., 24(4), pp. 205-218.

Haukka, T. M. & Thomas, I. L., 1977. Total X-ray Fluorescence Analysis of Geological Samples Using a Low-dilution Lithium Metaborate Fusion Method, Matrix Corrections for Major Elements. X-ray Spectrom., 6(6), pp. 204-211.

ISO/IEC, 17025., 2005. General requirements for the competence of testing and calibration laboratories. ISO Geneva.

ISO/IEC, 17025., 2005 - General Requirements for the competence of testing and calibration laboratories, SADCAS TR 26-03 – Criteria for validation of methods used by Chemical laboratories in the Coal, Oil, Petroleum, Metals and Minerals, Food, Pharmaceuticals, water and related industries.

Kadachi, A.N. & Al-Eshaikh, A., 2012. Limits of detection in XRF spectroscopy. X-Ray spectrometry, 41, pp. 350-354.

Kusano, Y. et al., 2015. Quantitative analysis of major elements in igneous rocks with X-ray fluorescence spectrometer "ZSX primus II" using a 1:10 dilution glass bead. Sci. Rep. Kanazawa Univ., Volume 58, p. 31–44.

Lachance, G. R., 1981. The role of alpha coefficients in X-ray Spectrom, Paper Presented at the International Conference on Industrial Inorganic Elemental Analysis, Metz, France.

Lachance, G. R. & Traill, R. J., 1966. A practical solution to the matrix problem in X-ray analysis. Canadian Journal of Spectroscopy, Volume 11, pp. 43-48.

Lee, R. F. & McConchie, D. M., 1982. Comprehensive major and trace element analysis of geological material by x-ray fluorescence, using low dilution fusions. X-Ray Spectrometry, 11(2), pp. 41-98.

Lezzerini, M., Tamponi, M. & Bertoli, M., 2014. Calibration of XRF data on silicate rocks using chemicals as in-house standards. Atti. Soc. Tosc. Sci. Nat., Mem., Serie A (121), pp. 65-70.

Li X.L., An S.Q., Liu Y.X., Yu Z.S., Zhang Q., 2018. Investigation of a high-pressure pressed powder pellet technique for the analysis of coal by wavelength dispersive X-ray fluorescence spectroscopy Appl. Radiat. Isotopes,132, pp. 170-177.

Loubser, M., Strydom, C. & Potgieter, H., 2004. A thermogravimetric analysis study of volatilisation of flux mixtures used in XRF sample preparation. X-ray Spectrometry, 33(3), pp. 212-215.

Lucas-Tooth, H. & Pyne, C., 1964. The accurate determination of major constituents by X-ray fluorescent analysis in the presence of large interelement effects. Advances in X-ray, Volume 7, pp. 523-541.

Lucas-Tooth, H. J. & Price, B. J., 1961. A Mathematical Method for the Investigation of Interelement Effects in X-Ray Fluorescence Analysis. Metallurgia, 64(2), pp. 149-152.

Marguí, E., Queralt, I. & Van Grieken, R., 2016. Sample preparation for X-ray fluorescence analysis, John Wiley & Sons, Encyclopedia of Analytical Chemistry.

Mashima, H. & Mori, Y., 2005. X-ray fluorescence analysis of major and trace elements in silicate rocks using 1:5 dilution glass beads. Bull. Kitakyushu Mus. Nat. Hist. Hum. Hist. Ser. A, Volume 3, pp. 1-12.

Mashima, H., 2016. XRF analyses of major and trace elements in silicate rocks calibrated with synthetic standard samples. Natural Resource Environment and Humans, Volume 6, pp. 39-50.

Miller, J. N. & Miller, J. C., 2018. Statistics and chemometrics for analytical chemistry. 7 ed. Harlow: Prentice Hall.

Nettles, H. S., 2000. Effect of calibration specimen preparation techniques on narrow range X-ray fluorescence calibration accuracy, International centre for diffraction data. Advances in X-ray analysis, Volume 43.

Norrish, K. & Hutton, J. T., 1969. An accurate X-Ray spectrographic method for the analysis of a wide range of geological samples. Geochimica et Cosmochimica Acta, Volume 33, pp. 431-453.

Ogasawara, M., Mikoshiba, M., Shimoda, G. & Ishizuka, Y., 2018. Optimization of analytical conditions for major element analysis of geological samples with XRF using glass beads. Bulletin of the Geological Survey of Japan, 69 (2), p. 91–103.

Philander, C., Rozendaal, A., Le Rouxb, S. G. & du Plessis, A., 2018. Grade and product quality control by microCT scanning of the world class Namakwa Sands Ti-Zr placer deposit West Coast, South Africa: An orientation study. Minerals Engineering, Volume 116, p. 152–162.

Potts, P. J., 2013. A Handbook of Silicate Rock Analysis. 1 ed. New York: Springer.

Prichard, E. & Barwick, V., 2007. Quality Assurance in Analytical Chemistry. Chichester: John Wiley.

Rasberry, S. D. & Heinrich, K. J., 1974. Calibration for interelement effects in X-ray fluorescence analysis. Analytical Chemistry, Volume 46, pp. 81-89.

Richard, R. M., 2001. Detection limit and estimate of uncertainty of analytical XRF results. The Rigaku journal, 18(2).

Rousseau, R. M., 2006. Corrections for Matrix Effects in X-ray Fluorescence Analysis – A tutorial, Part B. Spectrochimica Acta, Volume 61, pp. 9-777.

Rousseeuw, P. J. & Hubert, M., 2018. Anomaly Detection by Robust Statistics. Wires Data Mining Knowl. Discov., Volume 8, pp. 1-4.

Schlotz, R. & Uhlig, S., 2006. Introduction to X-ray Fluorescence Analysis (XRF). Bruker AXS GmbH, Karlruhe, West Germany.

Sherman, J., 1955. The theoretical derivation of fluorescent X-ray intensities from mixtures. Spectrochimical Acta, Volume 7, pp. 283-306.

Sieber, J. R., 2002. Matrix-independent XRF methods for certification of standard reference materials. Advances in X-ray anal., Volume 45.

Smoliński A., Stempin M., Howaniec N., 2016. Determination of Rare Earth Elements in Combustion Ashes from Selected Polish Coal Mines by Wavelength Dispersive X-ray Fluorescence Spectrometry, Spectrochim. Acta B, 116, pp. 63-74.

Staats, G., 1989. Synthetic macro-reference samples for the calibration of instruments in inorganic bulk analysis. Fresenius Z Anal Chem., Volume 4, pp. 326-330.

Thompson, M., Potts, P. J., Kane, J. S. & Wilson, S., 1999. An International Proficiency Test for Analytical Geochemistry Laboratories. Geostandards Newsletter.

Van Grieken E.R. & Markowicz, A.A., 2001. Handbook of X-Ray Spectrometry, Second Edition, New York: Marcel Dekker, Inc.

Willis, J. P., Feather, C. & Turner, K., 2014. Guidelines for XRF Spectrometry. 1 ed. Cape Town, South Africa: James Willis Consultants cc.

Willis, J. P., Turner, K. & Pritchard, G., 2011. XRF in the Workplace: A Guide to Practical XRF Spectrometry. PAnalytical Australia.

Willis, P. J., 2010. XRF sample preparation - glass beads by borate fusion. Netherlands: PANalytical BV, 33(1), pp. 431-453.

Yamasaki, T., 2014. XRF major element analyses of silicate rocks using 1:10 dilution ratio glass bead and a synthetically extended calibration curve method. Bulletin of the Geological Survey of Japan, 65(7/8), pp. 97-103.

Appendix A.1: Al-Kα wavelength scan

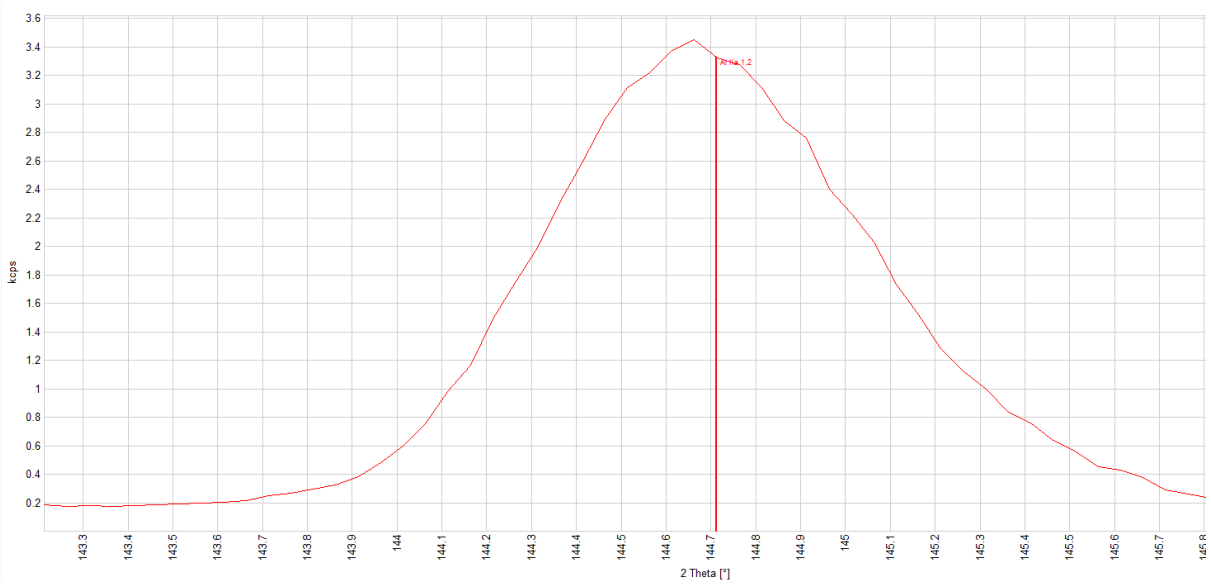

Appendix A.2: Ca-Kα wavelength scan

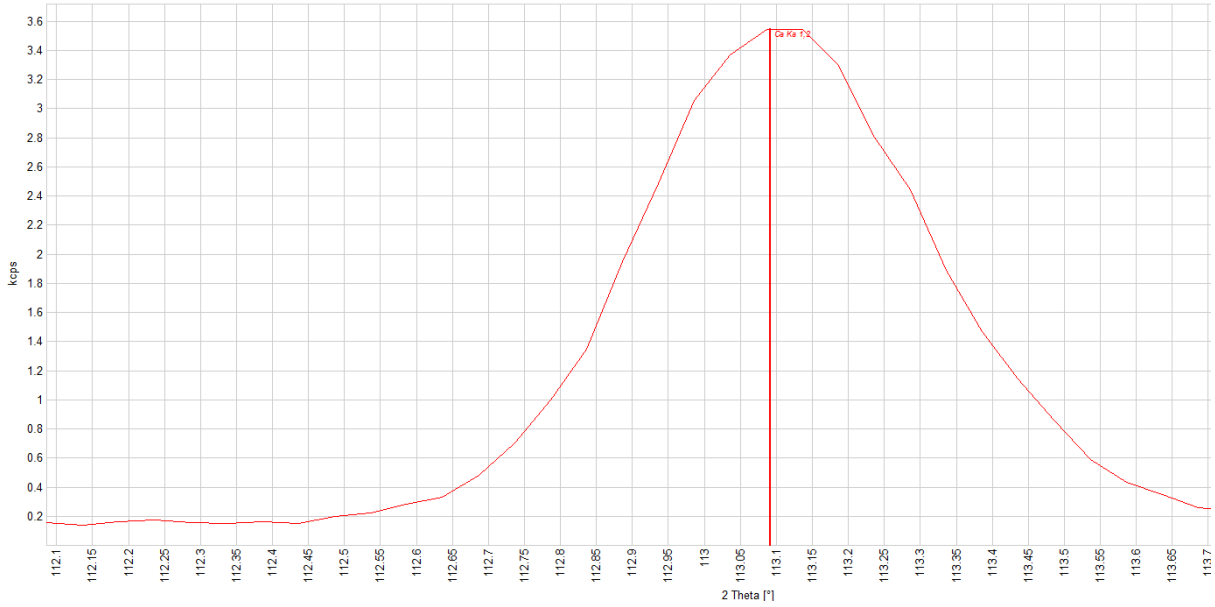

Appendix A.3: Fe-Kα wavelength scan

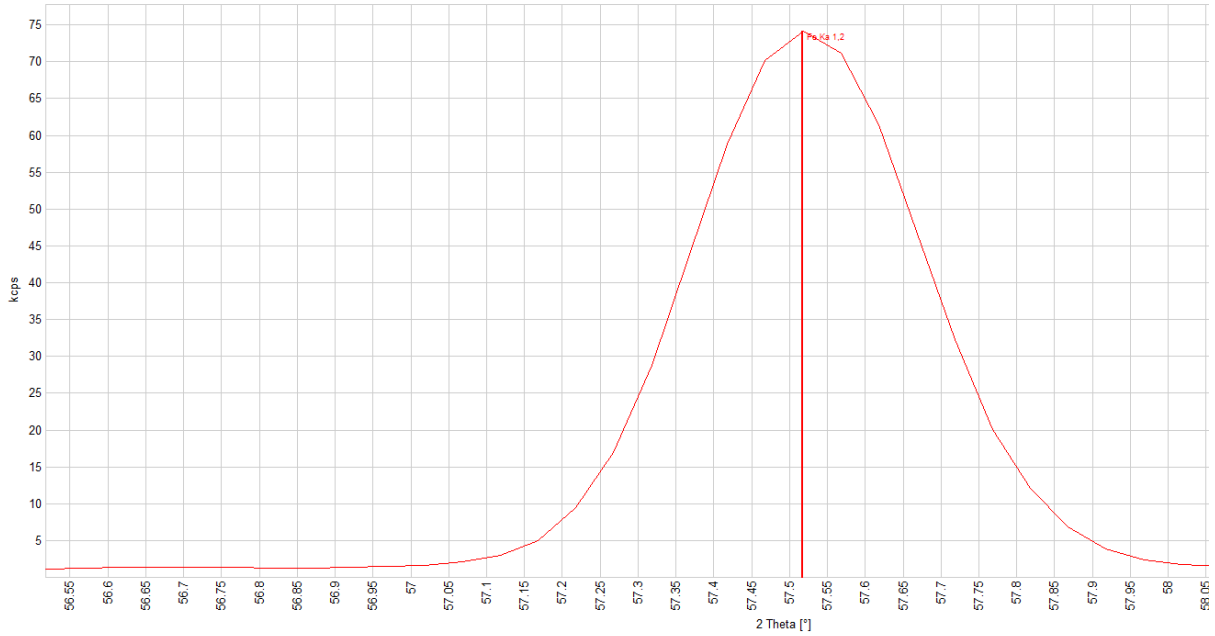

Appendix A.4: Hf-Lβ wavelength scan

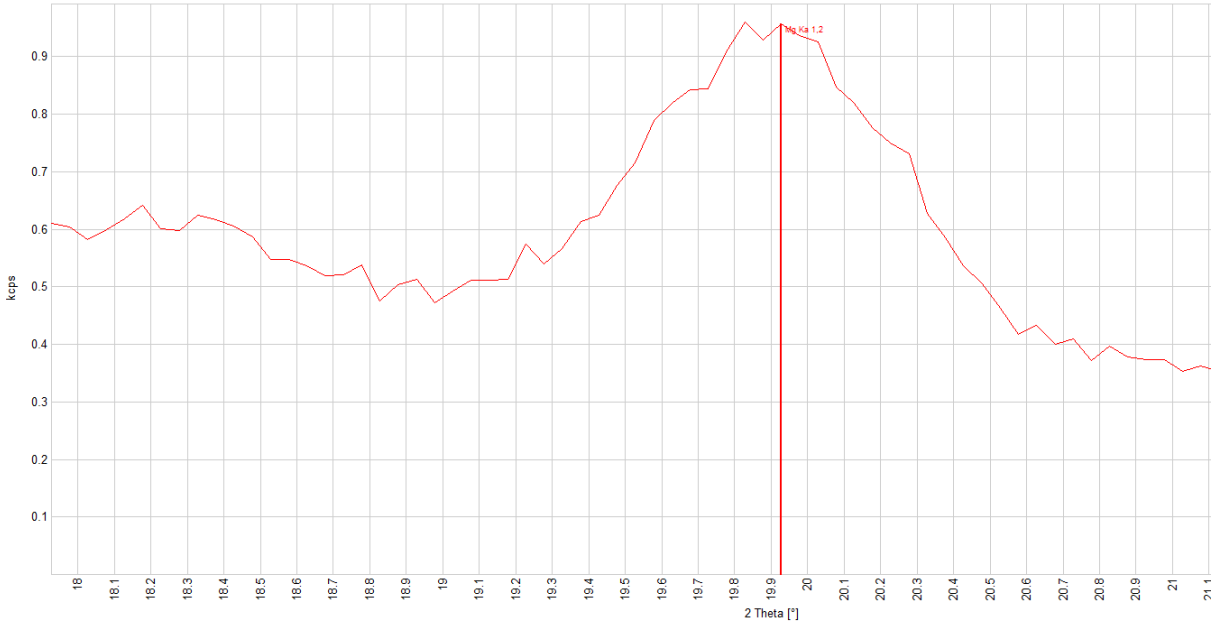

Appendix A.5: Mg-Kα wavelength scan

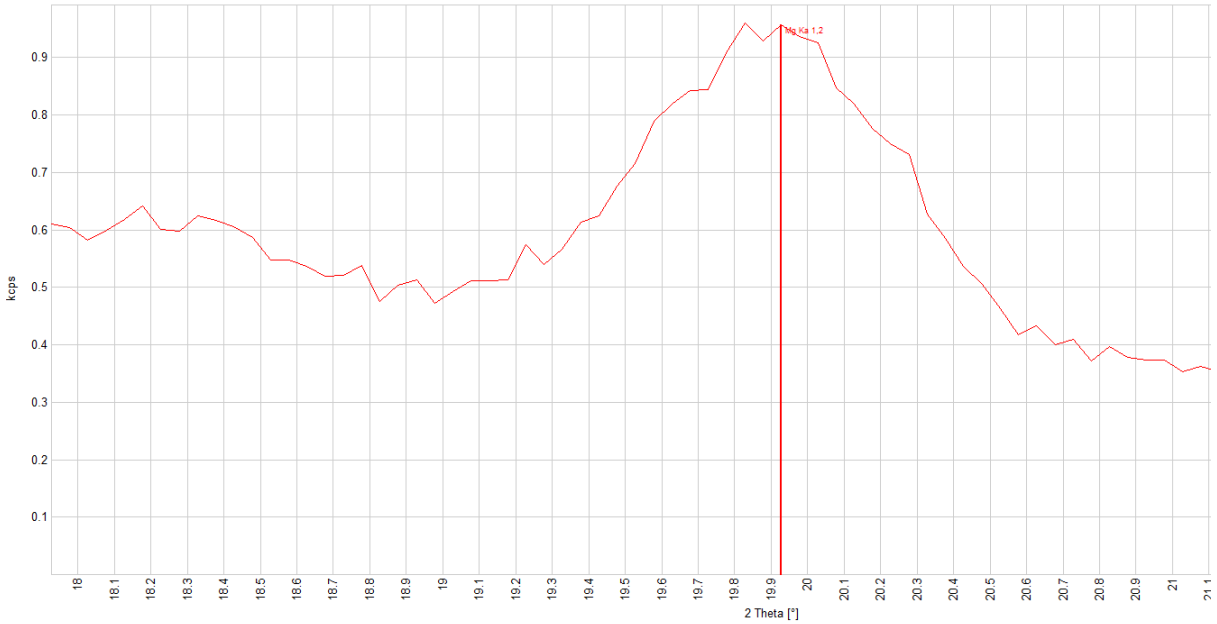

Appendix A.6: P-Kα wavelength scanx

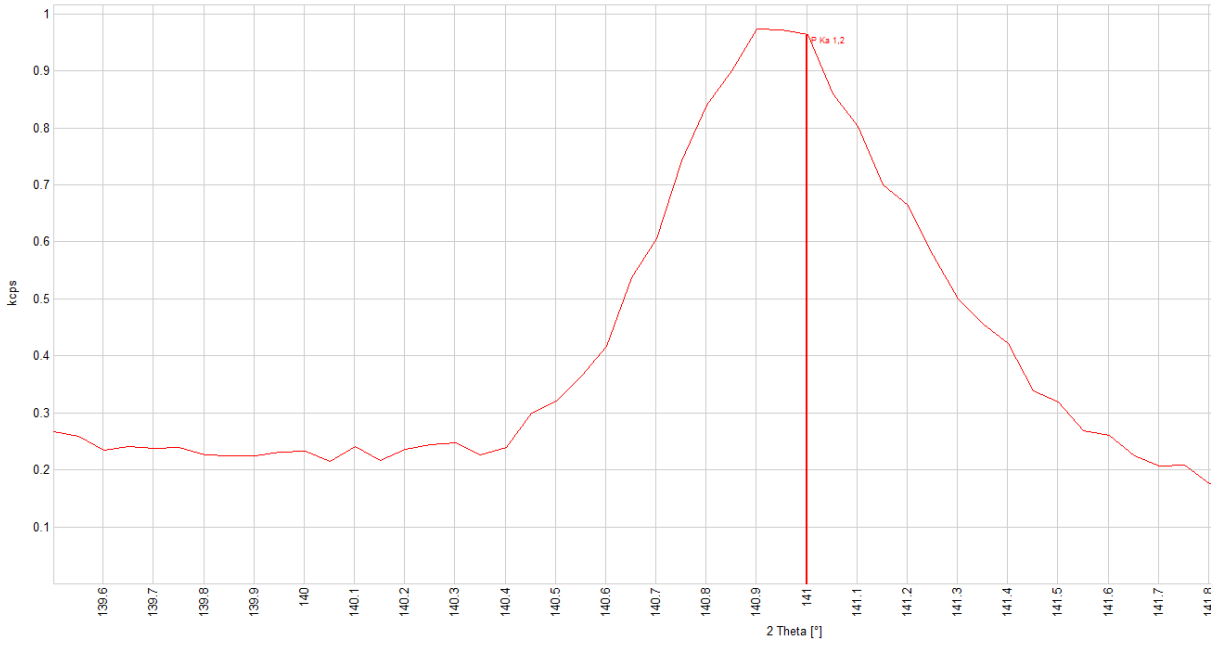

Appendix A.7: Si-Kα wavelength scan

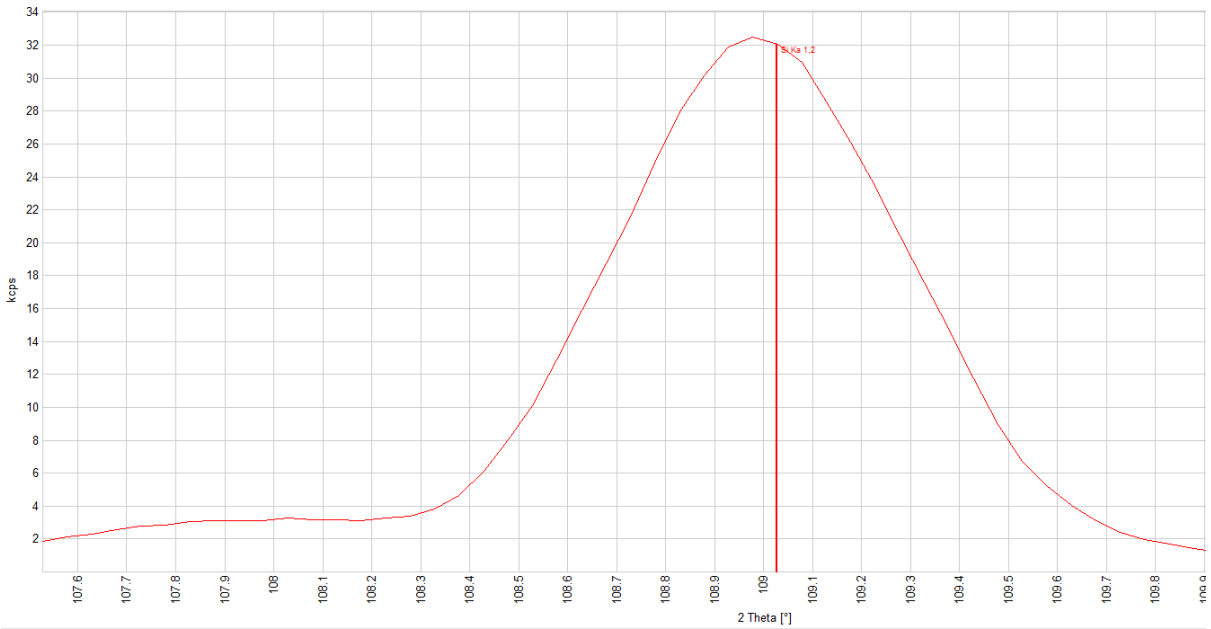

Appendix A.8: Ti-Kα wavelength scan

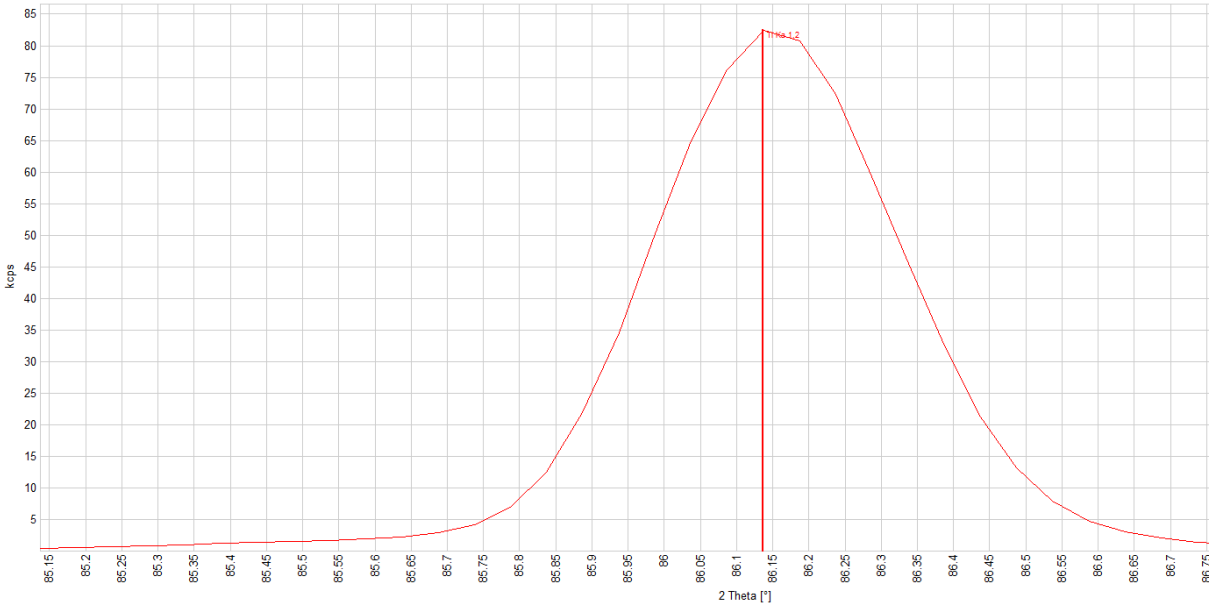

Appendix A.9: Zr-Lα wavelength scan

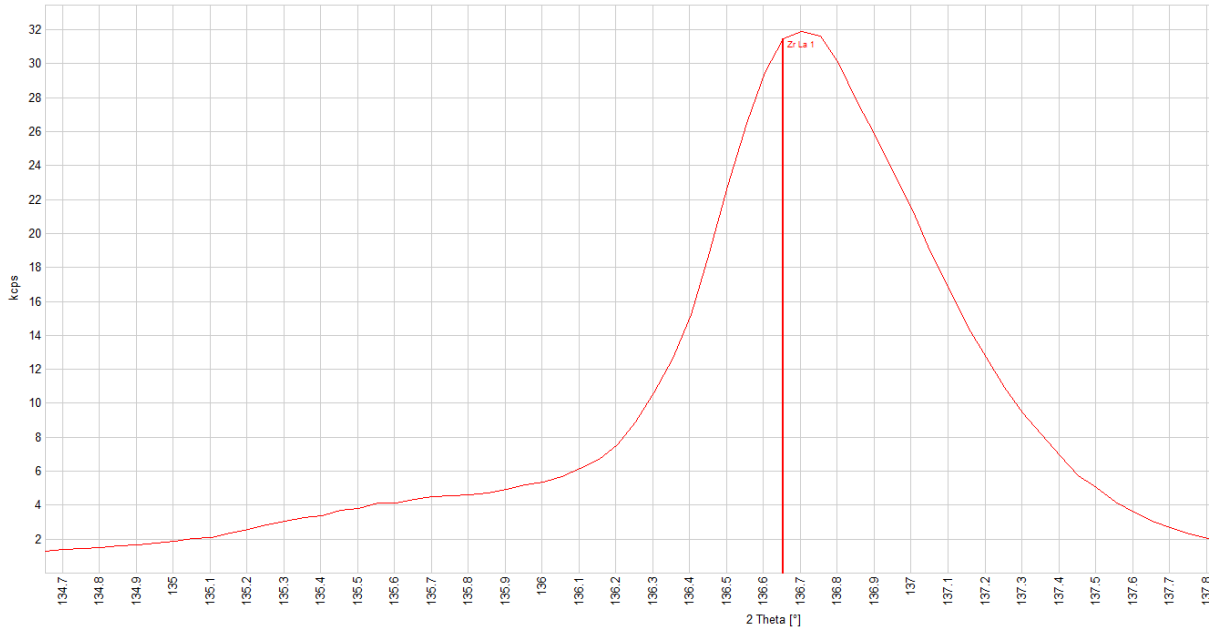

Appendix A.10: Th-Lα wavelength scan

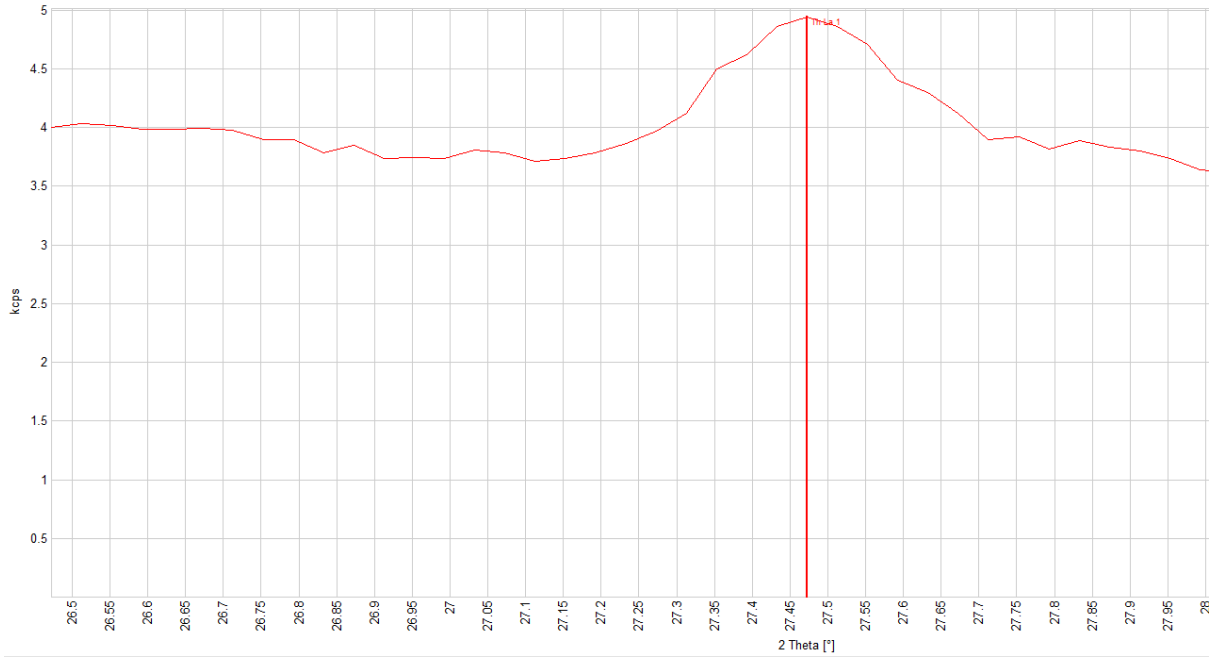

Appendix A.11: U-Lα wavelength scan

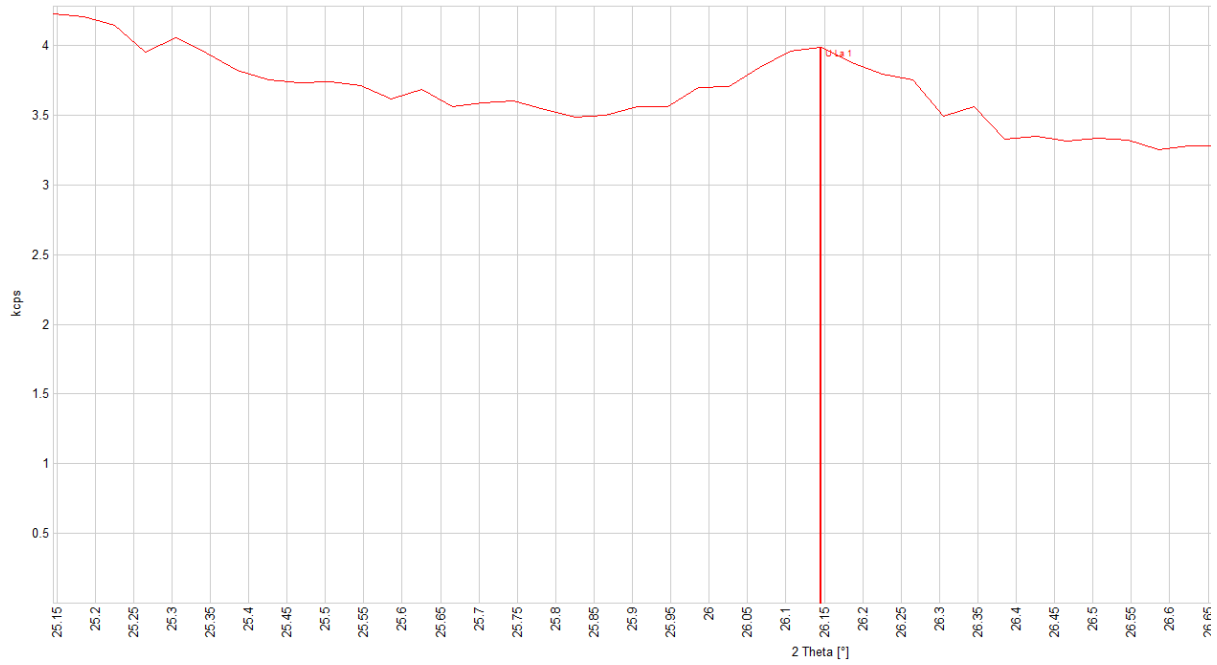

Appendix B.1: Al-Kα Energy Profile

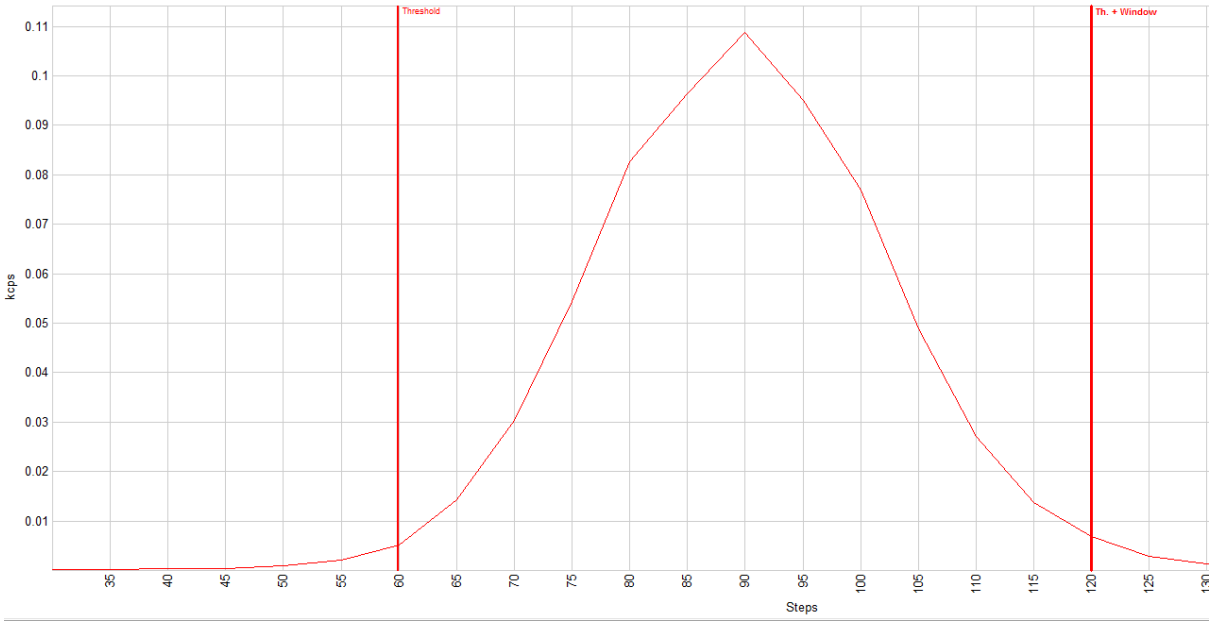

Appendix B.2: Ca-Kα Energy Profile

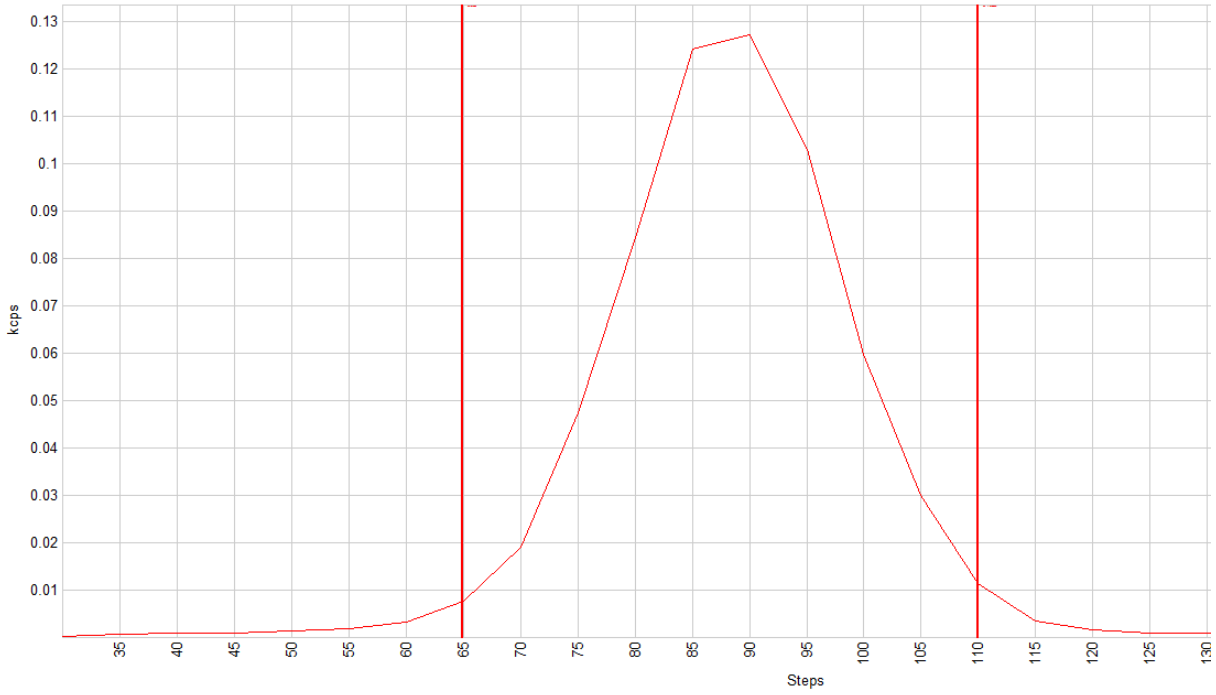

Appendix B.3: Fe-Kα Energy Profile

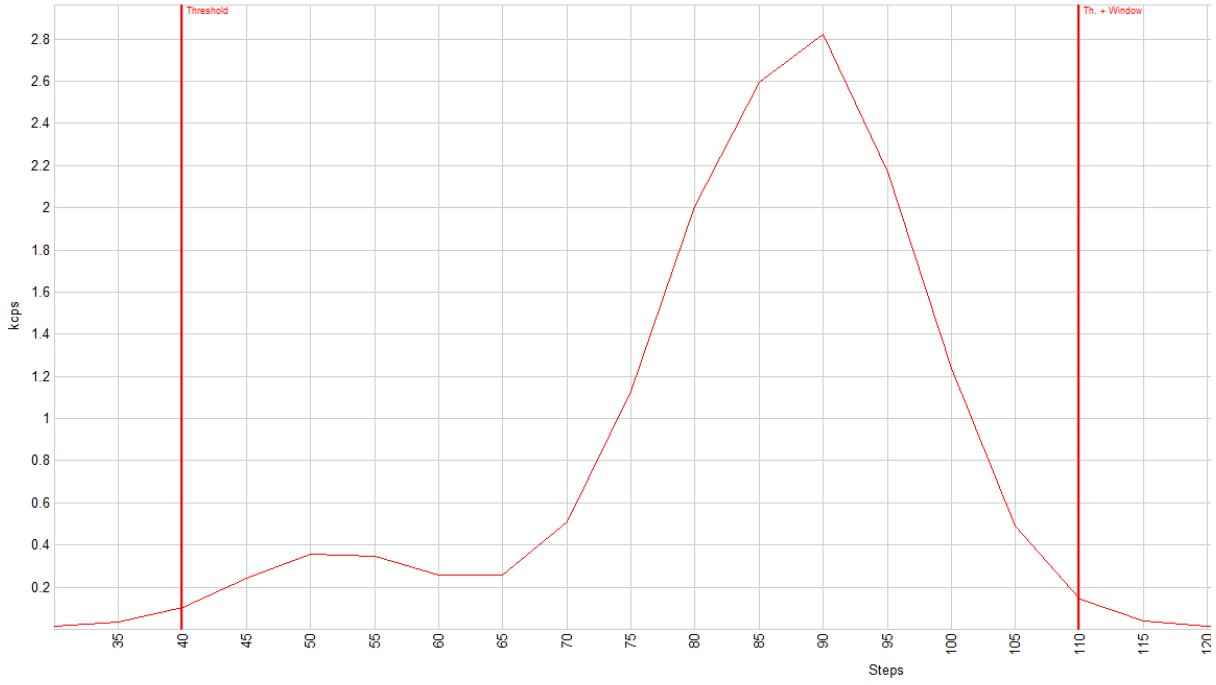

Appendix B.4: Hf-Lβ Energy Profile

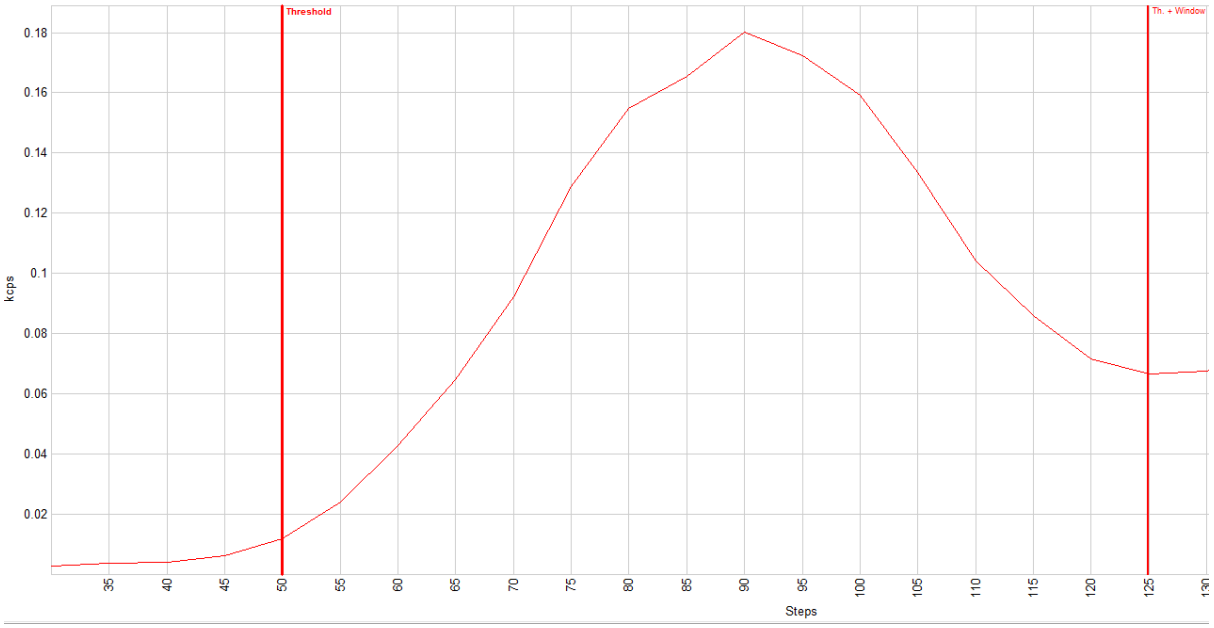

Appendix B.5: Mg-Kα Energy Profile

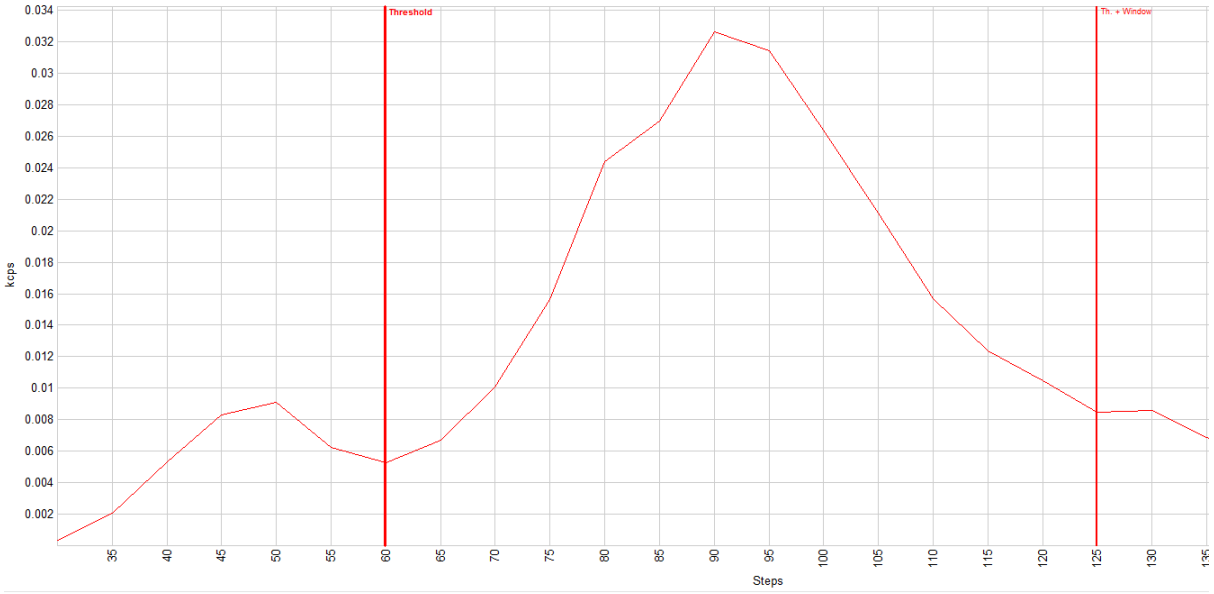

Appendix B.6: P-Kα Energy Profile

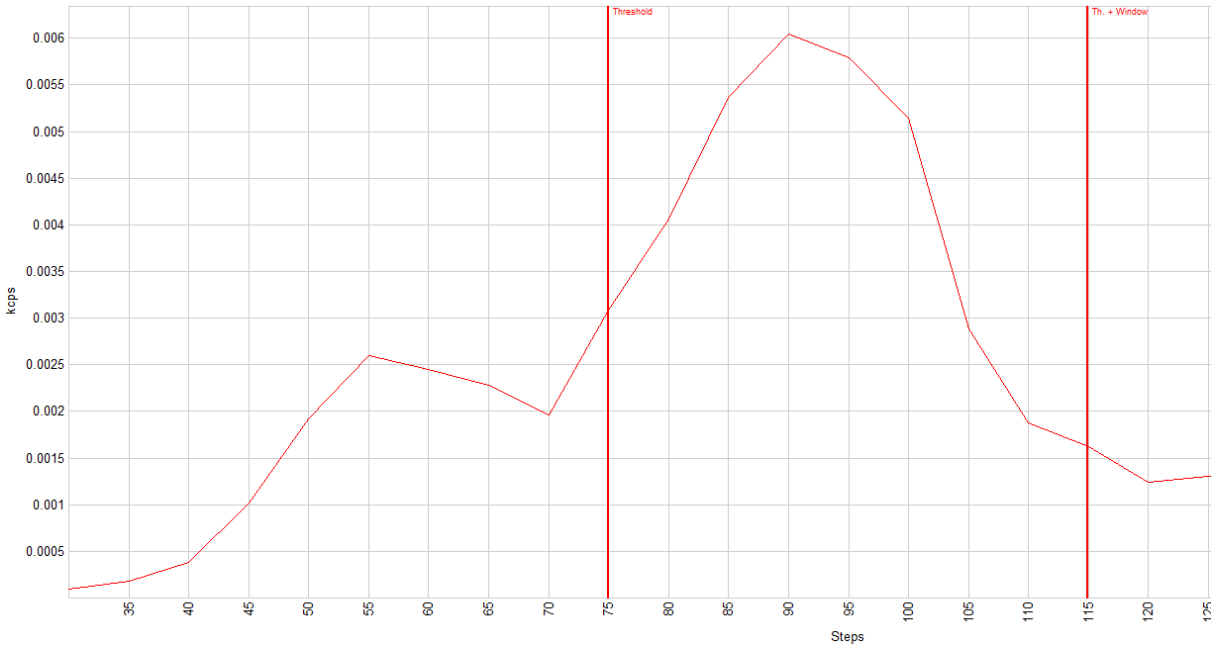

Appendix B.7: Si-Kα Energy Profile

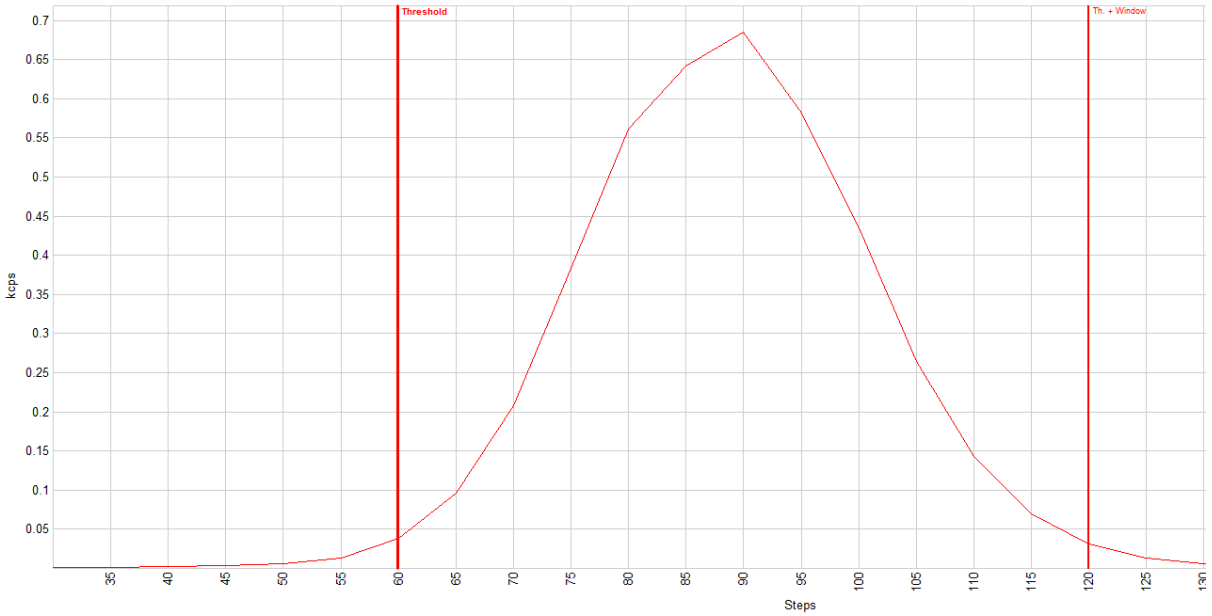

Appendix B.8: Ti-Kα Energy Profile

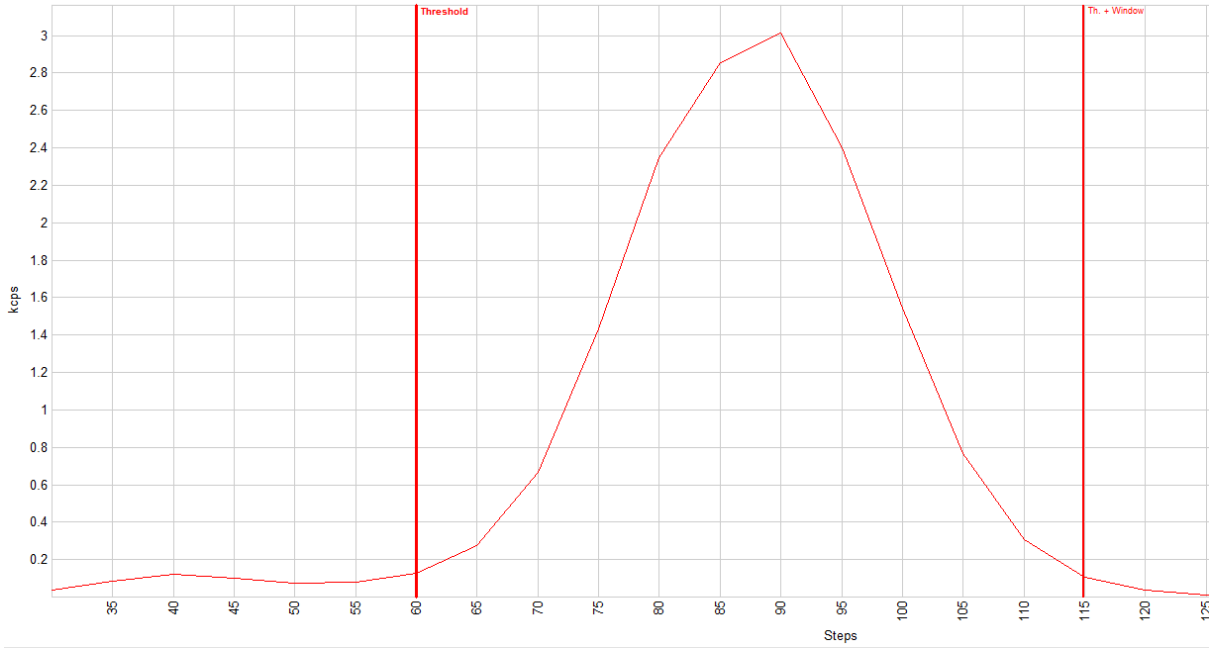

Appendix B.9: Zr-Lα Energy Profile

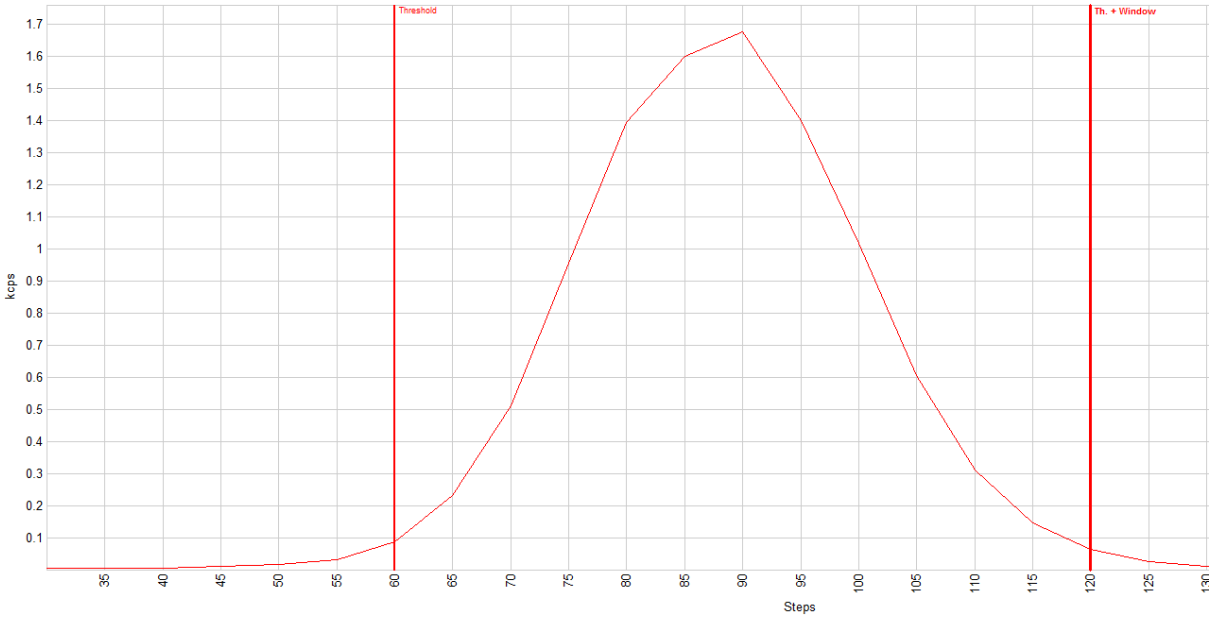

Appendix B.10: Th-Lα Energy Profile

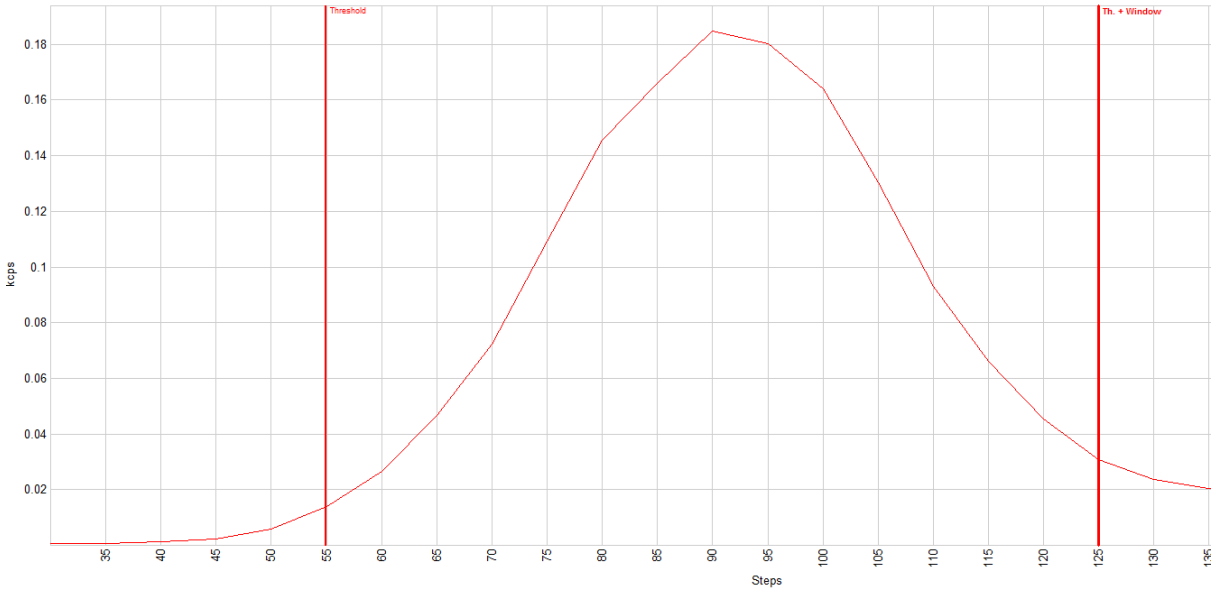

Appendix B.11: U-Lα Energy Profile

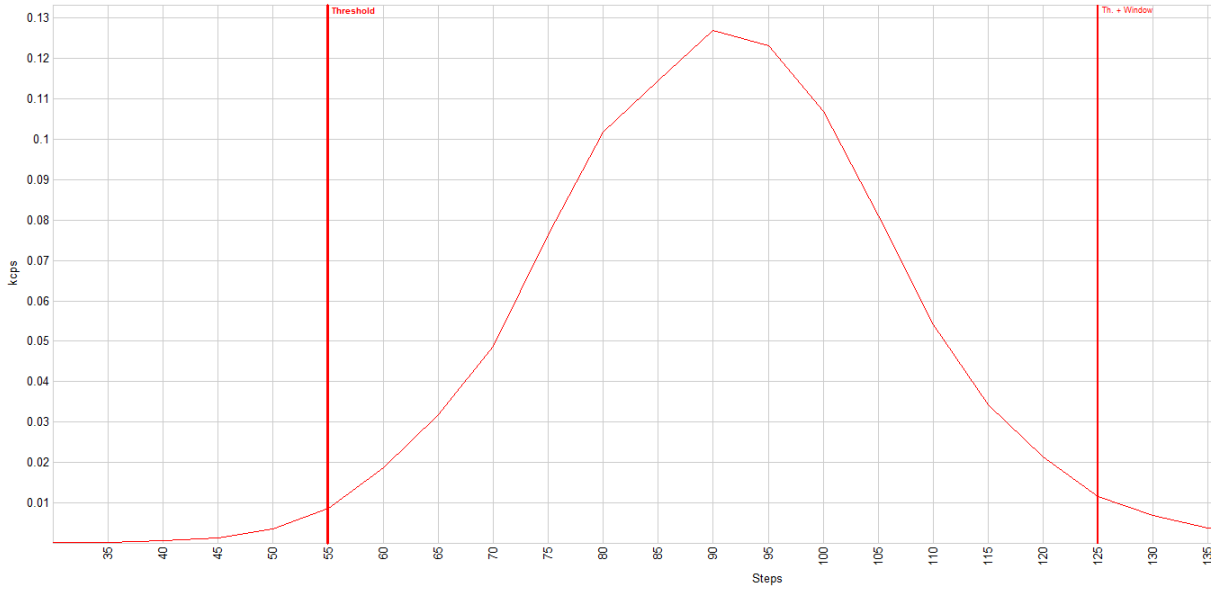

Appendix C.1: Al-Kα calibration line

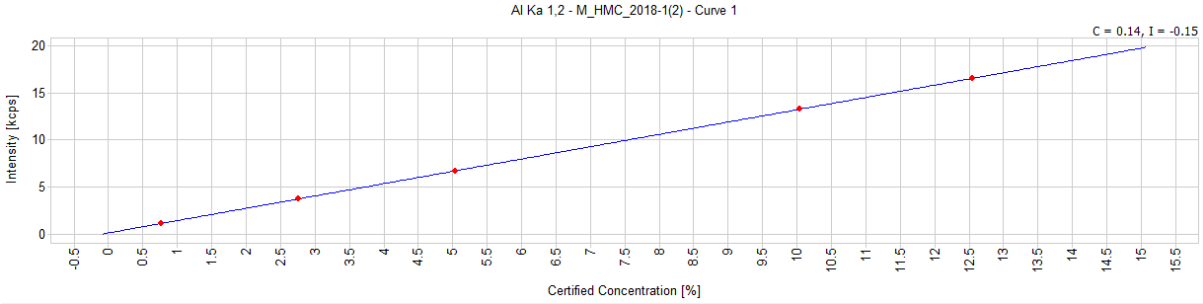

Appendix C.2: Ca-Kα calibration line

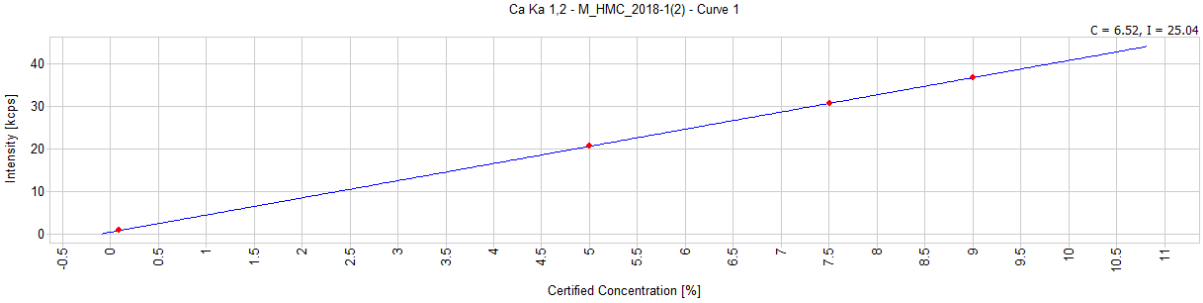

Appendix C.3: Fe-Kα calibration line

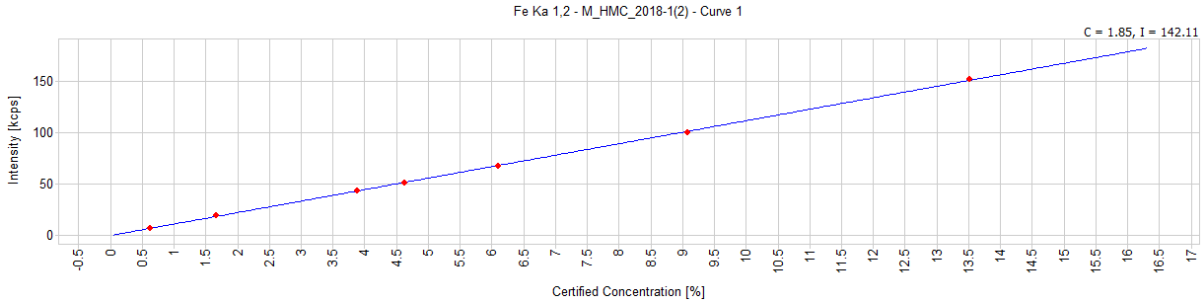

Appendix C.4: Hf-Lβ calibration line

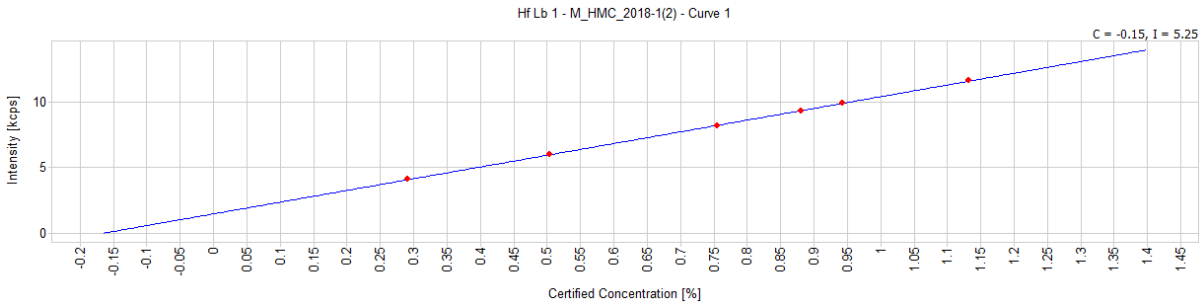

Appendix C.5: Mg-Kα calibration line

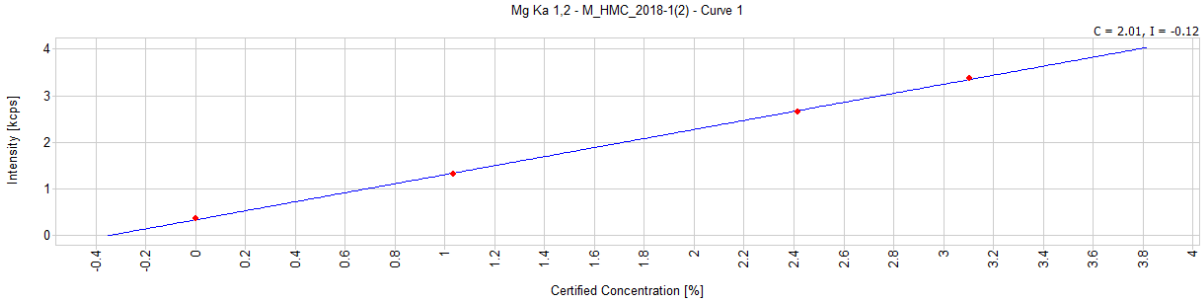

Appendix C.6: P-Kα calibration line

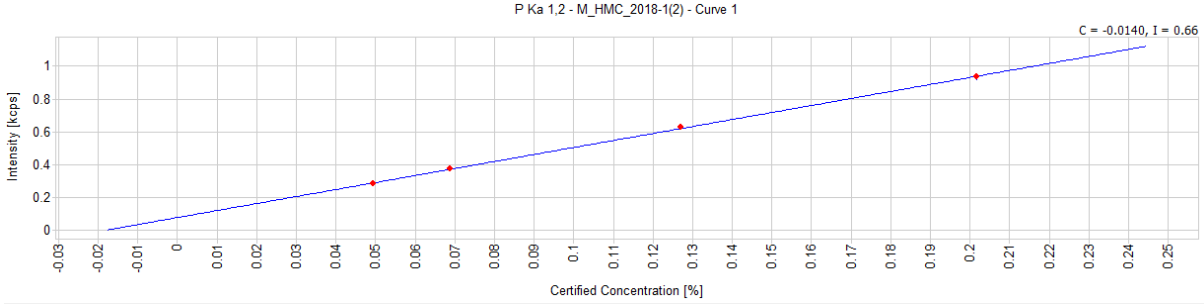

Appendix C.7: Si-Kα calibration line

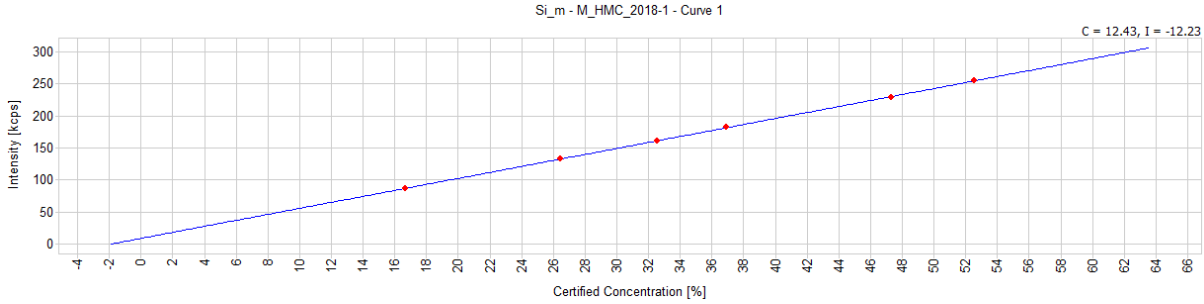

Appendix C.8: Ti-Kα calibration line

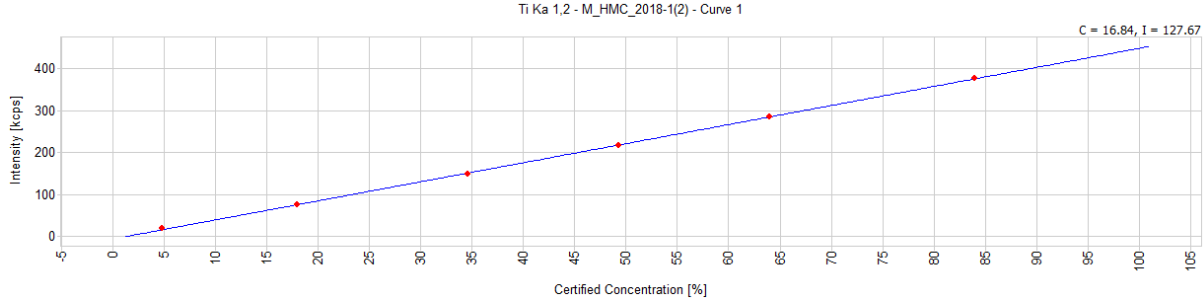

Appendix C.9: Zr-Lα calibration line

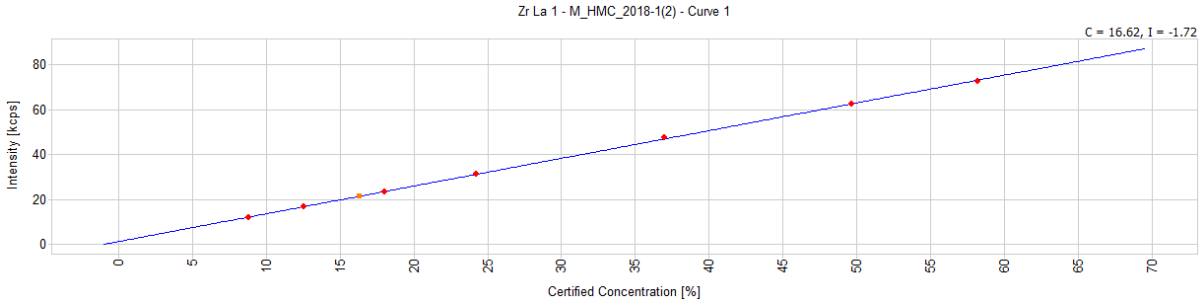

Appendix C.10: Th-Lα calibration line

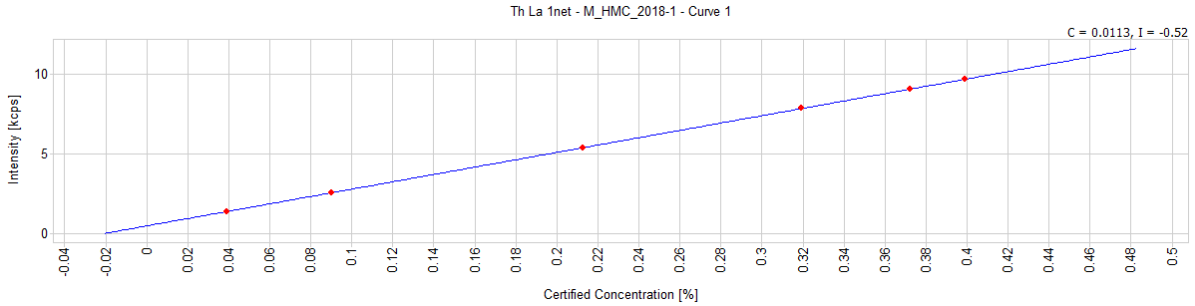

Appendix C.11: U-Lα calibration line

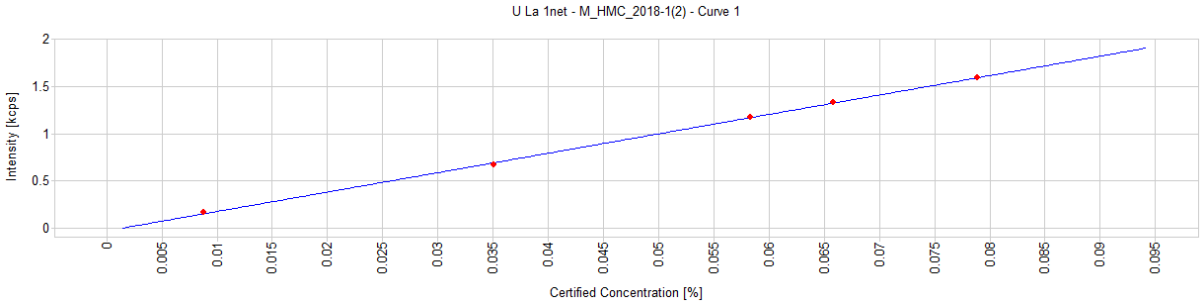

Appendix D.1: Regression Analysis Al_2O_3

Regression Analysis: INT (kcps) yi versus %Al2O3

Analysis of Variance

Source	DF	Adj SS	Adj MS	F-Value	P-Value
Regression	1	9,31600	9,31600	5331,77	0,000
%Al2O3	1	9,31600	9,31600	5331,77	0,000
Error	6	0,01048	0,00175		
Total	7	9,32648			

Model Summary

S	R-sq	R-sq(adj)	R-sq(pred)
0,0418003	99,89%	99,87%	98,49%

Coefficients

Term	Coef	SE Coef	T-Value	P-Value	VIF
Constant	0,1493	0,0190	7,86	0,000	
%Al2O3	0,72337	0,00991	73,02	0,000	1,00

Regression Equation

INT (kcps) yi = 0,1493 + 0,72337 %Al2O3

Appendix D.2: Regression Analysis CaO

Regression Analysis: INT (kcps) yi versus %CaO

Analysis of Variance

Source	DF	Adj SS	Adj MS	F-Value	P-Value
Regression	1	909,606	909,606	1259,66	0,000
%CaO	1	909,606	909,606	1259,66	0,000
Error	9	6,499	0,722		
Total	10	916,105			

Model Summary

S	R-sq	R-sq(adj)	R-sq(pred)
0,849766	99,29%	99,21%	99,03%

Coefficients

Term	Coef	SE Coef	T-Value	P-Value	VIF
Constant	-0,068	0,452	-0,15	0,884	
%CaO	2,6963	0,0760	35,49	0,000	1,00

Regression Equation

INT (kcps) yi = -0,068 + 2,6963 %CaO

Appendix D.3: Regression Analysis Fe_2O_3

Regression Analysis: INT (kcps) yi versus %Fe2O3

Analysis of Variance

Source	DF	Adj SS	Adj MS	F-Value	P-Value
Regression	1	5411,6	5411,58	501,51	0,000
%Fe2O3	1	5411,6	5411,58	501,51	0,000
Error	10	107,9	10,79		
Total	11	5519,5			

Model Summary

S	R-sq	R-sq(adj)	R-sq(pred)
3,28491	98,04%	97,85%	97,36%

Coefficients

Term	Coef	SE Coef	T-Value	P-Value	VIF
Constant	1,17	1,49	0,78	0,451	
%Fe2O3	4,446	0,199	22,39	0,000	1,00

Regression Equation

INT (kcps) yi = 1,17 + 4,446 %Fe2O3

Appendix D.4: Regression Analysis HfO_2

Regression Analysis: INT (kcps) yi versus %HfO2

Analysis of Variance

Source	DF	Adj SS	Adj MS	F-Value	P-Value
Regression	1	44,4958	44,4958	4667,08	0,000
%HfO2	1	44,4958	44,4958	4667,08	0,000
Error	4	0,0381	0,0095		
Total	5	44,5339			

Model Summary

S	R-sq	R-sq(adj)	R-sq(pred)
0,0976420	99,91%	99,89%	99,46%

Coefficients

Term	Coef	SE Coef	T-Value	P-Value	VIF
Constant	0,146	0,108	1,35	0,250	
%HfO2	7,816	0,114	68,32	0,000	1,00

Regression Equation

INT (kcps) yi = 0,146 + 7,816 %HfO2

Appendix D.5: Regression Analysis MgO

Regression Analysis: INT (kcps) yi versus %MgO

Analysis of Variance

Source	DF	Adj SS	Adj MS	F-Value	P-Value
Regression	1	3,22918	3,22918	9009,41	0,000
%MgO	1	3,22918	3,22918	9009,41	0,000
Error	3	0,00108	0,00036		
Total	4	3,23026			

Model Summary

S	R-sq	R-sq(adj)	R-sq(pred)
0,0189321	99,97%	99,96%	99,93%

Coefficients

Term	Coef	SE Coef	T-Value	P-Value	VIF
Constant	0,4223	0,0117	36,19	0,000	
%MgO	0,51067	0,00538	94,92	0,000	1,00

Regression Equation

INT (kcps) yi = 0,4223 + 0,51067 %MgO

Appendix D.6: Regression Analysis P_2O_5

Regression Analysis: INT (kcps) yi versus %P2O5

Analysis of Variance

Source	DF	Adj SS	Adj MS	F-Value	P-Value
Regression	1	0,030319	0,030319	10821,02	0,000
%P2O5	1	0,030319	0,030319	10821,02	0,000
Error	2	0,000006	0,000003		
Total	3	0,030325			

Model Summary

S	R-sq	R-sq(adj)	R-sq(pred)
0,0016739	99,98%	99,97%	99,94%

Coefficients

Term	Coef	SE Coef	T-Value	P-Value	VIF
Constant	-0,04235	0,00161	-26,27	0,001	
%P2O5	1,1091	0,0107	104,02	0,000	1,00

Regression Equation

INT (kcps) yi = -0,04235 + 1,1091 %P2O5

Appendix D.7: Regression Analysis SiO_2

Regression Analysis: INT (kcps) yi versus %SiO2

Analysis of Variance

Source	DF	Adj SS	Adj MS	F-Value	P-Value
Regression	1	28768,8	28768,8	33021,28	0,000
%SiO2	1	28768,8	28768,8	33021,28	0,000
Error	10	8,7	0,9		
Total	11	28777,5			

Model Summary

S	R-sq	R-sq(adj)	R-sq(pred)
0,933392	99,97%	99,97%	99,96%

Coefficients

Term	Coef	SE Coef	T-Value	P-Value	VIF
Constant	1,933	0,449	4,31	0,002	
%SiO2	2,8102	0,0155	181,72	0,000	1,00

Regression Equation

INT (kcps) yi = 1,933 + 2,8102 %SiO2

Appendix D.8: Regression Analysis TiO_2

Regression Analysis: INT (kcps) yi versus %TiO2

Analysis of Variance

Source	DF	Adj SS	Adj MS	F-Value	P-Value
Regression	1	798,975	798,975	54287,00	0,000
%TiO2	1	798,975	798,975	54287,00	0,000
Error	4	0,059	0,015		
Total	5	799,033			

Model Summary

S	R-sq	R-sq(adj)	R-sq(pred)
0,121316	99,99%	99,99%	99,98%

Coefficients

Term	Coef	SE Coef	T-Value	P-Value	VIF
Constant	-1,971	0,117	-16,88	0,000	
%TiO2	0,52772	0,00226	233,00	0,000	1,00

Regression Equation

INT (kcps) yi = -1,971 + 0,52772 %TiO2

Appendix D.9: Regression Analysis ZrO_2

Regression Analysis: INT (kcps) yi versus %ZrO2

Analysis of Variance

Source	DF	Adj SS	Adj MS	F-Value	P-Value
Regression	1	2856,87	2856,87	13711,75	0,000
%ZrO2	1	2856,87	2856,87	13711,75	0,000
Error	12	2,50	0,21		
Total	13	2859,37			

Model Summary

S	R-sq	R-sq(adj)	R-sq(pred)
0,456456	99,91%	99,91%	99,88%

Coefficients

Term	Coef	SE Coef	T-Value	P-Value	VIF
Constant	0,740	0,255	2,90	0,013	
%ZrO2	0,75297	0,00643	117,10	0,000	1,00

Regression Equation

INT (kcps) yi = 0,740 + 0,75297 %ZrO2

Appendix D.10: Regression Analysis U_3O_5

Regression Analysis: INT (kcps) yi versus %U3O5

Analysis of Variance

Source	DF	Adj SS	Adj MS	F-Value	P-Value
Regression	1	1,45193	1,45193	5799,87	0,000
%U3O5	1	1,45193	1,45193	5799,87	0,000
Error	3	0,00075	0,00025		
Total	4	1,45268			

Model Summary

S	R-sq	R-sq(adj)	R-sq(pred)
0,0158221	99,95%	99,93%	99,91%

Coefficients

Term	Coef	SE Coef	T-Value	P-Value	VIF
Constant	0,2102	0,0124	16,97	0,000	
%U3O5	17,441	0,229	76,16	0,000	1,00

Regression Equation

INT (kcps) yi = 0,2102 + 17,441 %U3O5

Appendix D.11: Regression Analysis ThO_2

Regression Analysis: INT (kcps) yi versus %ThO2

Analysis of Variance

Source	DF	Adj SS	Adj MS	F-Value	P-Value
Regression	1	3,38017	3,38017	8928,10	0,000
%ThO2	1	3,38017	3,38017	8928,10	0,000
Error	4	0,00151	0,00038		
Total	5	3,38168			

Model Summary

S	R-sq	R-sq(adj)	R-sq(pred)
0,0194576	99,96%	99,94%	99,83%

Coefficients

Term	Coef	SE Coef	T-Value	P-Value	VIF
Constant	0,2918	0,0115	25,36	0,000	
%ThO2	16,272	0,172	94,49	0,000	1,00

Regression Equation

INT (kcps) yi = 0,2918 + 16,272 %ThO2

Appendix E.1: Precision Analysis Al_2O_3

Descriptive Statistics: 1 fused bead 10 measurements

Statistics

Variable	Mean	StDev	CoefVar
1 fused bead 10 measurements	2,3414	0,0132	0,56

Descriptive Statistics: 40 days

Statistics

Variable	Mean	StDev	CoefVar
40 days	2,3205	0,0471	2,03

Appendix E.2: Precision Analysis CaO

Descriptive Statistics: 1 fused bead 10 measurements

Statistics

Variable	Mean	StDev	CoefVar
1 fused bead 10 measurements	1,2602	0,00346	0,27

Descriptive Statistics: 40 days

Statistics

Variable	Mean	StDev	CoefVar
40 days	1,2401	0,0306	2,47

Appendix E.3: Precision Analysis Fe_2O_3

Descriptive Statistics: 1 fused bead 10 measurements

Statistics

Variable	Mean	StDev	CoefVar
1 fused bead 10 measurements	6,7001	0,00854	0,13

Descriptive Statistics: 40 days

Statistics

Variable	Mean	StDev	CoefVar
40 days	6,5810	0,0972	1,48

Appendix E.4: Precision Analysis HfO_2

Descriptive Statistics: 1 fused bead 10 measurements

Statistics

Variable	Mean	StDev	CoefVar
1 fused bead 10 measurements	0,77670	0,00200	0,26

Descriptive Statistics: 40 days

Statistics

Variable	Mean	StDev	CoefVar
40 days	0,77100	0,01480	1,92

Appendix E.5: Precision Analysis Mg

Descriptive Statistics: 1 fused bead 10 measurements

Statistics

Variable	Mean	StDev	CoefVar
1 fused bead 10 measurements	0,80010	0,02591	3,24

Descriptive Statistics: 40 days

Statistics

Variable	Mean	StDev	CoefVar
40 days	0,74740	0,02177	2,91

Appendix E.6: Precision Analysis P_2O_5

Descriptive Statistics: 1 fused bead 10 measurements

Statistics

Variable	Mean	StDev	CoefVar
1 fused bead 10 measurements	0,32120	0,00204	0,64

Descriptive Statistics: 40 days

Statistics

Variable	Mean	StDev	CoefVar
40 days	0,31712	0,00559	1,76

Appendix E.7: Precision Analysis SiO_2

Descriptive Statistics: 1 fused bead 10 measurements

Statistics

Variable	Mean	StDev	CoefVar
1 fused bead 10 measurements	28,260	0,0403	0,14

Descriptive Statistics: 40 days

Statistics

Variable	Mean	StDev	CoefVar
40 days	28,208	0,0830	0,29

Appendix E.8: Precision Analysis TiO_2

Descriptive Statistics: 1 fused bead 10 measurements

Statistics

Variable	Mean	StDev	CoefVar
1 fused bead 10 measurements	20,687	0,0660	0,32

Descriptive Statistics: 40 days

Statistics

Variable	Mean	StDev	CoefVar
40 days	20,629	0,146	0,71

Appendix E.9: Precision Analysis ZrO_2

Descriptive Statistics: 1 fused bead 10 measurements

Statistics

Variable	Mean	StDev	CoefVar
1 fused bead 10 measurements	37,620	0,0400	0,11

Descriptive Statistics: 40 days

Statistics

Variable	Mean	StDev	CoefVar
40 days	37,791	0,399	1,06

Appendix E.10: Precision Analysis U_3O_5

Descriptive Statistics: 1 fused bead 10 measurements

Statistics

Variable	Mean	StDev	CoefVar
1 fused bead 10 measurements	228,10	4,75	2,08

Descriptive Statistics: 40 days

Statistics

Variable	Mean	StDev	CoefVar
40 days	234,38	11,03	4,71

Appendix E.11: Precision Analysis ThO_2

Descriptive Statistics: 1 fused bead 10 measurements

Statistics

Variable	Mean	StDev	CoefVar
1 fused bead 10 measurements	664,60	13,62	2,05

Descriptive Statistics: 40 days

Statistics

Variable	Mean	StDev	CoefVar
40 days	679,02	25,73	3,79

Appendix F: Proficiency Testing

Results of
Non mags Round Robin

Sample ID: RR005e/18
Date: Jun-19

All results are reported in %, unless otherwise indicated
Grubbs min or max outliers indicated in red
Other outliers in green

	Laboratory																												Average	Std Dev
Element	**1**	**2**	**3**	**4**	**5**	**6**	**7**	**8**	**9**	**10**	**11**	**12**	**13**	**14**	**15**	**16**	**17**	**18**	**19**	**20**	**21**	**22**	**23**	**24**	**25**	**26**	**27**	**28**		
Al_2O_3	2,56	2,64	2,54	2,72	2,71	2,63	2,88	3,62	-	2,75	2,63	2,64	2,66	2,70	2,67	3,04	2,70	2,69	2,75	2,77	2,70	0,30	1,19	2,55	2,71	1,82	2,83	1,83	2,69	0,08
CaO	1,13	1,59	1,61	1,68	1,68	1,62	1,55	2,16	1,70	1,52	1,62	1,62	1,60	1,60	1,62	2,13	1,55	1,59	1,64	1,68	1,62	0,12	1,60	1,48	1,60	-	1,48	1,64	1,607	0,06
Fe_2O_3	6,51	6,03	6,09	6,10	6,22	6,67	8,15	6,23	5,91	6,14	6,14	6,26	6,18	6,15	6,68	6,37	6,04	6,61	6,55	6,35	6,19	0,13	3,48	6,02	6,15	6,52	6,18	6,16	6,20	0,17
TiO_2	21,0	21,2	21,9	22,1	21,8	21,2	22,8	21,7	21,1	21,5	21,6	21,7	21,4	21,6	21,5	23,3	20,9	20,9	22,3	22,6	21,6	1,64	24,0	21,0	21,4	21,3	23,9	21,5	21,5	0,44
ZrO_2	35,3	35,2	36,5	35,9	35,8	36,2	30,5	37,3	37,4	38,1	35,6	35,4	36,0	36,3	35,7	36,2	34,5	36,5	35,1	36,1	36,3	59,1	39,1	32,4	36,3	36,6	35,5	36,0	36,0	0,68
HfO_2	0,21	0,80	0,77	0,74	0,76	-	0,67	0,95	1,06	0,73	0,74	0,88	0,81	0,77	0,86	0,74	0,78	0,73	0,89	0,76	0,82	-	1,06	0,76	0,76	-	0,79	0,75	0,77	0,05
SiO_2	27,2	27,7	28,5	28,0	28,1	27,7	26,4	24,9	27,5	24,3	28,3	28,1	28,4	28,4	28,3	28,8	27,4	28,6	27,5	28,2	28,7	34,8	28,6	32,1	29,2	33,6	28,4	28,4	28,2	0,5
P_2O_5	0,51	0,56	0,73	0,34	0,33	0,48	0,55	0,60	0,47	-	0,53	0,51	0,52	0,48	0,49	0,54	0,47	0,51	0,51	0,54	0,53	0,36	0,21	0,50	0,51	0,19	0,51	0,49	0,50	0,07
U ppm	-	260	211	-	-	-	244	331	-	-	250	267	238	274	250	309	1780	280	248	115	300	366	-	458	232	260	119	-	259	53
Th ppm	-	660	594	-	-	-	768	1529	-	-	640	673	636	668	654	660	978	763	712	596	800	365	-	870	375	690	615	-	666	53